Bipedal Walking for a Full-sized Humanoid Robot Utilizing Sinusoidal Feet Trajectories and Its Energy Consumption

Jeakweon Han

Dissertation submitted to the faculty of the Virginia Polytechnic Institute and State University in partial fulfillment of the requirements for the degree of

Doctor of Philosophy

In

Mechanical Engineering

Dennis W. Hong, Chair
Andrew J, Kurdila
Robert L, West
Robert H, Sturges
Thurmon E, Lockhart

April 24, 2012
Blacksburg, Virginia

Keywords: Bipedal, Humanoid, Robot, CHARLI, Energy, Walking method, ZMP, Sinusoidal foot movement, Energy consumption

Bipedal Walking for a Full-sized Humanoid Robot Utilizing Sinusoidal Feet Trajectories and Its Energy Consumption

Jeakweon Han

ABSTRACT

This research effort aims to develop a series of full-sized humanoid robots, and to research a simple but reliable bipedal walking method.

Since the debut of Wabot from Waseda University in 1973, several full-sized humanoid robots have been developed around the world that can walk, and run. Although various humanoid robots have successfully demonstrated their capabilities, bipedal walking methods are still one of the main technical challenges that robotics researchers are attempting to solve. It is still challenging because most bipedal walking methods, including ZMP (Zero Moment Point) require not only fast sensor feedback, but also fast and precise control of actuators. For this reason, only a small number of research groups have the ability to create full-sized humanoid robots that can walk and run.

However, if we consider this problem from a different standpoint, the development of a full-sized humanoid robot can be simplified as long as the bipedal walking method is easily formulated. Therefore, this research focuses on developing a simple but reliable bipedal walking method. It then presents the designs of two versions of a new class of super lightweight (less than 13 kg), full-sized (taller than 1.4 m) humanoid robots called CHARLI-L (Cognitive Humanoid Autonomous Robot with Learning Intelligence – Lightweight) and CHARLI-2. These robots have unique designs compared to other full-sized humanoid robots. CHARLI-L utilizes spring assisted parallel four-bar linkages with synchronized actuation to achieve the goals of lightweight and low cost. Based on the experience and lesions learned from CHARLI-L, CHARLI-2 uses gear train reduction mechanisms, instead of parallel four-bar linkages, to increase actuation torque at the joints while further reducing weight.

Both robots successfully demonstrated untethered bipedal locomotion using an intuitive walking method with sinusoidal foot movement. This walking method is based on the ZMP method. Motion capture tests using six high speed infrared cameras validate the proposed bipedal walking method. Additionally, the total power and energy consumptions during walking are calculated from measured actuator currents.

Acknowledgements

My wife, Sheal, said, “If you achieve success, you should show appreciation to those who supported you along the way.” I feel like I am the luckiest person in world because of all the lovely people that have helped me along my journey.

I give my true and sincere gratitude to Dr. Dennis Hong for his dedication and encouragement. I would never make anything successful without him. His passion and broad knowledge in robotics nourished my growth as a successful roboticist.

In addition, I deeply appreciate my committee members, Dr. Thurmon Lockhart, Dr. Andrew Kurdila, Dr. Robert Sturges and Dr. Robert West. They provided guidance, support and patience to keep me on the right track. I would especially like to thank Dr. Thurmon Lockhart. He allowed me to use his test equipment, so that I could meet with good results.

I would like to thank visiting Researchers, Dr. Bohee Lee and Dr. Young-Jae Ryoo for their help, support and encouragement. Also, I would like to thank Brandy McCoy. She helped me with her cheerful heart and mind.

I want to say thanks to my amazing lab mates: Joe Hays, Ping Ren, Blake Jeans, Rob Nguyen, Ryan Colby, Gabriel Goldman, Seungmoon Song, Eric Williams, Derek Lahr, Viktor Orekhov, Bryce Lee, Mike Hopkins, Paul D'Angio, Panit Howard, David Henry, Coleman Knabe, Taylor Pesek and Jack Newton. They were always my friends who cheered me up and assisted me in the lab.

I give special thanks to RoboCup crew: Rob Nguyen, Paul D'Angio, Mike Hopkins, Seungmoon Song, Derek Lahr, Viktor Orekhov, Bryce Lee and Taylor Pesek. I’ll always cherish my memories of dominating the world with our robots.

Also, I would like to thank my mentor Bill Kim and Inyong Ha who supported me and helped me get into RoMeLa.

I would like to thank my mother, father, brother, mother-in-law, father-in-law, sister-in-law and my dog Bell. Even though they are in South Korea (except for Bell), they always assured me that I am loved, which gave me the energy to keep moving forward.

I send my heart to everyone who helped me during the last four years at Virginia Tech. I am grateful for the experience.

Lastly, I dedicate the successes I made during my graduate school years to my soul mate Sheal Eum.

Table of Contents

List of Figures

List of Tables

Section 1 Introduction

1.1 Motivation

As a child, I grew up watching the Japanese animated television program "Astro Boy," a show about a robot that helped and protected people. Since then, I have always dreamt of contributing to the development of intelligent robots that would help make the world a better place. However, most people associate the term *humanoid robot* with destructive machines such as "The Terminator" from Hollywood's recent movies. I don't think robots will ever become something as terrible as we have seen in movies; I believe that mankind will maintain an effective method for controlling robots when they do eventually become a part of our everyday lives. Instead of fearing robots, we should realize the enormous benefits that they can bring to the human race. We are facing an aging society and the ratio of workload to available human labor continues to fall. Intelligent robots such as these offer a promising solution to these types of problems.

Taking these factors into account, I believe it is my duty to build reliable, effective, and safe robots that can be easily integrated into our everyday lives. However, currently, building a full-sized humanoid robot is one of the most challenging tasks in the robotics research area. There are many factors contributing to its difficulty, but one of the biggest challenges is that bipedal walking requires fast and precise control of the robot's legs. Then, is it possible to design a simple and reliable bipedal walking method?

This research began from the question above. If a bipedal walking method was sufficiently simple and reliable that many researchers could implement it readily, this would be a very positive contribution to the robotics society. For this reason, I propose in this work a simple walking method for humanoid robots that can be tuned and tweaked intuitively.

1.2 History and Background

The humanoid research group at Waseda University has had a long history of research in bipedal robots; making many significant contributions to the field since 1966. Ichiro Kato, a professor of Waseda University who is known as the father of bipedal robotics, devoted his life to researching bipedal locomotion and accomplished remarkable works in the field [1], [2], [3], [4], [5], [6]. In 1973, Waseda University developed the Wabot, which became the first well known series of humanoid robots capable of bipedal walking. Currently, Waseda University continues research on their WABIAN-2 (the WAseda BIpedal humANoid) humanoid platform.

One of the most famous humanoid robots to date is the Honda ASIMO, which made its debut in the year 2000. However, Honda developed three prototype predecessors of the ASIMO robot. Honda had secretly conducted a decade of research before revealing the development of their second humanoid robot and world's first self-regulating humanoid walking robot, the "P2" model, in 1996. Further improvements on these prototypes have helped ASIMO become recognized as the most advanced humanoid robot in the world considering its artificial intelligence (AI) and impressive movement capabilities. Honda has demonstrated the maturity of ASIMO's AI through advanced tasks such as multiple ASIMO robots working together to serve coffee to humans in a cafeteria. The mobility of the ASIMO robot has also been demonstrated through its running and stair climbing abilities. [7] [8]

Another impressive humanoid robot is the HRP (Humanoid Robotics Project) series developed by AIST (Japanese National Institute of Advanced Industrial Science and Technology) and Kawada Industries, Inc. The HRP-2 robot has the ability to stand up from either a front or back lying position on the floor, which is something that the Honda ASIMO robot is not capable of doing. The HRP-4C model can mimic human facial and head movements as well as execute dance steps. At Tokyo's Digital Content Expo 2010, this model gave the most realistic human performance by a robot yet. [9] [10]

In 2003, the Technical University of Munich created JOHNNIE, an autonomous bipedal walking robot. Their main objective was to realize an anthropomorphic walking machine with a human-like, dynamically stable gait. They also released a new 25-degree of freedom (DOF) humanoid walking robot, called LOLA, in 2009. The goal of this project was to realize fast and human-like walking motion. [11]

In 2009, Boston Dynamics, already famous for its BigDog robot, released a video of its bipedal robot called PETMAN. The quadruped robot BigDog shocked the world with its superior balance and mobility which allowed it to run and hop on rough-terrain. Likewise, the prototype of PETMAN also demonstrated the ability to balance during walking at a level which was unprecedented in the history of bipedal robots. Unfortunately, the technical paper describing the research behind the PETMAN has not been released as the research itself is part of a military project.

1.3 Problem Statement

It has been only 40 years since humanoid robots sprung from science fiction to reality. Although humanoid robot technology has made remarkable progress during this relatively short period, our expectations are always beyond the current level of technology. Humans wish for robots to take over all of their complicated daily tasks, however, our most advanced humanoid robot technology is only capable of a few, simple tasks in laboratory environments.

Likewise, we expect for robots to be able to walk and run with the same skill as humans, but only a small portion of research groups have the ability to create full-sized humanoid robots that can walk and run at all. Bipedal walking is still one of the main technical issues robot researchers are attempting to accomplish. As stated previously, the reason why this task is still challenging is that bipedal walking requires fast and precise control of the robot's legs. To overcome these difficulties, many robot researchers are using high performance sensors and sophisticated control methods. As a result, limited funds and technological barriers hinder the development of a robot society.

If we consider the issue from another viewpoint, a simple bipedal walking method could effectively solve this problem. Thus, the main objective of this work is to create a full-sized humanoid robot that can walk using a relatively simple method. To reach this objective, it is necessary to investigate bipedal walking methods which can be implemented without any sophisticated skill or specialized technology. Once achieved, the usefulness and reliability of the proposed bipedal walking method should be proven in both a theoretical and practical manner.

In addition to the stability of the walking algorithm, energy consumption is a crucial issue related to the use of robots in real environments, since the amount of energy a robot consumes limits the length of time it is able to perform a task. For this reason, whenever a bipedal walking method is proposed it is important to analyze the energy consumed by the walking gait. Therefore, the second objective of this work is to measure the energy consumed by the proposed walking method.

1.4 Review of Literature

Since Waseda University introduced the Wabot series, many research groups have seen success in the development of bipedal humanoid robots. The HONDA research group has developed the humanoid platforms P2, P3, and ASIMO [7]. The Japanese National Institute of Advanced Industrial Science and Technology (AIST) and Kawada Industries, Inc. have developed HRP-2P [8]. The University of Tokyo has built the H6 and H7 [9], and the Technical University of Munich has developed JOHNNIE [11]. The Korea Advanced Institute of Science and Technology (KAIST) has developed the 41-DOF KHR-2 and HUBO [12].

Since Miomir Vukobratović suggested the ZMP (Zero Moment Point) algorithm, it has become one of the most popular bipedal walking methods [13]. Most full-sized humanoid robots use the ZMP method for walking. Many research studies have been performed utilizing the ZMP method for bipedal walking, and the algorithm has evolved since it was first introduced. Sardain, P. et al. investigated the use of foot pressure for the ZMP walking method [14]. Qinghua Li et al. showed how to measure ZMP using force moment sensors [15]. Sorao, K et al. showed how to estimate the robot's motion based on the sensed ZMP data [16]. Takanishi, A. suggested a ZMP control method for eliminating external disturbances and proved its performance through experiments.[6]

Although the ZMP method makes dynamic bipedal walking feasible, the walking stability depends on the sensing and processing speed, because the controller should send appropriate control signals to the actuators in a short period of time when a robot falls down. Many researchers have tried to overcome this disadvantage. Nishiwaki Koichi [17], Sugihara, T et al. [18] investigated fast generation methods for ZMP motion patterns. Each proposed a different approach. Kagami, S. showed his walking pattern could be updated every 40ms [19].

Alternatively, Okumura, Y et al. compensated for ZMP trajectories by adjusting feedback parameters, instead of changing the walking pattern [20]. Kajita, S. et al. suggested auxiliary ZMP control to increase the sensing speed. With this approach the controller estimates disturbances and changes in the ZMP trajectory before a disturbance actually occurs, as opposed to waiting for sensor data [21]. Johannes Strom et al, added a preview controller to improve the walking stability. The primary goal was to generate balanced center of mass trajectories based on the dynamics [22].

Numerous other studies have been conducted. Jinsu Liu et al. suggested an online sampling algorithm to search for the ZMP efficiently and simulated its performance [23]. Kajita, S. et al. used preview control theory to compensate for the ZMP error caused by the differences between a simple model and the precise multi-body model. This method was used to allow a simulated robot to walk on spiral stairs [24]. Sato, T. et al. designed a ZMP disturbance observer to increase walking stability. It was confirmed through simulations and experiments [25]. Kyu-Cheon Choi et al. used fuzzy posture control to improve walking stability [26]. Jong Hyeon Park et al. also used fuzzy-logic to reduce the

swing motion of the trunk to minimize disturbances [27]. Erbatur, K et al. suggested the use of Fourier series approximation to generate a smooth ZMP reference signal [28].

Meanwhile, some researchers have focused on the relationship between the center of mass (COM) and ZMP which is the one of the main ideas of this research. Sugihara, T. studied the relationship between COM and ZMP [29]. Youngjin Choi et al. used the position of the COM to estimate the ZMP [30]. Bum-Joo Lee et al. independently changed the position and velocity of the center of mass within single stance status to simplify the ZMP function [31].

1.5 Outline of Dissertation

The motivation, history, problem statement and review of literature for this dissertation were presented in the previous subsections. Section 2 presents methods for solving the forward and inverse kinematics for humanoid robotic legs. These kinematic solutions lead up to the dynamics solution presented in Section 3 which utilizes the Jacobian matrix and Euler-Lagrange equations. These dynamic equations are fundamental to bipedal walking theory. Section 4 discusses the ZMP walking method as well as an intuitive walking method with sinusoidal foot movement. Section 5 presents methods for simulating bipedal walking performances and the corresponding results. Section 6 introduces the design and fabrication of the CHARLI-L and CHARLI-2 robots and outlines critical design considerations for building full-sized humanoid robots. Section 7 presents test results related to the walking ability, stability, ZMP trajectories, and energy consumption. It also includes a discussion of the effectiveness of the proposed walking method. Section 8 outlines the conclusions of this research, including its contributions and future work to be considered.

Section 2 Kinematics

The first step in developing bipedal walking in humanoids is defining the kinematics. In this section, forward and inverse kinematics of CHARLI-2's leg will be introduced.

2.1 Forward Kinematics

CHARLI-2 has 6-DOF(Degree Of Freedom) in each leg. The hip joint has 3-DOF, arranged to move as a spherical joint. The knee joint has 1DOF and the ankle joint has 2-DOF.

As shown in Figure 2.1, an origin $\{x_0, y_0, z_0\}$ is established at the hip joint and each joint has a coordinate system following the Denavit-Hartenberg (DH) definition. The foot coordinate is a special case in which it corresponds with the origin coordinate. This allows us to think about foot movement more intuitively.

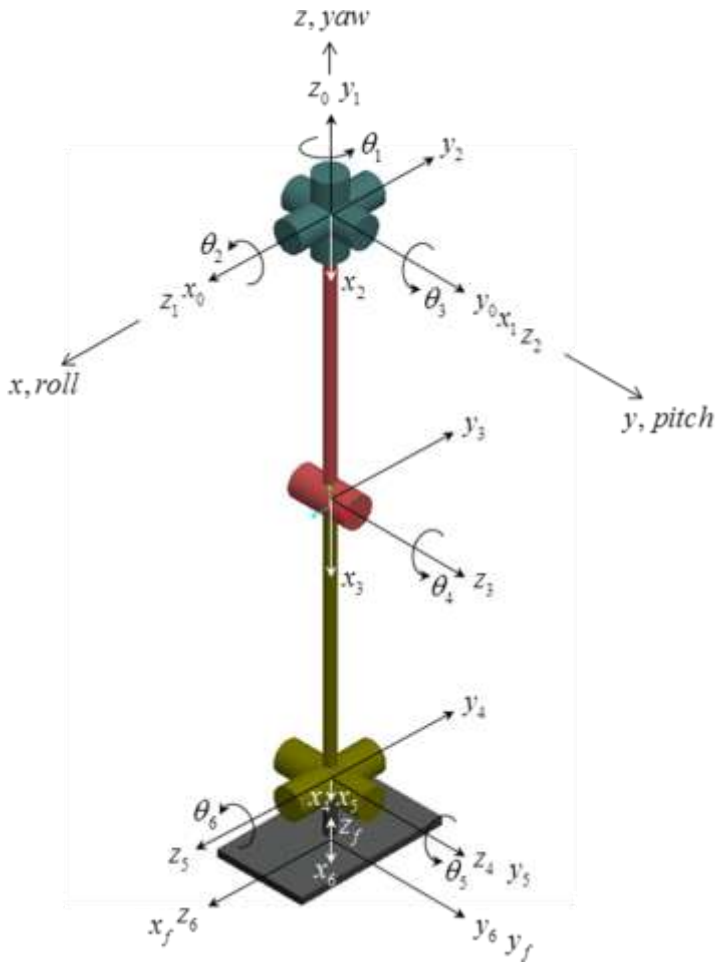

Figure 2.1 Coordinate frames and joint definition of CHARLI-2's leg

Table 2.1 lists DH parameters used to solve the DH matrixes. Equation 2.1 is a homogeneous transformation matrix which expresses the position and the orientation of each joint. The transformation matrix of each joint can be readily obtained by substituting DH parameters into Equation 2.1. The Equations from 2.2 to 2.8 are the transformation matrixes of each joint.

Table 2.1 D-H parameters of CHRALI-2's leg

i	θ_i	α_i	a_i	d_i
1	90	90	0	0
2	-90	-90	0	0
3	0	0	l_3	0
4	0	0	l_4	0
5	0	90	0	0
6	0	0	l_6	0

$$H_i^{i-1} = \begin{bmatrix} \cos\theta_i & -\cos\alpha_i \sin\theta_i & \sin\alpha_i \sin\theta_i & a_i \cos\theta_i \\ \sin\theta_i & \cos\alpha_i \cos\theta_i & -\sin\alpha_i \cos\theta_i & a_i \sin\theta_i \\ 0 & \sin\alpha_i & \cos\alpha_i & d_i \\ 0 & 0 & 0 & 1 \end{bmatrix} \quad \text{(Eq. 2.1)}$$

$$H_1^0 = \begin{bmatrix} \cos(\theta_1+90^\circ) & 0_i & \sin(\theta_1+90^\circ) & 0 \\ \sin(\theta_1+90^\circ) & 0 & -\cos(\theta_1+90^\circ) & 0 \\ 0 & 1 & 0 & 0 \\ 0 & 0 & 0 & 1 \end{bmatrix} = \begin{bmatrix} -\sin\theta_1 & 0 & \cos\theta_1 & 0 \\ \cos\theta_1 & 0 & \sin\theta_1 & 0 \\ 0 & 1 & 0 & 0 \\ 0 & 0 & 0 & 1 \end{bmatrix} \quad \text{(Eq. 2.2)}$$

$$H_2^1 = \begin{bmatrix} \cos(\theta_2-90^\circ) & 0_i & -\sin(\theta_2-90^\circ) & 0 \\ \sin(\theta_2-90^\circ) & 0 & \cos(\theta_2-90^\circ) & 0 \\ 0 & -1 & 0 & 0 \\ 0 & 0 & 0 & 1 \end{bmatrix} = \begin{bmatrix} \sin\theta_2 & 0 & \cos\theta_2 & 0 \\ -\cos\theta_2 & 0 & \sin\theta_2 & 0 \\ 0 & -1 & 0 & 0 \\ 0 & 0 & 0 & 1 \end{bmatrix} \quad \text{(Eq. 2.3)}$$

$$H_3^2 = \begin{bmatrix} \cos\theta_3 & -\sin\theta_3 & 0 & l_3\cos\theta_3 \\ \sin\theta_3 & \cos\theta_3 & 0 & l_3\sin\theta_3 \\ 0 & 0 & 1 & 0 \\ 0 & 0 & 0 & 1 \end{bmatrix} \quad \text{(Eq. 2.4)}$$

$$H_4^3 = \begin{bmatrix} \cos\theta_4 & -\sin\theta_4 & 0 & l_4\cos\theta_4 \\ \sin\theta_4 & \cos\theta_4 & 0 & l_4\sin\theta_4 \\ 0 & 0 & 1 & 0 \\ 0 & 0 & 0 & 1 \end{bmatrix} \quad \text{(Eq. 2.5)}$$

$$H_5^4 = \begin{bmatrix} \cos\theta_5 & 0 & \sin\theta_5 & 0 \\ \sin\theta_5 & 0 & -\cos\theta_5 & 0 \\ 0 & 1 & 0 & 0 \\ 0 & 0 & 0 & 1 \end{bmatrix} \quad \text{(Eq. 2.6)}$$

$$H_6^5 = \begin{bmatrix} \cos\theta_6 & -\sin\theta_6 & 0 & l_6\cos\theta_6 \\ \sin\theta_6 & \cos\theta_6 & 0 & l_6\sin\theta_6 \\ 0 & 0 & 1 & 0 \\ 0 & 0 & 0 & 1 \end{bmatrix} \quad \text{(Eq. 2.7)}$$

$$H_F^6 = \begin{bmatrix} 0 & 0 & -1 & 0 \\ 0 & 1 & 0 & 0 \\ 1 & 0 & 0 & 0 \\ 0 & 0 & 0 & 1 \end{bmatrix} \quad \text{(Eq. 2.8)}$$

The continuous homogeneous transformation from H_1^0 to H_F^6 transforms the foot coordinate to the origin, as shown in Equation 2.9.

$$H_F^0 = H_1^0 H_2^1 H_3^2 H_4^3 H_5^4 H_6^5 H_F^6 \quad \text{(Eq. 2.9)}$$

2.2 Inverse Kinematics

The purpose of solving the inverse kinematics is to find the angle of each joint for a known foot position. Equation ( ) provides the solution of the forward kinematics with matrix P being the result. The translation vector $\{P_x, P_y, P_z\}$ gives the position of the foot and the orientation matrix $\begin{bmatrix} r_{11} & r_{12} & r_{13} \\ r_{21} & r_{22} & r_{23} \\ r_{31} & r_{32} & r_{33} \end{bmatrix}$ shows the direction of the foot.
Based on the assumption that the values in P are known, the joint angles can be calculated.

$$H_F^0 = H_1^0 H_2^1 H_3^2 H_4^3 H_5^4 H_6^5 H_F^6 = P = \begin{bmatrix} r_{11} & r_{12} & r_{13} & P_x \\ r_{21} & r_{22} & r_{23} & P_y \\ r_{31} & r_{32} & r_{33} & P_z \\ 0 & 0 & 0 & 1 \end{bmatrix} \quad \text{(Eq. 2.10)}$$

A geometrical solution should be done first to simplify the inverse kinematics. If we select the plane perpendicular to the z_2, z_3, z_4 axes, we can draw Figure 2.2.

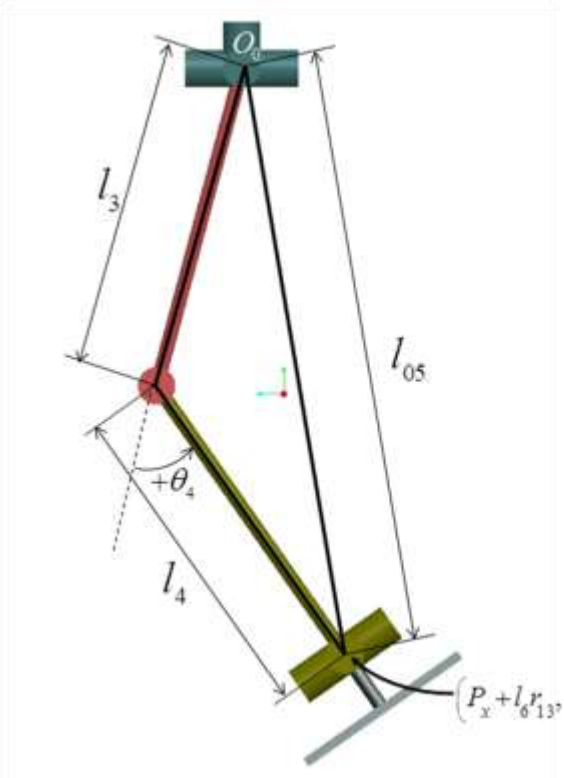

Figure 2.2 Geometical relationship among the links
on the perpendicular plane to z_2, z_3, z_4 axes

Here , the postion of ankle origin (o_5) can be obtained from the inverse matrix of ${}^{5}_{6}H\,{}^{6}_{F}H$. If we multiply the inverse matrix with Equation 2.10, we can obtain Equation 2.11 and the translation vector of the right hand side $\{P_x + l_6 r_{13}, P_y + l_6 r_{23}, P_z + l_6 r_{33}\}$ gives the position of the ankle origin.

$$
{}^{0}_{5}H = {}^{0}_{1}H\,{}^{1}_{2}H\,{}^{2}_{3}H\,{}^{3}_{4}H\,{}^{4}_{5}H = P\left({}^{5}_{6}H\,{}^{6}_{F}H\right)^{-1} = \begin{bmatrix} r_{11} & r_{12} & r_{13} & P_x \\ r_{21} & r_{22} & r_{23} & P_y \\ r_{31} & r_{32} & r_{33} & P_z \\ 0 & 0 & 0 & 1 \end{bmatrix} \left({}^{5}_{6}H\,{}^{6}_{F}H\right)^{-1} \qquad \text{(Eq. 2.11)}
$$

$$
= \begin{bmatrix} * & * & * & P_x + l_6 r_{13} \\ * & * & * & P_y + l_6 r_{23} \\ * & * & * & P_z + l_6 r_{33} \\ 0 & 0 & 0 & 1 \end{bmatrix}
$$

Then, the distance from the hip origin to the ankle origin can be calculated with Equation 2.12.

$$
l_{05} = \sqrt{\left(P_x + l_6 r_{13}\right)^2 + \left(P_y + l_6 r_{23}\right)^2 + \left(P_z + l_6 r_{33}\right)^2} \qquad \text{(Eq. 2.12)}
$$

Now, the knee angle (θ_4) can be calculated from the law of cosines using Equation 2.13, with known values for the link lengths (l_3, l_4) and the distance (l_{05} .)

$$
\theta_4 = \cos^{-1}\left(\frac{{l_{05}}^2 - {l_3}^2 - {l_4}^2}{2 l_3 l_4}\right) \qquad \text{(Eq. 2.13)}
$$

If we consider the plane perpendicular to the z_5 axis, we can draw Figure 2.3 Also, if we inverse the P matrix as shown in Equation 2.14, we can find the vector $\{P^{-1}(2,4), P^{-1}(3,4)\}$ which is the vector going from the foot position to the origin.

$$
P^{-1} = \begin{bmatrix} * & * & * & * \\ * & * & * & \dfrac{P_x\left(r_{21}r_{33} - r_{23}r_{31}\right) - P_y\left(r_{11}r_{33} - r_{13}r_{31}\right) + P_z\left(r_{11}r_{23} - r_{13}r_{21}\right)}{r_{11}r_{22}r_{33} - r_{11}r_{23}r_{32} - r_{12}r_{21}r_{33} + r_{12}r_{23}r_{31} + r_{13}r_{21}r_{32} - r_{13}r_{22}r_{31}} \\ * & * & * & \dfrac{-P_x\left(r_{21}r_{31} - r_{22}r_{31}\right) - P_y\left(r_{11}r_{32} - r_{12}r_{31}\right) + P_z\left(r_{11}r_{22} - r_{12}r_{21}\right)}{r_{11}r_{22}r_{33} - r_{11}r_{23}r_{32} - r_{12}r_{21}r_{33} + r_{12}r_{23}r_{31} + r_{13}r_{21}r_{32} - r_{13}r_{22}r_{31}} \\ 0 & 0 & 0 & 1 \end{bmatrix} \qquad \text{(Eq. 2.14)}
$$

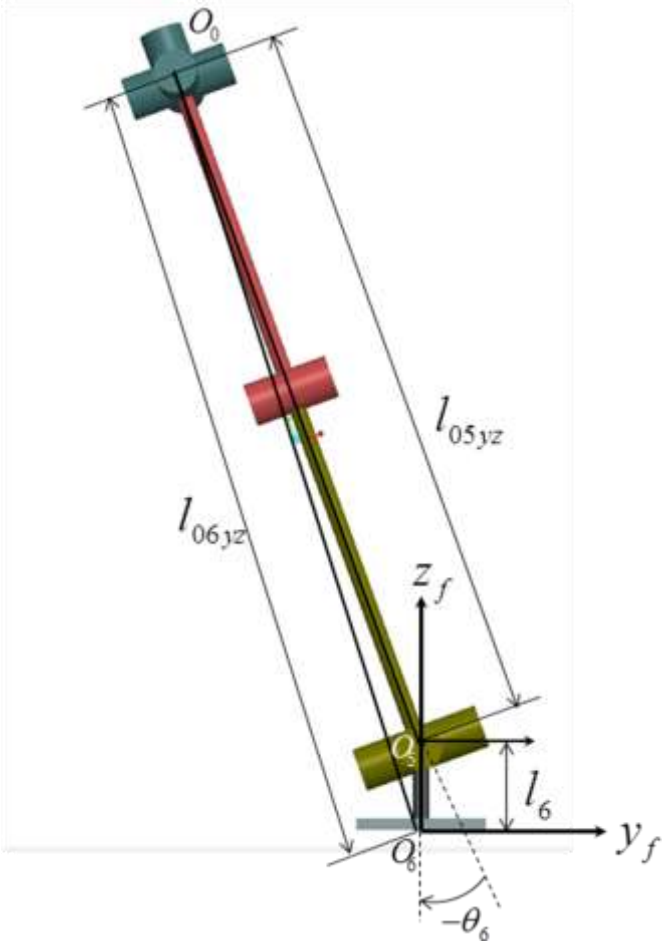

Figure 2.3 Geometical relationship among the links
on the perpendicular plane to z_5 axis

From the geometry in Figure 2.3, the distance l_{06yz} and l_{05yz} can be calculated using Equation 2.15 and 2.16

$$l_{06yz} = \sqrt{\left\{P^{-1}(2,4)\right\}^2 + \left\{P^{-1}(3,4)\right\}^2} \qquad \text{(Eq. 2.15)}$$

$$l_{05yz} = \sqrt{\left\{P^{-1}(2,4)\right\}^2 + \left\{P^{-1}(3,4) - l_6\right\}^2} \qquad \text{(Eq. 2.16)}$$

The ankle roll angle can be calculated by the law of cosine based on the length l_6 and the distances l_{06yz}, l_{05yz}.

$$\theta_6 = sign(P^{-1}(2,4))\cos^{-1}\left(\frac{{l_{06yz}}^2 - {l_{05yz}}^2 - {l_6}^2}{2 l_{05yz} l_6}\right) \qquad \text{(Eq. 2.17)}$$

These geometrical solutions help simplify the inverse kinematics. If we inverse ${}^{4}_{5}H\,{}^{5}_{6}H\,{}^{6}_{F}H$ and multiply it with Equation 2.10, we can get Equation 2.18, 2.19 and 2.20.

$$ {}^{0}_{1}H\,{}^{1}_{2}H\,{}^{2}_{3}H\,{}^{3}_{4}H = P\left({}^{4}_{5}H\,{}^{5}_{6}H\,{}^{6}_{F}H\right)^{-1} \qquad \text{(Eq. 2.18)} $$

$$ RHS = \begin{bmatrix} * & * & r_{12}\cos\theta_6 - r_{13}\sin\theta_6 & * \\ * & * & r_{22}\cos\theta_6 - r_{23}\sin\theta_6 & * \\ * & * & r_{32}\cos\theta_6 - r_{33}\sin\theta_6 & * \\ 0 & 0 & 0 & 1 \end{bmatrix} \qquad \text{(Eq. 2.19)} $$

$$ LHS = \begin{bmatrix} * & * & -\sin\theta_1\cos\theta_2 & * \\ * & * & \cos\theta_1\cos\theta_2 & * \\ * & * & \sin\theta_2 & * \\ 0 & 0 & 0 & 1 \end{bmatrix} \qquad \text{(Eq. 2.20)} $$

From the element (3, 3), we can obtain the solution of the hip roll angle.

$$ \theta_2 = \sin^{-1}\left(r_{32}\cos\theta_6 - r_{33}\sin\theta_6\right) \qquad \text{(Eq. 2.21)} $$

Also the element (1, 3) and (2, 3), the hip yaw angle can be calculated with Equation 2.22.

$$ \theta_1 = a\tan 2\left(\frac{r_{12}\cos\theta_6 - r_{13}\sin\theta_6}{-\cos\theta_2}, \frac{r_{22}\cos\theta_6 - r_{23}\sin\theta_6}{\cos\theta_2}\right) \qquad \text{(Eq. 2.22)} $$

Now, If we inverse ${}^{0}_{1}H\,{}^{1}_{2}H, {}^{5}_{6}H\,{}^{6}_{F}H$ and multiply them with Equation 2.10, we can get Equation 2.23, 2.24 and 2.25.

$$ {}^{2}_{3}H\,{}^{3}_{4}H\,{}^{4}_{5}H = \left({}^{0}_{1}H\,{}^{1}_{2}H\right)^{-1} P\left({}^{5}_{6}H\,{}^{6}_{F}H\right)^{-1} \qquad \text{(Eq. 2.23)} $$

$$ RHS = \begin{bmatrix} * & * & * & -P_x\sin\theta_1\sin\theta_2 + P_y\cos\theta_1\sin\theta_2 - P_z\cos\theta_2 - l_6\left(r_{13}\sin\theta_1\sin\theta_2 - r_{23}\cos\theta_1\sin\theta_2 + r_{33}\cos\theta_2\right) \\ * & * & * & -P_x\cos\theta_1 - P_y\sin\theta_1 - l_6\left(r_{13}\cos\theta_1 + r_{23}\sin\theta_1\right) \\ * & * & * & * \\ 0 & 0 & 0 & 1 \end{bmatrix} \qquad \text{(Eq. 2.24)} $$

$$ LHS = \begin{bmatrix} * & * & * & \left(l_3 + l_4\cos\theta_4\right)\cos\theta_3 - l_4\sin\theta_4\sin\theta_3 \\ * & * & * & l_4\sin\theta_4\cos\theta_3 + \left(l_3 + l_4\cos\theta_4\right)\sin\theta_3 \\ * & * & * & * \\ 0 & 0 & 0 & 1 \end{bmatrix} \qquad \text{(Eq. 2.25)} $$

Let α and β represent elements (1, 4) and (2, 4), respectively, of the right hand side,

$$\alpha = -P_x \sin\theta_1 \sin\theta_2 + P_y \cos\theta_1 \sin\theta_2 - P_z \cos\theta_2 - l_6\left(r_{13}\sin\theta_1 \sin\theta_2 - r_{23}\cos\theta_1 \sin\theta_2 + r_{33}\cos\theta_2\right)$$
$$\beta = -P_x \cos\theta_1 - P_y \sin\theta_1 - l_6\left(r_{13}\cos\theta_1 + r_{23}\sin\theta_1\right) \quad \text{(Eq. 2.26)}$$

We then have two simultaneous Equations 2.27.

$$\left(l_3 + l_4\cos\theta_4\right)\cos\theta_3 - l_4 \sin\theta_4 \sin\theta_3 = \alpha$$
$$l_4 \sin\theta_4 \cos\theta_3 + \left(l_3 + l_4\cos\theta_4\right)\sin\theta_3 = \beta \quad \text{(Eq. 2.27)}$$

Solving for θ_3, the sine and cosine values are,

$$\sin\theta_3 = \frac{-l_4 \sin\theta_4 \cdot \alpha + \left(l_3 + l_4\cos\theta_4\right)\beta}{{l_3}^2 + {l_4}^2 + 2l_3 l_4 \cos\theta_4}$$
$$\cos\theta_3 = \frac{\left(l_3 + l_4\cos\theta_4\right)\alpha + l_4 \sin\theta_4 \cdot \beta}{{l_3}^2 + {l_4}^2 + 2l_3 l_4 \cos\theta_4} \quad \text{(Eq. 2.28)}$$

Here, the denominator can be given as l_{05}

$${l_3}^2 + {l_4}^2 + 2l_3 l_4 \cos\theta_4 = {l_{05}}^2 \geq 0 \quad \text{(Eq. 2.29)}$$

Thus, the hip roll angle is,

$$\theta_3 = a\tan 2\left(-l_4 \sin\theta_4 \cdot \alpha + \left(l_3 + l_4\cos\theta_4\right)\beta\ ,\ \left(l_3 + l_4\cos\theta_4\right)\alpha + l_4 \sin\theta_4 \cdot \beta\right) \quad \text{(Eq. 2.30)}$$

Again, from Equation 2.24, 2.25, if we compare elements (1, 3) and (2, 3) and define θ_{pitch} as shown in Equation 2.31, 2.32 and 2.33.

$$RHS = \begin{bmatrix} * & * & -r_{11}\sin\theta_1 \sin\theta_2 + r_{21}\cos\theta_1 \sin\theta_2 - r_{31}\cos\theta_2 & * \\ * & * & -r_{11}\cos\theta_1 - r_{21}\sin\theta_1 & * \\ * & * & * & * \\ 0 & 0 & 0 & 1 \end{bmatrix} \quad \text{(Eq. 2.31)}$$

$$LHS = \begin{bmatrix} * & * & \sin\left(\theta_3 + \theta_4 + \theta_5\right) & * \\ * & * & -\cos\left(\theta_3 + \theta_4 + \theta_5\right) & * \\ * & * & * & * \\ 0 & 0 & 0 & 1 \end{bmatrix} \quad \text{(Eq. 2.32)}$$

$$\theta_{pitch} = \theta_3 + \theta_4 + \theta_5 \quad \text{(Eq. 2.33)}$$

The sum of $\theta_3, \theta_4, \theta_5$ is,

$$\theta_{pitch} = a\tan 2\left(-r_{11}\sin\theta_1\sin\theta_2 + r_{21}\cos\theta_1\sin\theta_2 - r_{31}\cos\theta_2,\ r_{11}\cos\theta_1 + r_{21}\sin\theta_1\right) \quad \text{(Eq. 2.34)}$$

Then, the ankle pitch angle can be obtained,

$$\theta_5 = \theta_{pitch} - \theta_3 - \theta_4 \quad \text{(Eq. 2.35)}$$

In summary, for given values of $P = \begin{bmatrix} r_{11} & r_{12} & r_{13} & P_x \\ r_{21} & r_{22} & r_{23} & P_y \\ r_{31} & r_{32} & r_{33} & P_z \\ 0 & 0 & 0 & 1 \end{bmatrix}$ and l_3, l_4, l_6

$$\theta_6 = sign(P^{-1}(2,4))\cos^{-1}\left(\frac{l_{06yz}{}^2 - l_{05yz}{}^2 - l_6{}^2}{2l_{05yz}l_6}\right) \quad \text{(Eq. 2.17)}$$

$$l_{06yz} = \sqrt{\left\{P^{-1}(2,4)\right\}^2 + \left\{P^{-1}(3,4)\right\}^2}, \quad l_{05yz} = \sqrt{\left\{P^{-1}(2,4)\right\}^2 + \left\{P^{-1}(3,4) - l_6\right\}^2}$$

$$P^{-1}(2,4) = \frac{P_x\left(r_{21}r_{33} - r_{23}r_{31}\right) - P_y\left(r_{11}r_{33} - r_{13}r_{31}\right) + P_z\left(r_{11}r_{23} - r_{13}r_{21}\right)}{r_{11}r_{22}r_{33} - r_{11}r_{23}r_{32} - r_{12}r_{21}r_{33} + r_{12}r_{23}r_{31} + r_{13}r_{21}r_{32} - r_{13}r_{22}r_{31}}$$

$$P^{-1}(3,4) = \frac{-P_x\left(r_{21}r_{31} - r_{22}r_{31}\right) - P_y\left(r_{11}r_{32} - r_{12}r_{31}\right) + P_z\left(r_{11}r_{22} - r_{12}r_{21}\right)}{r_{11}r_{22}r_{33} - r_{11}r_{23}r_{32} - r_{12}r_{21}r_{33} + r_{12}r_{23}r_{31} + r_{13}r_{21}r_{32} - r_{13}r_{22}r_{31}}$$

$$\theta_2 = \sin^{-1}\left(r_{32}\cos\theta_6 - r_{33}\sin\theta_6\right) \quad \text{(Eq. 2.21)}$$

$$\theta_1 = a\tan 2\left(\frac{r_{12}\cos\theta_6 - r_{13}\sin\theta_6}{-\cos\theta_2}, \frac{r_{22}\cos\theta_6 - r_{23}\sin\theta_6}{\cos\theta_2}\right) \quad \text{(Eq. 2.22)}$$

$$\theta_4 = \cos^{-1}\left(\frac{l_{05}{}^2 - l_3{}^2 - l_4{}^2}{2l_3l_4}\right) \quad \text{(Eq. 2.13)}$$

$$l_{05} = \sqrt{\left(P_x + l_6r_{13}\right)^2 + \left(P_y + l_6r_{23}\right)^2 + \left(P_z + l_6r_{33}\right)^2}$$

$$\theta_3 = a\tan 2\left(-l_4\sin\theta_4\cdot\alpha + \left(l_3 + l_4\cos\theta_4\right)\beta\ ,\ \left(l_3 + l_4\cos\theta_4\right)\alpha + l_4\sin\theta_4\cdot\beta\right) \quad \text{(Eq. 2.30)}$$

$$\alpha = -P_x\sin\theta_1\sin\theta_2 + P_y\cos\theta_1\sin\theta_2 - P_z\cos\theta_2 - l_6\left(r_{13}\sin\theta_1\sin\theta_2 - r_{23}\cos\theta_1\sin\theta_2 + r_{33}\cos\theta_2\right)$$

$$\beta = -P_x\cos\theta_1 - P_y\sin\theta_1 - l_6\left(r_{13}\cos\theta_1 + r_{23}\sin\theta_1\right)$$

$$\theta_5 = \theta_{pitch} - \theta_3 - \theta_4 \quad \text{(Eq. 2.35)}$$

$$\theta_{pitch} = a\tan 2\left(-r_{11}\sin\theta_1\sin\theta_2 + r_{21}\cos\theta_1\sin\theta_2 - r_{31}\cos\theta_2,\ r_{11}\cos\theta_1 + r_{21}\sin\theta_1\right)$$

Section 3 Dynamics

The second step in developing bipedal walking in humanoid robot is defining the dynamics. In this section, Jaconbian matrixes and Euler-Lagrange equations of CHARLI-2's leg will be introduced to determine its dynamic characteristics such as velocity, acceleration and torque. These performances will be the basec information not only for the design of a full-sized humanoid robot but also for the estimation of its energy consumption.

3.1 Jacobian Matrixes

In estimating the bipedal robot's walking status, Jacobian matrixes are the basic elements in building a dynamic model. Jacobian matrixes are divided by actuation types, linear or revolution, based on whether the motions are rectilinear or rotary. In the case of CHARLI, all joints are revolute, so the general form of the matrix can be written as,

$$J_i = \begin{bmatrix} J_{vi} \\ J_{\omega i} \end{bmatrix} = \begin{bmatrix} z_{i-1} \times (o_n - o_{i-1}) \\ z_{i-1} \end{bmatrix} \qquad \text{(Eq. 3.1)}$$

Also, if the masses are considered as three concentrated material point such as thigh, shin and foot, we can define the dynamic system as like Figure 3.1.

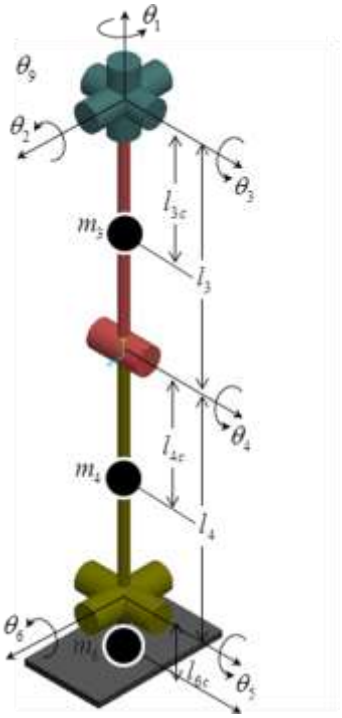

Figure 3.1 The definition of masses and joints for the dynamic model of CHARLI-2's leg

Each mass needs a Jacobian matrix; J_3, J_4, J_6 means the Jacobian matrix of thigh, shin and foot respectively. If we separate this Jacobian matrix into rectilinear and rotary elements, the Jacobian matrix can be written as shown below.

$$J_{v3} = \begin{bmatrix} z_0 \times (o_{3C} - o_0) & z_1 \times (o_{3C} - o_1) & z_2 \times (o_{3C} - o_2) & 0 & 0 & 0 \end{bmatrix} \quad \text{(Eq. 3.1)}$$
$$J_{\omega 3} = \begin{bmatrix} z_0 & z_1 & z_2 & 0 & 0 & 0 \end{bmatrix}$$

$$J_{v4} = \begin{bmatrix} z_0 \times (o_{4C} - o_0) & z_1 \times (o_{4C} - o_1) & z_2 \times (o_{4C} - o_2) & z_3 \times (o_{4C} - o_3) & 0 & 0 \end{bmatrix} \quad \text{(Eq. 3.2)}$$
$$J_{\omega 4} = \begin{bmatrix} z_0 & z_1 & z_2 & z_3 & 0 & 0 \end{bmatrix}$$

$$J_{v6} = \begin{bmatrix} z_0 \times (o_{6C} - o_0) & z_1 \times (o_{6C} - o_1) & z_2 \times (o_{6C} - o_2) & z_3 \times (o_{6C} - o_3) & z_4 \times (o_{6C} - o_4) & z_5 \times (o_{6C} - o_5) \end{bmatrix}$$
$$J_{\omega 6} = \begin{bmatrix} z_0 & z_1 & z_2 & z_3 & z_4 & z_5 \end{bmatrix} \quad \text{(Eq. 3.3)}$$

where,

$$z_0 = \begin{bmatrix} 0 & 0 & 1 \end{bmatrix}^T$$

$$z_1 = \begin{bmatrix} H_1^0(1,3) \\ H_1^0(2,3) \\ H_1^0(3,3) \end{bmatrix} = \begin{bmatrix} \cos\theta_1 \\ \sin\theta_1 \\ 0 \end{bmatrix}$$

$$z_2 = \begin{bmatrix} H_2^0(1,3) \\ H_2^0(2,3) \\ H_2^0(3,3) \end{bmatrix} = \begin{bmatrix} -\sin\theta_1 \cos\theta_2 \\ \cos\theta_1 \cos\theta_2 \\ \sin\theta_2 \end{bmatrix}$$

$$z_3 = \begin{bmatrix} H_3^0(1,3) \\ H_3^0(2,3) \\ H_3^0(3,3) \end{bmatrix} = \begin{bmatrix} -\sin\theta_1 \cos\theta_2 \\ \cos\theta_1 \cos\theta_2 \\ \sin\theta_2 \end{bmatrix}$$

$$z_4 = \begin{bmatrix} H_4^0(1,3) \\ H_4^0(2,3) \\ H_4^0(3,3) \end{bmatrix} = \begin{bmatrix} -\sin\theta_1 \cos\theta_2 \\ \cos\theta_1 \cos\theta_2 \\ \sin\theta_2 \end{bmatrix}$$

$$z_5 = \begin{bmatrix} H_5^0(1,3) \\ H_5^0(2,3) \\ H_5^0(3,3) \end{bmatrix} = \begin{bmatrix} \cos\theta_1 \cos\theta_{345} - \sin\theta_1 \sin\theta_2 \sin\theta_{345} \\ \sin\theta_1 \cos\theta_{345} + \cos\theta_1 \sin\theta_2 \sin\theta_{345} \\ -\cos\theta_2 \sin\theta_{345} \end{bmatrix}$$

$$o_0 = \begin{bmatrix} 0 & 0 & 0 \end{bmatrix}^T$$

$$o_1 = \begin{bmatrix} H_1^0(1,4) & H_1^0(2,4) & H_1^0(3,4) \end{bmatrix}^T = \begin{bmatrix} 0 & 0 & 0 \end{bmatrix}^T$$

$$o_2 = \begin{bmatrix} H_2^0(1,4) & H_2^0(2,4) & H_2^0(3,4) \end{bmatrix}^T = \begin{bmatrix} 0 & 0 & 0 \end{bmatrix}^T$$

$$o_3 = \begin{bmatrix} H_3^0(1,4) \\ H_3^0(2,4) \\ H_3^0(3,4) \end{bmatrix} = \begin{bmatrix} -l_3 \cos\theta_1 \sin\theta_3 - l_3 \sin\theta_1 \sin\theta_2 \cos\theta_3 \\ -l_3 \sin\theta_1 \sin\theta_3 + l_3 \cos\theta_1 \sin\theta_2 \cos\theta_3 \\ -l_3 \cos\theta_2 \cos\theta_3 \end{bmatrix}$$

$$o_4 = \begin{bmatrix} H_4^0(1,4) \\ H_4^0(2,4) \\ H_4^0(3,4) \end{bmatrix} = \begin{bmatrix} -\cos\theta_1 \left(l_3 \sin\theta_3 + l_4 \sin\theta_{34} \right) - \sin\theta_1 \sin\theta_2 \left(l_3 \cos\theta_3 + l_4 \cos\theta_{34} \right) \\ -\sin\theta_1 \left(l_3 \sin\theta_3 + l_4 \sin\theta_{34} \right) + \cos\theta_1 \sin\theta_2 \left(l_3 \cos\theta_3 + l_4 \cos\theta_{34} \right) \\ -\cos\theta_2 \left(l_3 \cos\theta_3 + l_4 \cos\theta_{34} \right) \end{bmatrix}$$

$$o_5 = \begin{bmatrix} H_5^0(1,4) \\ H_5^0(2,4) \\ H_5^0(3,4) \end{bmatrix} = \begin{bmatrix} -\cos\theta_1 \left(l_3 \sin\theta_3 + l_4 \sin\theta_{34} \right) - \sin\theta_1 \sin\theta_2 \left(l_3 \cos\theta_3 + l_4 \cos\theta_{34} \right) \\ -\sin\theta_1 \left(l_3 \sin\theta_3 + l_4 \sin\theta_{34} \right) + \cos\theta_1 \sin\theta_2 \left(l_3 \cos\theta_3 + l_4 \cos\theta_{34} \right) \\ -\cos\theta_2 \left(l_3 \cos\theta_3 + l_4 \cos\theta_{34} \right) \end{bmatrix}$$

$$o_{3C} = \begin{bmatrix} H_3^0(1,4) \\ H_3^0(2,4) \\ H_3^0(3,4) \end{bmatrix} = \begin{bmatrix} -l_{3C} \cos\theta_1 \sin\theta_3 - l_{3C} \sin\theta_1 \sin\theta_2 \cos\theta_3 \\ -l_{3C} \sin\theta_1 \sin\theta_3 + l_{3C} \cos\theta_1 \sin\theta_2 \cos\theta_3 \\ -l_{3C} \cos\theta_2 \cos\theta_3 \end{bmatrix}$$

$$o_{4C} = \begin{bmatrix} H_4^0(1,4) \\ H_4^0(2,4) \\ H_4^0(3,4) \end{bmatrix} = \begin{bmatrix} -\cos\theta_1 \left(l_3 \sin\theta_3 + l_{4C} \sin\theta_{34} \right) - \sin\theta_1 \sin\theta_2 \left(l_3 \cos\theta_3 + l_{4C} \cos\theta_{34} \right) \\ -\sin\theta_1 \left(l_3 \sin\theta_3 + l_{4C} \sin\theta_{34} \right) + \cos\theta_1 \sin\theta_2 \left(l_3 \cos\theta_3 + l_{4C} \cos\theta_{34} \right) \\ -\cos\theta_2 \left(l_3 \cos\theta_3 + l_{4C} \cos\theta_{34} \right) \end{bmatrix}$$

$$o_{6C} = \begin{bmatrix} H_6^0(1,4) \\ H_6^0(2,4) \\ H_6^0(3,4) \end{bmatrix} = \begin{bmatrix} -\cos\theta_1 \left(l_3 \sin\theta_3 + l_4 \sin\theta_{34} \right) - \sin\theta_1 \sin\theta_2 \left(l_3 \cos\theta_3 + l_4 \cos\theta_{34} \right) \\ +l_{6C} \left\{ \sin\theta_1 \cos\theta_2 \sin\theta_6 - \cos\theta_6 \left(\cos\theta_1 \sin\theta_{345} + \sin\theta_1 \sin\theta_2 \cos\theta_{345} \right) \right\} \\ \\ -\sin\theta_1 \left(l_3 \sin\theta_3 + l_4 \sin\theta_{34} \right) + \cos\theta_1 \sin\theta_2 \left(l_3 \cos\theta_3 + l_4 \cos\theta_{34} \right) \\ +l_{6C} \left\{ \cos\theta_1 \cos\theta_2 \sin\theta_6 - \cos\theta_6 \left(\sin\theta_1 \sin\theta_{345} - \cos\theta_1 \sin\theta_2 \cos\theta_{345} \right) \right\} \\ \\ -\cos\theta_2 \left(l_3 \cos\theta_3 + l_4 \cos\theta_{34} \right) + l_{6C} \left(\sin\theta_2 \sin\theta_6 - \cos\theta_2 \cos\theta_6 \cos\theta_{345} \right) \end{bmatrix}$$

3.2 Euler-Lagrange Equation

The final goal of the dynamics is to obtain the equations of motion of the system. In the case of CHARLI's leg, it is not easy to derive the equations of motion, because it is a multi degree of freedom system consisted of 6 joints and 3 masses. However, the equations of motion of a multi DOF system can be readily derived by energy methods. Euler-Lagrange equations are the equations of motion obtained by energy methods.

If we represent the variable of the system as generalized coordinates, then we can write the equations of motion for an n-DOF system utilizing Euler-Lagrange equation as,

$$\frac{d}{dt}\frac{\partial L}{\partial \dot{q}_i} - \frac{\partial L}{\partial q_i} = \tau_i \qquad \text{(Eq. 3.4)}$$

$$L = K - P \qquad \text{(Eq. 3.5)}$$

Where, L is Lagrangian, K is kinetic energy and P is potential energy.
The kinetic energy of a rigid body is the sum of two terms;

$$K = \frac{1}{2} m v^T v + \frac{1}{2} \omega^T \mathrm{I} \omega \qquad \text{(Eq. 3.6)}$$

The inertia tensor, I, should be transferred into the global coordinate, so equation 3.6 should be multiplied by rotational transfer matrix R.

$$K = \frac{1}{2} m v^T v + \frac{1}{2} \omega^T R I R^T \omega \qquad \text{(Eq. 3.7)}$$

The total kinetic energy is the sum of each link's.

$$K = \sum_{i=1}^{n} \left\{ \frac{1}{2} m_i v_i^T v_i + \frac{1}{2} \omega_i^T R_i I_i R_i^T \omega_i \right\} \qquad \text{(Eq. 3.8)}$$

If we apply the Jacobian matrix, the kinetic energy can be written as the function of the joint variables like Equation 3.9.

$$K = \frac{1}{2} \dot{q}^T \left[\sum_{i=1}^{n} \left\{ m_i J_{vi}(q)^T J_{vi}(q) + J_{\omega i}(q)^T R_i(q) I_i R(q)^T J_{\omega i}(q) \right\} \right] \dot{q} \qquad \text{(Eq. 3.9)}$$

In the case of CHARLI's leg, it has 3 masses, so we finally have the kinetic energy in Equation 3.10.

$$K = \frac{1}{2}\dot{q}^T \begin{Bmatrix} m_3 J_{v3}(q)^T J_{v3}(q) + m_4 J_{v4}(q)^T J_{v4}(q) + m_6 J_{v6}(q)^T J_{v6}(q) \\ + J_{\omega 3}(q)^T R_3(q) I_3 R_3(q)^T J_{\omega 3}(q) + J_{\omega 4}(q)^T R_4(q) I_4 R_4(q)^T J_{\omega 4}(q) \\ + J_{\omega 6}(q)^T R_6(q) I_6 R_6(q)^T J_{\omega 6}(q) \end{Bmatrix} \dot{q} \qquad \text{(Eq. 3.10)}$$

Then, if we define the inertia matrix $D(q)$ as in Equation 3.11,

$$\begin{aligned} D(q) = {} & m_3 J_{v3}(q)^T J_{v3}(q) + m_4 J_{v4}(q)^T J_{v4}(q) + m_6 J_{v6}(q)^T J_{v6}(q) \\ & + J_{\omega 3}(q)^T R_3(q) I_3 R_3(q)^T J_{\omega 3}(q) + J_{\omega 4}(q)^T R_4(q) I_4 R_4(q)^T J_{\omega 4}(q) \\ & + J_{\omega 6}(q)^T R_6(q) I_6 R_6(q)^T J_{\omega 6}(q) \end{aligned} \qquad \text{(Eq. 3.11)}$$

The kinetic energy can be simplified as,

$$K = \frac{1}{2}\dot{q}^T D(q)\dot{q} = \frac{1}{2}\sum_{j=1}^{n}\sum_{i=1}^{n} d_{ij}(q)\dot{q}_i\dot{q}_j \qquad \text{(Eq. 3.12)}$$

Where, $D(q)$ is 6 by 6 symmetric matrix. Equation 3.13 shows its elements.

$$D(q) = \begin{bmatrix} d_{11}(q) & d_{12}(q) & d_{13}(q) & d_{14}(q) & d_{15}(q) & d_{16}(q) \\ * & d_{22}(q) & d_{23}(q) & d_{24}(q) & d_{25}(q) & d_{26}(q) \\ * & * & d_{33}(q) & d_{34}(q) & d_{35}(q) & d_{36}(q) \\ * & * & * & d_{44}(q) & d_{45}(q) & d_{46}(q) \\ * & * & * & * & d_{55}(q) & d_{56}(q) \\ * & * & * & * & * & d_{66}(q) \end{bmatrix} \qquad \text{(Eq. 3.13)}$$

Also, Potential Energy of the leg is,

$$P = mgh = \sum_{i=1}^{n} m_i g h_{ci}(q) \qquad \text{(Eq. 3.14)}$$

Therefore, the Lagrangian L is shown as the function of the joint variables like Equation 3.15,

$$L = K - P = \frac{1}{2}\dot{q}^T D(q)\dot{q} - P(q) = \frac{1}{2}\sum_{j=1}^{n}\sum_{i=1}^{n} d_{ij}(q)\dot{q}_i\dot{q}_j - \sum_{i=1}^{n} m_i g h_{ci}(q) \qquad \text{(Eq. 3.15)}$$

The partial derivatives of the Lagrangian with respect to the velocity is,

$$\frac{\partial L}{\partial \dot{q}_k} = \frac{\partial}{\partial \dot{q}_k}\left(\frac{1}{2}\sum_{j=1}^{n}\sum_{i=1}^{n} d_{ij}(q)\dot{q}_i\dot{q}_j\right) - \frac{\partial}{\partial \dot{q}_k}P(q) = \sum_{j=1}^{n} d_{kj}(q)\dot{q}_j \qquad \text{(Eq. 3.16)}$$

The differentiation of Equation 3.16 is,

$$\frac{d}{dt}\frac{\partial L}{\partial \dot{q}_k} = \sum_{j=1}^{n} d_{kj}\ddot{q}_j + \sum_{j=1}^{n}\frac{d}{dt}d_{kj}\dot{q}_j = \sum_{j=1}^{n} d_{kj}\ddot{q}_j + \sum_{j=1}^{n}\sum_{i=1}^{n}\frac{\partial d_{kj}}{\partial q_i}\dot{q}_i\dot{q}_j \qquad \text{(Eq. 3.17)}$$

Additionally, the partial derivatives of the Lagrangian with respect to the position is,

$$\frac{\partial L}{\partial q_k} = \frac{1}{2}\sum_{j=1}^{n}\sum_{i=1}^{n}\frac{\partial d_{ij}}{\partial q_k}\dot{q}_i\dot{q}_j - \frac{\partial P}{\partial q_k} \qquad \text{(Eq. 3.18)}$$

Therefore, the Euler-Lagrange equation can be obtained by the subtraction of Equation 3.18 from Equation 3.17.

$$\sum_{j=1}^{n} d_{kj}\ddot{q}_j + \sum_{j=1}^{n}\sum_{i=1}^{n}\left\{\frac{\partial d_{kj}}{\partial q_i} - \frac{1}{2}\frac{\partial d_{ij}}{\partial q_k}\right\}\dot{q}_i\dot{q}_j + \frac{\partial P}{\partial q_k} = \tau_k \qquad \text{(Eq. 3.19)}$$

If we define the Christoffel symbols C_{ijk} and gravity force $g_k(q)$ as in Equation 3.20 and 3.21.

$$C_{ijk} \equiv \frac{1}{2}\left(\frac{\partial d_{kj}}{\partial q_i} + \frac{\partial d_{ki}}{\partial q_j} - \frac{\partial d_{ij}}{\partial q_k}\right) \qquad \text{(Eq. 3.20)}$$

$$g_k(q) \equiv \frac{\partial P(q)}{\partial q_k} \qquad \text{(Eq. 3.21)}$$

The equations of motion can be shown as in Equation 3.22.

$$\sum_{j=1}^{6} d_{kj}(q)\ddot{q}_j + \sum_{j=1}^{6}\sum_{i=1}^{6} c_{ijk}(q)\dot{q}_i\dot{q}_j + g_k(q) = \tau_k \qquad \text{(Eq. 3.22)}$$

Where, the second term of Equation 3.22, $\sum_{j=1}^{6}\sum_{i=1}^{6} c_{ijk}(q)\dot{q}_i\dot{q}_j$, has two meanings.
When $i = j$, this term means centrifugal force. When $i \neq j$, this term means Coriolis effect. If we disregard the Coriolis effect, because the product of inertia is much smaller than moment of inertia, as will be discussed again in Chapter 5, the equations of motion can be finally written as Equation 3.23.

$$\tau_1 = d_{11}\ddot{\theta}_1 + d_{12}\ddot{\theta}_2 + d_{13}\ddot{\theta}_3 + d_{14}\ddot{\theta}_4 + d_{15}\ddot{\theta}_5 + d_{16}\ddot{\theta}_6 + c_{111}\dot{\theta}_1^2 + c_{221}\dot{\theta}_2^2 + c_{331}\dot{\theta}_3^2 + c_{441}\dot{\theta}_4^2 + c_{551}\dot{\theta}_5^2 + c_{661}\dot{\theta}_6^2 + g_1$$
$$\tau_2 = d_{21}\ddot{\theta}_1 + d_{22}\ddot{\theta}_2 + d_{23}\ddot{\theta}_3 + d_{24}\ddot{\theta}_4 + d_{25}\ddot{\theta}_5 + d_{26}\ddot{\theta}_6 + c_{112}\dot{\theta}_1^2 + c_{222}\dot{\theta}_2^2 + c_{332}\dot{\theta}_3^2 + c_{442}\dot{\theta}_4^2 + c_{552}\dot{\theta}_5^2 + c_{662}\dot{\theta}_6^2 + g_2$$
$$\tau_3 = d_{31}\ddot{\theta}_1 + d_{32}\ddot{\theta}_2 + d_{33}\ddot{\theta}_3 + d_{34}\ddot{\theta}_4 + d_{35}\ddot{\theta}_5 + d_{36}\ddot{\theta}_6 + c_{113}\dot{\theta}_1^2 + c_{223}\dot{\theta}_2^2 + c_{333}\dot{\theta}_3^2 + c_{443}\dot{\theta}_4^2 + c_{553}\dot{\theta}_5^2 + c_{663}\dot{\theta}_6^2 + g_3$$
$$\tau_4 = d_{41}\ddot{\theta}_1 + d_{42}\ddot{\theta}_2 + d_{43}\ddot{\theta}_3 + d_{44}\ddot{\theta}_4 + d_{45}\ddot{\theta}_5 + d_{46}\ddot{\theta}_6 + c_{114}\dot{\theta}_1^2 + c_{224}\dot{\theta}_2^2 + c_{334}\dot{\theta}_3^2 + c_{444}\dot{\theta}_4^2 + c_{554}\dot{\theta}_5^2 + c_{664}\dot{\theta}_6^2 + g_4$$
$$\tau_5 = d_{51}\ddot{\theta}_1 + d_{52}\ddot{\theta}_2 + d_{53}\ddot{\theta}_3 + d_{54}\ddot{\theta}_4 + d_{55}\ddot{\theta}_5 + d_{56}\ddot{\theta}_6 + c_{115}\dot{\theta}_1^2 + c_{225}\dot{\theta}_2^2 + c_{335}\dot{\theta}_3^2 + c_{445}\dot{\theta}_4^2 + c_{555}\dot{\theta}_5^2 + c_{665}\dot{\theta}_6^2 + g_5$$
$$\tau_6 = d_{61}\ddot{\theta}_1 + d_{62}\ddot{\theta}_2 + d_{63}\ddot{\theta}_3 + d_{64}\ddot{\theta}_4 + d_{65}\ddot{\theta}_5 + d_{66}\ddot{\theta}_6 + c_{116}\dot{\theta}_1^2 + c_{226}\dot{\theta}_2^2 + c_{336}\dot{\theta}_3^2 + c_{446}\dot{\theta}_4^2 + c_{556}\dot{\theta}_5^2 + c_{666}\dot{\theta}_6^2 + g_6$$

(Eq. 3.23)

Where, each element of inertia matrix is,

$$
\begin{aligned}
d_{11} &= m_3 {l_{3C}}^2 \left(\sin^2\theta_3 + \sin^2\theta_2 \cos^2\theta_3\right) \\
&\quad + m_4 \left\{\left(l_3 \sin\theta_3 + l_{4C} \sin\theta_{34}\right)^2 + \sin^2\theta_2 \left(l_3 \cos\theta_3 + l_{4C} \cos\theta_{34}\right)^2\right\} \\
&\quad + m_6 \left[\left(l_3 \sin\theta_3 + l_4 \sin\theta_{34} + l_{6C} \sin\theta_{345} \cos\theta_6\right)^2 + \left\{\sin\theta_2 \left(l_3 \cos\theta_3 + l_4 \cos\theta_{34} - l_{6C} \cos\theta_{345} \cos\theta_6\right) + l_{6C} \cos\theta_2 \sin\theta_6\right\}^2\right] \\
&\quad + I_{3x} \cos^2\theta_2 \cos^2\theta_3 + I_{3y} \cos^2\theta_2 \sin^2\theta_3 + I_{3z} \sin^2\theta_2 \\
&\quad + I_{4x} \cos^2\theta_2 \cos^2\theta_{34} + I_{4y} \cos^2\theta_2 \sin^2\theta_{34} + I_{4z} \sin^2\theta_2 \\
&\quad + I_{6x} \left(\sin\theta_2 \sin\theta_6 - \cos\theta_2 \cos\theta_{345} \cos\theta_6\right)^2 + I_{6y} \left(\sin\theta_2 \cos\theta_6 + \cos\theta_2 \cos\theta_{345} \sin\theta_6\right)^2 + I_{6z} \cos^2\theta_2 \sin^2\theta_{345} \\
d_{12} &= -m_3 {l_{3C}}^2 \cos\theta_2 \cos\theta_3 \sin\theta_3 \\
&\quad - m_4 \cos\theta_2 \left(l_3^2 \cos\theta_3 \sin\theta_3 + {l_{4C}}^2 \cos\theta_{34} \sin\theta_{34} + l_3 l_{4C} \sin\left(2\theta_{34}\right)\right) \\
&\quad - m_6 \left(l_3 \sin\theta_3 + l_4 \sin\theta_{34} + l_{6C} \sin\theta_{345} \cos\theta_6\right)\left\{\cos\theta_2 \left(l_3 \cos\theta_3 + l_4 \cos\theta_{34}\right) - l_{6C} \left(\sin\theta_2 \sin\theta_6 + \cos\theta_2 \cos\theta_{345} \cos\theta_6\right)\right\} \\
&\quad + I_{3x} \cos\theta_2 \cos\theta_3 \sin\theta_3 - I_{3y} \cos\theta_2 \cos\theta_3 \sin\theta_3 \\
&\quad + I_{4x} \cos\theta_2 \cos\theta_{34} \sin\theta_{34} - I_{4y} \cos\theta_2 \cos\theta_{34} \sin\theta_{34} \\
&\quad - I_{6x} \left(\sin\theta_2 \sin\theta_{345} \cos\theta_6 \sin\theta_6 - \cos\theta_2 \cos\theta_{345} \sin\theta_{345} \cos^2\theta_6\right) \\
&\quad + I_{6y} \left(\sin\theta_2 \sin\theta_{345} \cos\theta_6 \sin\theta_6 + \cos\theta_2 \cos\theta_{345} \sin\theta_{345} \sin^2\theta_6\right) \\
&\quad - I_{6z} \cos\theta_2 \cos\theta_{345} \sin\theta_{345} \\
d_{13} &= m_3 {l_{3C}}^2 \sin\theta_2 \\
&\quad + m_4 \sin\theta_2 \left(l_3^2 + {l_{4C}}^2 + 2 l_3 l_{4C} \cos\theta_4\right) \\
&\quad + m_6 \begin{Bmatrix} l_3^2 \sin\theta_2 + l_4^2 \sin\theta_2 + {l_{6C}}^2 \left(\sin\theta_2 \cos^2\theta_6 + \cos\theta_2 \cos\theta_{345} \cos\theta_6 \sin\theta_6\right) \\ + l_3 l_4 \left(\sin 2\theta_{34} + \cos\theta_4\right) + l_3 l_{6C} \left(\cos\theta_2 \cos\theta_3 \sin\theta_6 + 2 \sin\theta_2 \cos\theta_{45} \cos\theta_6\right) \\ l_4 l_{6C} \left(\cos\theta_2 \cos\theta_{34} \sin\theta_6 + 2 \sin\theta_2 \cos\theta_5 \cos\theta_6\right) \end{Bmatrix} \\
&\quad + I_{3z} \left(\cos^2\theta_2 \sin\theta_2 + \sin^3\theta_2\right) + I_{4z} \left(\cos^2\theta_2 \sin\theta_2 + \sin^3\theta_2\right) \\
&\quad + I_{6x} \sin\theta_6 \left(\sin\theta_2 \sin\theta_6 - \cos\theta_2 \cos\theta_{345} \cos\theta_6\right) + I_{6y} \cos\theta_6 \left(\sin\theta_2 \cos\theta_6 + \cos\theta_2 \cos\theta_{345} \sin\theta_6\right) \\
d_{14} &= m_4 \left({l_{4C}}^2 \sin\theta_2 + l_3 l_{4C} \sin\theta_2 \cos\theta_4\right) \\
&\quad + m_6 \begin{Bmatrix} l_4^2 + {l_{6C}}^2 \left(\cos^2\theta_6 + \cos\theta_2 \sin\theta_6 \left(\cos\theta_2 \sin\theta_6 + 2 \sin\theta_2 \cos\theta_{345} \cos\theta_6\right)\right) \\ + l_3 l_4 \left(\sin\theta_3 \sin\theta_{34} + \sin^2\theta_2 \cos\theta_3 \cos\theta_{34}\right) \\ + l_3 l_{6C} \left(\cos\theta_2 \sin\theta_2 \cos\theta_3 \sin\theta_6 + \sin\theta_3 \sin\theta_{345} \cos\theta_6 + \sin^2\theta_2 \cos\theta_3 \cos\theta_{345} \cos\theta_6\right) \\ + 2 l_4 l_{6C} \left(\cos\theta_5 \cos\theta_6 + \cos\theta_2 \sin\theta_2 \cos\theta_{34} \sin\theta_6\right) \end{Bmatrix} \\
&\quad + I_{4z} \sin\theta_2 \\
&\quad + I_{6x} \sin\theta_6 \left(\sin\theta_2 \sin\theta_6 - \cos\theta_2 \cos\theta_{345} \cos\theta_6\right) + I_{6y} \cos\theta_6 \left(\sin\theta_2 \cos\theta_6 + \cos\theta_2 \cos\theta_{345} \sin\theta_6\right) \\
d_{15} &= m_6 l_{6C} \left(\sin\theta_2 \sin\theta_6 - \cos\theta_2 \cos\theta_{345} \cos\theta_6\right)\left(l_3 \sin\theta_3 + l_4 \sin\theta_{34} + l_{6C} \cos\theta_6 \sin\theta_{345}\right) \\
&\quad + I_{6x} \sin\theta_6 \left(\sin\theta_2 \sin\theta_6 - \cos\theta_2 \cos\theta_{345} \cos\theta_6\right) + I_{6y} \cos\theta_6 \left(\sin\theta_2 \cos\theta_6 + \cos\theta_2 \cos\theta_{345} \sin\theta_6\right) \\
&\quad - I_{6z} \cos^2\theta_2 \sin^2\theta_{345} \sin\theta_2 \\
d_{16} &= m_6 l_{6C} \left(l_3 \sin\theta_2 \cos\theta_{45} \cos\theta_6 + l_4 \sin\theta_2 \cos\theta_5 \cos\theta_6 + l_{6C} \cos\theta_6 \left(\sin\theta_2 \cos\theta_6 + \cos\theta_2 \cos\theta_{345} \sin\theta_6\right)\right) \\
&\quad - I_{6z} \cos\theta_2 \sin\theta_{345} \cos^2\theta_{345}
\end{aligned}
$$

$$
\begin{aligned}
d_{22} &= m_3 l_{3C}{}^2 \cos^2\theta_3 \\
&\quad + m_4 \sin^2\theta_2 \left(l_3\cos\theta_3 + l_4\cos\theta_{34}\right)^2 \\
&\quad + m_6\left\{\left(l_3\cos\theta_3 + l_4\cos\theta_{34}\right)^2 + 2l_{6C}\cos\theta_{345}\cos\theta_6\left(l_3\cos\theta_3 + l_4\cos\theta_{34}\right) + l_{6C}{}^2\left(\sin^2\theta_6 + \cos^2\theta_{345}\cos^2\theta_6\right)\right\} \\
&\quad + I_{3x}\sin^2\theta_3 + I_{3y}\cos^2\theta_3 + I_{4x}\sin^2\theta_{34} + I_{4y}\cos^2\theta_{34} + I_{6x}\sin^2\theta_{345}\cos^2\theta_6 + I_{6y}\sin^2\theta_{345}\sin^2\theta_6 + I_{6z}\cos^2\theta_{345} \\
d_{23} &= m_6 l_{6C}\sin\theta_6\left(l_3\sin\theta_3 + l_4\sin\theta_{34} + l_{6C}\sin\theta_{345}\cos\theta_6\right) \\
&\quad - I_{6x}\sin\theta_{345}\cos\theta_6\sin\theta_6 + I_{6y}\sin\theta_{345}\cos\theta_6\sin\theta_6 \\
d_{24} &= -m_6\left(l_4\sin\theta_{34} + l_{6C}\sin\theta_{345}\cos\theta_6\right)\left\{l_3\cos\theta_2\cos\theta_3 + l_4\cos\theta_2\cos\theta_{34} - l_{6C}\left(\sin\theta_2\sin\theta_6 - \cos\theta_2\cos\theta_{345}\cos\theta_6\right)\right\} \\
&\quad - I_{6x}\sin\theta_{345}\cos\theta_6\sin\theta_6 + I_{6y}\sin\theta_{345}\cos\theta_6\sin\theta_6 \\
d_{25} &= m_6 l_{6C}\cos\theta_6\left\{l_3\cos\theta_3\cos\theta_{345} + l_4\cos\theta_{34}\cos\theta_{345} + l_{6C}\left(\sin^2\theta_6 + \cos^2\theta_{345}\cos\theta_6\right)\right\} \\
&\quad + I_{6x}\sin\theta_{345}\cos\theta_6\sin\theta_6 + I_{6y}\sin\theta_{345}\cos\theta_6\sin\theta_6 \\
d_{26} &= m_6 l_{6C}{}^2\sin\theta_{345}\cos\theta_6\sin\theta_6 + I_{6z}\cos\theta_{345}
\end{aligned}
$$

$$
\begin{aligned}
d_{33} &= m_3 l_{3C}{}^2 \\
&\quad + m_4\left(l_3{}^2 + l_{4C}{}^2 + 2l_3 l_{4C}\cos\theta_4\right) \\
&\quad + m_6\left\{l_3{}^2 + l_4{}^2 + l_{6C}{}^2\cos^2\theta_6 + 2l_3 l_4\cos\theta_4 + 2l_3 l_{6C}\cos\theta_{45}\cos\theta_6 + 2l_4 l_{6C}\cos\theta_5\cos\theta_6\right\} \\
&\quad + I_{3z} + I_{4z} + I_{6x}\sin^2\theta_6 + I_{6y}\cos^2\theta_6 \\
d_{34} &= m_4 l_{4C}\left(l_3\cos\theta_4 + l_{4C}\right) \\
&\quad + m_6\begin{Bmatrix} l_4{}^2\sin\theta_2 + l_{6C}{}^2\cos\theta_6\left(\sin\theta_2\cos\theta_6 + \cos\theta_2\cos\theta_{345}\sin\theta_6\right) \\ + l_3 l_4\sin\theta_2\cos\theta_4 \\ + l_3 l_{6C}\left\{\cos\theta_2\cos\theta_3\sin\theta_6 + \sin\theta_2\cos\theta_{45}\cos\theta_6\left(2 - \cos\theta_3\right)\right\} \\ + l_4 l_{6C}\left(\cos\theta_2\cos\theta_{34}\sin\theta_6 + 2\sin\theta_2\cos\theta_5\cos\theta_6\right) \end{Bmatrix} \\
&\quad + I_{4z} + I_{6x}\sin^2\theta_6 + I_{6y}\cos^2\theta_6 \\
d_{35} &= m_6 l_{6C}\sin\theta_6\left(l_3\sin\theta_3 + l_4\sin\theta_{34} + l_{6C}\sin\theta_{345}\cos\theta_6\right) + I_{6x}\sin^2\theta_6 + I_{6y}\cos^2\theta_6 \\
d_{36} &= m_6 l_{6C}\cos\theta_6\left(l_3\cos\theta_{45} + l_4\cos\theta_5 + l_{6C}\cos\theta_6\right)
\end{aligned}
$$

$$
\begin{aligned}
d_{44} &= m_4 l_{4C}{}^2 \\
&\quad + m_6\begin{Bmatrix} + l_4{}^2\left(\sin^2\theta_{34} + \sin^2\theta_2\cos^2\theta_{34}\right) \\ + l_{6C}{}^2\left\{\left(\cos\theta_2\sin\theta_6 + \sin\theta_2\cos\theta_{345}\cos\theta_6\right)^2 + \sin^2\theta_{345}\cos^2\theta_6\right\} \\ + 2l_4 l_{6C}\left(\sin\theta_{34}\sin\theta_{345}\cos\theta_6 + \sin^2\theta_2\cos\theta_{34}\cos\theta_{345}\cos\theta_6 + \cos\theta_2\sin\theta_2\cos\theta_{34}\sin\theta_6\right) \end{Bmatrix} \\
&\quad + I_{4z} + I_{6x}\sin^2\theta_6 + I_{6y}\cos^2\theta_6 \\
d_{45} &= m_6 l_{6C}\left(\sin\theta_2\sin\theta_6 - \cos\theta_2\cos\theta_{345}\cos\theta_6\right)\left(l_4\sin\theta_{34} + l_{6C}\sin\theta_{345}\cos\theta_6\right) + I_{6x}\sin^2\theta_6 + I_{6y}\cos^2\theta_6 \\
d_{46} &= m_6 l_{6C}\left\{l_4\sin\theta_2\cos\theta_5\cos\theta_6 + l_{6C}\cos\theta_6\left(\sin\theta_2\cos\theta_6 + \cos\theta_2\cos\theta_{345}\sin\theta_6\right)\right\}
\end{aligned}
$$

$$
\begin{aligned}
d_{55} &= m_6 l_{6C}{}^2\left(\sin^2\theta_6 + \cos^2\theta_{345}\cos^2\theta_6\right) + I_{6x}\sin^2\theta_6 + I_{6y}\cos^2\theta_6 \\
d_{56} &= m_6 l_{6C}{}^2\sin\theta_{345}\cos\theta_6\sin\theta_6
\end{aligned}
$$

$$
d_{66} = m_6 l_{6C}{}^2\cos^2\theta_6\left[\left\{\left(\sin\theta_1 + \cos\theta_1\right)\sin\theta_2 + \cos\theta_2\right\}\sin\theta_{345} + \left(\sin\theta_1 - \cos\theta_1\right)\cos\theta_{345}\right]^2 + I_{6z}
$$

Each element of the Christoffel symbols is,

$$c_{111}=\frac{1}{2}\left\{\frac{\partial d_{11}}{\partial q_1}+\frac{\partial d_{11}}{\partial q_1}-\frac{\partial d_{11}}{\partial q_1}\right\}=\frac{1}{2}\frac{\partial d_{11}}{\partial q_1}=0$$

$$\begin{aligned}c_{221}&=\frac{1}{2}\left\{\frac{\partial d_{12}}{\partial q_2}+\frac{\partial d_{12}}{\partial q_2}-\frac{\partial d_{22}}{\partial q_1}\right\}=\frac{\partial d_{12}}{\partial q_2}-\frac{1}{2}\frac{\partial d_{22}}{\partial q_1}\\&=m_3{l_{3C}}^2\sin\theta_2\cos\theta_3\sin\theta_3\\&+m_4\sin\theta_2\left({l_3}^2\cos\theta_3\sin\theta_3+{l_{4C}}^2\cos\theta_{34}\sin\theta_{34}+l_3l_{4C}\sin\left(2\theta_{34}\right)\right)\\&+m_6\left(l_3\sin\theta_3+l_4\sin\theta_{34}+l_{6C}\sin\theta_{345}\cos\theta_6\right)\\&\times\left\{\sin\theta_2\left(l_3\cos\theta_3+l_4\cos\theta_{34}\right)+l_{6C}\left(\cos\theta_2\sin\theta_6-\sin\theta_2\cos\theta_{345}\cos\theta_6\right)\right\}\\&-\sin\theta_2\cos\theta_3\sin\theta_3\left(I_{3x}-I_{3y}\right)-\sin\theta_2\cos\theta_{34}\sin\theta_{34}\left(I_{4x}-I_{4y}\right)\\&-I_{6x}\sin\theta_{345}\cos\theta_6\left(\cos\theta_2\sin\theta_6+\sin\theta_2\cos\theta_{345}\cos\theta_6\right)\\&+I_{6y}\sin\theta_{345}\sin\theta_6\left(\cos\theta_2\cos\theta_6-\sin\theta_2\cos\theta_{345}\sin\theta_6\right)+I_{6z}\sin\theta_2\cos\theta_{345}\sin\theta_{345}\end{aligned}$$

$$\begin{aligned}c_{331}&=\frac{1}{2}\left\{\frac{\partial d_{13}}{\partial q_3}+\frac{\partial d_{13}}{\partial q_3}-\frac{\partial d_{33}}{\partial q_1}\right\}=\frac{\partial d_{13}}{\partial q_3}-\frac{1}{2}\frac{\partial d_{33}}{\partial q_1}\\&=-m_6\begin{Bmatrix}+{l_{6C}}^2\cos\theta_2\sin\theta_{345}\cos\theta_6\sin\theta_6\\-2l_3l_4\cos2\theta_{34}+l_3l_{6C}\cos\theta_2\sin\theta_3\sin\theta_6\\+l_4l_{6C}\cos\theta_2\sin\theta_{34}\sin\theta_6\end{Bmatrix}+\left(I_{6x}-I_{6y}\right)\cos\theta_2\sin\theta_{345}\cos\theta_6\sin\theta_6\end{aligned}$$

$$\begin{aligned}c_{441}&=\frac{1}{2}\left\{\frac{\partial d_{14}}{\partial q_4}+\frac{\partial d_{14}}{\partial q_4}-\frac{\partial d_{44}}{\partial q_1}\right\}=\frac{\partial d_{14}}{\partial q_4}-\frac{1}{2}\frac{\partial d_{44}}{\partial q_1}\\&=m_4\left(-l_3l_{4C}\sin\theta_2\sin\theta_4\right)\\&+m_6\begin{Bmatrix}-2{l_{6C}}^2\cos\theta_2\sin\theta_2\sin\theta_{345}\cos\theta_6\sin\theta_6+l_3l_4\left(\sin\theta_3\cos\theta_{34}-\sin^2\theta_2\cos\theta_3\sin\theta_{34}\right)\\+l_3l_{6C}\cos\theta_6\left(\sin\theta_3\cos\theta_{345}-\sin^2\theta_2\cos\theta_3\sin\theta_{345}\right)\\-2l_4l_{6C}\cos\theta_2\sin\theta_2\sin\theta_{34}\sin\theta_6\end{Bmatrix}\\&+\cos\theta_2\sin\theta_{345}\cos\theta_6\sin\theta_6\left(I_{6x}-I_{6y}\right)\end{aligned}$$

$$\begin{aligned}c_{551}&=\frac{1}{2}\left\{\frac{\partial d_{15}}{\partial q_5}+\frac{\partial d_{15}}{\partial q_5}-\frac{\partial d_{55}}{\partial q_1}\right\}=\frac{\partial d_{15}}{\partial q_5}-\frac{1}{2}\frac{\partial d_{55}}{\partial q_1}\\&=m_6l_{6C}\begin{Bmatrix}\cos\theta_2\sin\theta_{345}\cos\theta_6\left(l_3\sin\theta_3+l_4\sin\theta_{34}+l_{6C}\cos\theta_6\sin\theta_{345}\right)\\+l_{6C}\cos\theta_6\cos\theta_{345}\left(\sin\theta_2\sin\theta_6-\cos\theta_2\cos\theta_{345}\cos\theta_6\right)\end{Bmatrix}\\&+\cos\theta_2\sin\theta_{345}\left\{\left(I_{6x}-I_{6y}\right)\cos\theta_6\sin\theta_6-2I_{6z}\cos\theta_2\cos\theta_{345}\sin\theta_2\right\}\end{aligned}$$

$$\begin{aligned}c_{661}&=\frac{1}{2}\left\{\frac{\partial d_{16}}{\partial q_6}+\frac{\partial d_{16}}{\partial q_6}-\frac{\partial d_{66}}{\partial q_1}\right\}=\frac{\partial d_{16}}{\partial q_6}-\frac{1}{2}\frac{\partial d_{66}}{\partial q_1}\\&=-m_6l_{6C}\begin{bmatrix}\sin\theta_2\sin\theta_6\left(l_3\cos\theta_{45}+l_4\cos\theta_5\right)\\+l_{6C}\sin\theta_6\left(\sin\theta_2\cos\theta_6+\cos\theta_2\cos\theta_{345}\sin\theta_6\right)\\+l_{6C}\cos\theta_6\left(\sin\theta_2\sin\theta_6-\cos\theta_2\cos\theta_{345}\cos\theta_6\right)\\+l_{6C}\cos^2\theta_6\left\{\left(\cos\theta_1-\sin\theta_1\right)\sin\theta_2\sin\theta_{345}+\left(\cos\theta_1+\sin\theta_1\right)\cos\theta_{345}\right\}\\\times\left\{\left(\sin\theta_1+\cos\theta_1\right)\sin\theta_2\sin\theta_{345}+\cos\theta_2\sin\theta_{345}+\left(\sin\theta_1-\cos\theta_1\right)\cos\theta_{345}\right\}\end{bmatrix}\end{aligned}$$

$$c_{112}=\frac{1}{2}\left\{\frac{\partial d_{21}}{\partial q_1}+\frac{\partial d_{21}}{\partial q_1}-\frac{\partial d_{11}}{\partial q_2}\right\}=\frac{\partial d_{12}}{\partial q_1}-\frac{1}{2}\frac{\partial d_{11}}{\partial q_2}$$

$$\begin{aligned}
&=-m_3 l_{3C}{}^2\sin\theta_2\cos\theta_2\cos^2\theta_3-m_4\sin\theta_2\cos\theta_2\left(l_3\cos\theta_3+l_{4C}\cos\theta_{34}\right)^2\\
&-m_6\left[\begin{array}{l}\left\{\cos\theta_2\left(l_3\cos\theta_3+l_4\cos\theta_{34}-l_{6C}\cos\theta_{345}\cos\theta_6\right)-l_{6C}\sin\theta_2\sin\theta_6\right\}\\ \times\left\{\sin\theta_2\left(l_3\cos\theta_3+l_4\cos\theta_{34}-l_{6C}\cos\theta_{345}\cos\theta_6\right)+l_{6C}\cos\theta_2\sin\theta_6\right\}\end{array}\right]\\
&+\cos\theta_2\sin\theta_2\left(I_{3x}\cos^2\theta_3+I_{3y}\sin^2\theta_3-I_{3z}\right)+\cos\theta_2\sin\theta_2\left(I_{4x}\cos^2\theta_{34}+I_{4y}\sin^2\theta_{34}-I_{4z}\right)\\
&-I_{6x}\left(\sin\theta_2\sin\theta_6-\cos\theta_2\cos\theta_{345}\cos\theta_6\right)\left(\cos\theta_2\sin\theta_6+\sin\theta_2\cos\theta_{345}\cos\theta_6\right)\\
&-I_{6y}\left(\sin\theta_2\cos\theta_6+\cos\theta_2\cos\theta_{345}\sin\theta_6\right)\left(\cos\theta_2\cos\theta_6-\sin\theta_2\cos\theta_{345}\sin\theta_6\right)\\
&-I_{6z}\cos\theta_2\sin\theta_2\sin^2\theta_{345}
\end{aligned}$$

$$c_{222}=\frac{1}{2}\left\{\frac{\partial d_{22}}{\partial q_2}+\frac{\partial d_{22}}{\partial q_2}-\frac{\partial d_{22}}{\partial q_2}\right\}=\frac{1}{2}\frac{\partial d_{22}}{\partial q_2}=0$$

$$c_{332}=\frac{1}{2}\left\{\frac{\partial d_{23}}{\partial q_3}+\frac{\partial d_{23}}{\partial q_3}-\frac{\partial d_{33}}{\partial q_2}\right\}=\frac{\partial d_{23}}{\partial q_3}-\frac{1}{2}\frac{\partial d_{33}}{\partial q_2}$$

$$=m_6 l_{6C}\sin\theta_6\left(l_3\cos\theta_3+l_4\cos\theta_{34}+l_{6C}\cos\theta_{345}\cos\theta_6\right)-\cos\theta_{345}\cos\theta_6\sin\theta_6\left(I_{6x}-I_{6y}\right)$$

$$c_{442}=\frac{1}{2}\left\{\frac{\partial d_{24}}{\partial q_4}+\frac{\partial d_{24}}{\partial q_4}-\frac{\partial d_{44}}{\partial q_2}\right\}=\frac{\partial d_{24}}{\partial q_4}-\frac{1}{2}\frac{\partial d_{44}}{\partial q_2}$$

$$\begin{aligned}
&=-m_6\left[\begin{array}{l}\left(l_4\cos\theta_{34}+l_{6C}\cos\theta_{345}\cos\theta_6\right)\\ \times\left\{l_3\cos\theta_2\cos\theta_3+l_4\cos\theta_2\cos\theta_{34}-l_{6C}\left(\sin\theta_2\sin\theta_6-\cos\theta_2\cos\theta_{345}\cos\theta_6\right)\right\}\\ -\cos\theta_2\left(l_4\sin\theta_{34}+l_{6C}\sin\theta_{345}\cos\theta_6\right)^2\\ +l_4{}^2\sin\theta_2\cos\theta_2\cos^2\theta_{34}\\ +l_{6C}{}^2\left(\cos\theta_2\sin\theta_6+\sin\theta_2\cos\theta_{345}\cos\theta_6\right)\left(-\sin\theta_2\sin\theta_6+\cos\theta_2\cos\theta_{345}\cos\theta_6\right)\\ +l_4 l_{6C}\cos\theta_{34}\left(+2\cos\theta_2\sin\theta_2\cos\theta_{345}\cos\theta_6-\sin^2\theta_2\sin\theta_6+\cos^2\theta_2\sin\theta_6\right)\end{array}\right]\\
&-\cos\theta_{345}\cos\theta_6\sin\theta_6\left(I_{6x}-I_{6y}\right)
\end{aligned}$$

$$c_{552}=\frac{1}{2}\left\{\frac{\partial d_{25}}{\partial q_5}+\frac{\partial d_{25}}{\partial q_5}-\frac{\partial d_{55}}{\partial q_2}\right\}=\frac{\partial d_{25}}{\partial q_5}-\frac{1}{2}\frac{\partial d_{55}}{\partial q_2}$$

$$\begin{aligned}
&=-m_6 l_{6C}\sin\theta_{345}\cos\theta_6\left(l_3\cos\theta_3+l_4\cos\theta_{34}+2l_{6C}\cos\theta_{345}\cos\theta_6\right)\\
&+\cos\theta_{345}\cos\theta_6\sin\theta_6\left(I_{6x}+I_{6y}\right)
\end{aligned}$$

$$c_{662}=\frac{1}{2}\left\{\frac{\partial d_{26}}{\partial q_6}+\frac{\partial d_{26}}{\partial q_6}-\frac{\partial d_{66}}{\partial q_2}\right\}=\frac{\partial d_{26}}{\partial q_6}-\frac{1}{2}\frac{\partial d_{66}}{\partial q_2}$$

$$=m_6 l_{6C}{}^2\left[\begin{array}{l}\sin\theta_{345}\left(\cos^2\theta_6-\sin^2\theta_6\right)\\ -\sin\theta_{345}\cos^2\theta_6\left\{\left(\sin\theta_1+\cos\theta_1\right)\cos\theta_2-\sin\theta_2\right\}\\ \times\left[\left\{\left(\sin\theta_1+\cos\theta_1\right)\sin\theta_2+\cos\theta_2\right\}\sin\theta_{345}+\left(\sin\theta_1-\cos\theta_1\right)\cos\theta_{345}\right]\end{array}\right]$$

$$
\begin{aligned}
c_{113} &= \frac{1}{2}\left\{\frac{\partial d_{31}}{\partial q_1}+\frac{\partial d_{31}}{\partial q_1}-\frac{\partial d_{11}}{\partial q_3}\right\}=\frac{\partial d_{13}}{\partial q_1}-\frac{1}{2}\frac{\partial d_{11}}{\partial q_3} \\
&= -m_3 {l_{3C}}^2 \cos^2\theta_2 \cos\theta_3 \sin\theta_3 \\
&\quad -m_4 \cos^2\theta_2 \left(l_3 \sin\theta_3 + l_{4C} \sin\theta_{34}\right)\left(l_3 \cos\theta_3 + l_{4C} \cos\theta_{34}\right) \\
&\quad -m_6 \begin{bmatrix} \left(l_3 \sin\theta_3 + l_4 \sin\theta_{34} + l_{6C} \sin\theta_{345} \cos\theta_6\right)\left(l_3 \cos\theta_3 + l_4 \cos\theta_{34} + l_{6C} \cos\theta_{345} \cos\theta_6\right) \\ -\sin\theta_2 \left(l_3 \sin\theta_3 + l_4 \sin\theta_{34} - l_{6C} \sin\theta_{345} \cos\theta_6\right) \\ \times\left\{\sin\theta_2 \left(l_3 \cos\theta_3 + l_4 \cos\theta_{34} - l_{6C} \cos\theta_{345} \cos\theta_6\right) + l_{6C} \cos\theta_2 \sin\theta_6\right\} \end{bmatrix} \\
&\quad +\cos^2\theta_2 \cos\theta_3 \sin\theta_3 \left(I_{3x} - I_{3y}\right) + \cos^2\theta_2 \cos\theta_{34} \sin\theta_{34} \left(I_{4x} - I_{4y}\right) \\
&\quad -I_{6x} \cos\theta_2 \sin\theta_{345} \cos\theta_6 \left(\sin\theta_2 \sin\theta_6 - \cos\theta_2 \cos\theta_{345} \cos\theta_6\right) \\
&\quad +I_{6y} \cos\theta_2 \sin\theta_{345} \sin\theta_6 \left(\sin\theta_2 \cos\theta_6 + \cos\theta_2 \cos\theta_{345} \sin\theta_6\right) - I_{6z} \cos^2\theta_2 \cos\theta_{345} \sin\theta_{345} \\
c_{223} &= \frac{1}{2}\left\{\frac{\partial d_{32}}{\partial q_2}+\frac{\partial d_{32}}{\partial q_2}-\frac{\partial d_{22}}{\partial q_3}\right\}=\frac{\partial d_{23}}{\partial q_2}-\frac{1}{2}\frac{\partial d_{22}}{\partial q_3} \\
&= m_3 {l_{3C}}^2 \cos\theta_3 \sin\theta_3 + m_4 \sin^2\theta_2 \left(l_3 \cos\theta_3 + l_4 \cos\theta_{34}\right)\left(l_3 \sin\theta_3 + l_4 \sin\theta_{34}\right) \\
&\quad +m_6 \begin{bmatrix} +{l_{6C}}^2 \cos\theta_{345} \sin\theta_{345} \cos^2\theta_6 \\ +\left(l_3 \cos\theta_3 + l_4 \cos\theta_{34}\right)\left(l_3 \sin\theta_3 + l_4 \sin\theta_{34}\right) \\ +l_{6C} \cos\theta_6 \left\{\sin\theta_{345}\left(l_3 \cos\theta_3 + l_4 \cos\theta_{34}\right) + \cos\theta_{345}\left(l_3 \sin\theta_3 + l_4 \sin\theta_{34}\right)\right\} \end{bmatrix} \\
&\quad -\sin\theta_3 \cos\theta_3 \left(I_{3x} - I_{3y}\right) - \sin\theta_{34} \cos\theta_{34} \left(I_{4x} - I_{4y}\right) \\
&\quad -\sin\theta_{345} \cos\theta_{345} \left(I_{6x} \cos^2\theta_6 + I_{6y} \sin^2\theta_6 - I_{6z}\right) \\
c_{333} &= \frac{1}{2}\left\{\frac{\partial d_{33}}{\partial q_3}+\frac{\partial d_{33}}{\partial q_3}-\frac{\partial d_{33}}{\partial q_3}\right\}=\frac{1}{2}\frac{\partial d_{33}}{\partial q_3}=0 \\
c_{443} &= \frac{1}{2}\left\{\frac{\partial d_{34}}{\partial q_4}+\frac{\partial d_{34}}{\partial q_4}-\frac{\partial d_{44}}{\partial q_3}\right\}=\frac{\partial d_{34}}{\partial q_4}-\frac{1}{2}\frac{\partial d_{44}}{\partial q_3} \\
&= -m_4 l_3 l_{4C} \sin\theta_4 \\
&\quad -m_6 \begin{Bmatrix} +{l_4}^2 \cos^2\theta_2 \cos\theta_{34} \sin\theta_{34} \\ +{l_{6C}}^2 \sin\theta_{345} \cos\theta_6 \begin{pmatrix} \cos\theta_2 \sin\theta_6 - \sin\theta_2 \cos\theta_2 \sin\theta_6 \\ -\sin^2\theta_2 \cos\theta_{345} \cos\theta_6 + \cos\theta_{345} \cos\theta_6 \end{pmatrix} \\ +l_3 l_4 \sin\theta_2 \sin\theta_4 + l_3 l_{6C} \sin\theta_2 \sin\theta_{45} \cos\theta_6 \left(2 - \cos\theta_3\right) \\ +l_4 l_{6C} \begin{pmatrix} +\cos\theta_2 \sin\theta_{34} \sin\theta_6 \\ +\cos\theta_6 \left(\cos\theta_{34} \sin\theta_{345} + \sin\theta_{34} \cos\theta_{345}\right) \\ -\sin^2\theta_2 \cos\theta_6 \left(\sin\theta_{34} \cos\theta_{345} + \cos\theta_{34} \sin\theta_{345}\right) \\ -\cos\theta_2 \sin\theta_2 \sin\theta_{34} \sin\theta_6 \end{pmatrix} \end{Bmatrix} \\
c_{553} &= \frac{1}{2}\left\{\frac{\partial d_{35}}{\partial q_5}+\frac{\partial d_{35}}{\partial q_5}-\frac{\partial d_{55}}{\partial q_3}\right\}=\frac{\partial d_{35}}{\partial q_5}-\frac{1}{2}\frac{\partial d_{55}}{\partial q_3} \\
&= m_6 {l_{6C}}^2 \cos\theta_{345} \cos\theta_6 \left(\sin\theta_6 + \sin\theta_{345} \cos\theta_6\right)
\end{aligned}
$$

$$c_{663}=\frac{1}{2}\left\{\frac{\partial d_{36}}{\partial q_6}+\frac{\partial d_{36}}{\partial q_6}-\frac{\partial d_{66}}{\partial q_3}\right\}=\frac{\partial d_{36}}{\partial q_6}-\frac{1}{2}\frac{\partial d_{66}}{\partial q_3}$$

$$=m_6 l_{6C}\begin{bmatrix}-\sin\theta_6\left(l_3\cos\theta_{45}+l_4\cos\theta_5+2l_{6C}\cos\theta_6\right)\\ -l_{6C}\cos^2\theta_6\left[\left\{\left(\sin\theta_1+\cos\theta_1\right)\sin\theta_2+\cos\theta_2\right\}\cos\theta_{345}-\left(\sin\theta_1-\cos\theta_1\right)\sin\theta_{345}\right]\\ \times\left[\left\{\left(\sin\theta_1+\cos\theta_1\right)\sin\theta_2+\cos\theta_2\right\}\sin\theta_{345}+\left(\sin\theta_1-\cos\theta_1\right)\cos\theta_{345}\right]\end{bmatrix}$$

$$c_{114}=\frac{1}{2}\left\{\frac{\partial d_{41}}{\partial q_1}+\frac{\partial d_{41}}{\partial q_1}-\frac{\partial d_{11}}{\partial q_4}\right\}=\frac{\partial d_{14}}{\partial q_1}-\frac{1}{2}\frac{\partial d_{11}}{\partial q_4}$$

$$=-m_4\left\{l_{4C}\cos\theta_{34}\left(l_3\sin\theta_3+l_{4C}\sin\theta_{34}\right)-l_{4C}\sin\theta_{34}\sin^2\theta_2\left(l_3\cos\theta_3+l_{4C}\cos\theta_{34}\right)\right\}$$

$$-m_6\begin{bmatrix}\left(l_3\sin\theta_3+l_4\sin\theta_{34}+l_{6C}\sin\theta_{345}\cos\theta_6\right)\left(l_4\cos\theta_{34}+l_{6C}\cos\theta_{345}\cos\theta_6\right)\\ -\sin\theta_2\left(l_4\sin\theta_{34}-l_{6C}\sin\theta_{345}\cos\theta_6\right)\\ \times\left\{\sin\theta_2\left(l_3\cos\theta_3+l_4\cos\theta_{34}-l_{6C}\cos\theta_{345}\cos\theta_6\right)+l_{6C}\cos\theta_2\sin\theta_6\right\}\end{bmatrix}$$

$$+\cos^2\theta_2\cos\theta_{34}\sin\theta_{34}\left(I_{4x}-I_{4y}\right)$$

$$-\cos\theta_2\sin\theta_{345}\begin{Bmatrix}I_{6x}\cos\theta_6\left(\sin\theta_2\sin\theta_6-\cos\theta_2\cos\theta_{345}\cos\theta_6\right)\\ -I_{6y}\sin\theta_6\left(\sin\theta_2\cos\theta_6+\cos\theta_2\cos\theta_{345}\sin\theta_6\right)+I_{6z}\cos\theta_2\cos\theta_{345}\end{Bmatrix}$$

$$c_{224}=\frac{1}{2}\left\{\frac{\partial d_{42}}{\partial q_2}+\frac{\partial d_{42}}{\partial q_2}-\frac{\partial d_{22}}{\partial q_4}\right\}=\frac{\partial d_{24}}{\partial q_2}-\frac{1}{2}\frac{\partial d_{22}}{\partial q_4}$$

$$=m_4 l_4\sin\theta_{34}\sin^2\theta_2\left(l_3\cos\theta_3+l_4\cos\theta_{34}\right)$$

$$+m_6\begin{bmatrix}\left(l_4\sin\theta_{34}+l_{6C}\sin\theta_{345}\cos\theta_6\right)\\ \times\left\{\left(l_3\cos\theta_3+l_4\cos\theta_{34}\right)\left(\sin\theta_2+1\right)+l_{6C}\left(\cos\theta_2\sin\theta_6+\sin\theta_2\cos\theta_{345}\cos\theta_6\right)\right\}\\ +l_4 l_{6C}\sin\theta_{34}\cos\theta_{345}\cos\theta_6+{l_{6C}}^2\cos\theta_{345}\sin\theta_{345}\cos^2\theta_6\end{bmatrix}$$

$$-\cos\theta_{34}\sin\theta_{34}\left(I_{4x}-I_{4y}\right)-\cos\theta_{345}\sin\theta_{345}\left(I_{6x}\cos^2\theta_6+I_{6y}\sin^2\theta_6-I_{6z}\right)$$

$$c_{334}=\frac{1}{2}\left\{\frac{\partial d_{43}}{\partial q_3}+\frac{\partial d_{43}}{\partial q_3}-\frac{\partial d_{33}}{\partial q_4}\right\}=\frac{\partial d_{34}}{\partial q_3}-\frac{1}{2}\frac{\partial d_{33}}{\partial q_4}$$

$$=m_4 l_3 l_{4C}\sin\theta_4$$

$$-m_6\begin{Bmatrix}{l_{6C}}^2\cos\theta_2\sin\theta_{345}\cos\theta_6\sin\theta_6\\ -l_3 l_4\sin\theta_4+l_4 l_{6C}\cos\theta_2\sin\theta_{34}\sin\theta_6\\ l_3 l_{6C}\left(\cos\theta_2\sin\theta_3\sin\theta_6-\sin\theta_2\sin\theta_3\cos\theta_{45}\cos\theta_6-\sin\theta_{45}\cos\theta_6\right)\end{Bmatrix}$$

$$c_{444}=\frac{1}{2}\left\{\frac{\partial d_{44}}{\partial q_4}+\frac{\partial d_{44}}{\partial q_4}-\frac{\partial d_{44}}{\partial q_4}\right\}=\frac{1}{2}\frac{\partial d_{44}}{\partial q_4}$$

$$=m_6\begin{bmatrix}+{l_4}^2\cos\theta_{34}\sin\theta_{34}\cos^2\theta_2\\ +{l_{6C}}^2\sin\theta_{345}\cos\theta_6\left\{\cos\theta_{345}\cos\theta_6-\sin\theta_2\left(\cos\theta_2\sin\theta_6+\sin\theta_2\cos\theta_{345}\cos\theta_6\right)\right\}\\ \\ +l_4 l_{6C}\begin{Bmatrix}\cos\theta_6\left(\cos\theta_{34}\sin\theta_{345}+\sin\theta_{34}\cos\theta_{345}\right)\\ -\sin^2\theta_2\cos\theta_6\left(\sin\theta_{34}\cos\theta_{345}+\cos\theta_{34}\sin\theta_{345}\right)-\cos\theta_2\sin\theta_2\sin\theta_{34}\sin\theta_6\end{Bmatrix}\end{bmatrix}$$

$$c_{554}=\frac{1}{2}\left\{\frac{\partial d_{45}}{\partial q_5}+\frac{\partial d_{45}}{\partial q_5}-\frac{\partial d_{55}}{\partial q_4}\right\}=\frac{\partial d_{45}}{\partial q_5}-\frac{1}{2}\frac{\partial d_{55}}{\partial q_4}$$

$$=m_6 l_{6C}\begin{Bmatrix}\cos\theta_2\sin\theta_{345}\cos\theta_6\left(l_4\sin\theta_{34}+l_{6C}\sin\theta_{345}\cos\theta_6\right)\\+l_{6C}\cos\theta_{345}\cos\theta_6\left(\sin\theta_2\sin\theta_6-\cos\theta_2\cos\theta_{345}\cos\theta_6+\sin\theta_{345}\cos\theta_6\right)\end{Bmatrix}$$

$$c_{664}=\frac{1}{2}\left\{\frac{\partial d_{46}}{\partial q_6}+\frac{\partial d_{46}}{\partial q_6}-\frac{\partial d_{66}}{\partial q_4}\right\}=\frac{\partial d_{46}}{\partial q_6}-\frac{1}{2}\frac{\partial d_{66}}{\partial q_4}$$

$$=m_6 l_{6C}\begin{bmatrix}-l_4\sin\theta_2\cos\theta_5\sin\theta_6\\-l_{6C}\begin{Bmatrix}2\sin\theta_2\cos\theta_6\sin\theta_6+\cos\theta_2\cos\theta_{345}\left(\sin^2\theta_6-\cos^2\theta_6\right)\\+\cos^2\theta_6\left[\left\{\left(\sin\theta_1+\cos\theta_1\right)\sin\theta_2+\cos\theta_2\right\}\sin\theta_{345}+\left(\sin\theta_1-\cos\theta_1\right)\cos\theta_{345}\right]\\\times\left[\left\{\left(\sin\theta_1+\cos\theta_1\right)\sin\theta_2+\cos\theta_2\right\}\cos\theta_{345}-\left(\sin\theta_1-\cos\theta_1\right)\sin\theta_{345}\right]\end{Bmatrix}\end{bmatrix}$$

$$c_{115}=\frac{1}{2}\left\{\frac{\partial d_{51}}{\partial q_1}+\frac{\partial d_{51}}{\partial q_1}-\frac{\partial d_{11}}{\partial q_5}\right\}=\frac{\partial d_{15}}{\partial q_1}-\frac{1}{2}\frac{\partial d_{11}}{\partial q_5}$$

$$=-m_6 l_{6C}\cos\theta_6\begin{bmatrix}\cos\theta_{345}\left(l_3\sin\theta_3+l_4\sin\theta_{34}+l_{6C}\sin\theta_{345}\cos\theta_6\right)\\+\sin\theta_2\sin\theta_{345}\left\{\sin\theta_2\left(l_3\cos\theta_3+l_4\cos\theta_{34}-l_{6C}\cos\theta_{345}\cos\theta_6\right)+l_{6C}\cos\theta_2\sin\theta_6\right\}\end{bmatrix}$$

$$-\cos\theta_2\sin\theta_{345}\begin{Bmatrix}I_{6x}\cos\theta_6\left(\sin\theta_2\sin\theta_6-\cos\theta_2\cos\theta_{345}\cos\theta_6\right)\\-I_{6y}\sin\theta_6\left(\sin\theta_2\cos\theta_6+\cos\theta_2\cos\theta_{345}\sin\theta_6\right)\\+I_{6z}\cos\theta_2\cos\theta_{345}\end{Bmatrix}$$

$$c_{225}=\frac{1}{2}\left\{\frac{\partial d_{52}}{\partial q_2}+\frac{\partial d_{52}}{\partial q_2}-\frac{\partial d_{22}}{\partial q_5}\right\}=\frac{\partial d_{25}}{\partial q_2}-\frac{1}{2}\frac{\partial d_{22}}{\partial q_5}$$

$$=m_6 l_{6C}\sin\theta_{345}\cos\theta_6\left(l_3\cos\theta_3+l_4\cos\theta_{34}+l_{6C}\cos\theta_{345}\cos\theta_6\right)$$

$$-\cos\theta_{345}\sin\theta_{345}\left(I_{6x}\cos^2\theta_6+I_{6y}\sin^2\theta_6-I_{6z}\right)$$

$$c_{335}=\frac{1}{2}\left\{\frac{\partial d_{53}}{\partial q_3}+\frac{\partial d_{53}}{\partial q_3}-\frac{\partial d_{33}}{\partial q_5}\right\}=\frac{\partial d_{35}}{\partial q_3}-\frac{1}{2}\frac{\partial d_{33}}{\partial q_5}$$

$$=m_6 l_{6C}\left\{l_3\left(\cos\theta_3\sin\theta_6+\sin\theta_{45}\cos\theta_6\right)+l_4\left(\cos\theta_{34}\sin\theta_6+\sin\theta_5\cos\theta_6\right)+l_{6C}\cos\theta_{345}\cos\theta_6\sin\theta_6\right\}$$

$$c_{445}=\frac{1}{2}\left\{\frac{\partial d_{54}}{\partial q_4}+\frac{\partial d_{54}}{\partial q_4}-\frac{\partial d_{44}}{\partial q_5}\right\}=\frac{\partial d_{45}}{\partial q_4}-\frac{1}{2}\frac{\partial d_{44}}{\partial q_5}$$

$$=m_6 l_{6C}\begin{Bmatrix}\cos\theta_2\sin\theta_{345}\cos\theta_6\left(l_4\sin\theta_{34}+l_{6C}\sin\theta_{345}\cos\theta_6\right)\\-\left(\sin\theta_2\sin\theta_6-\cos\theta_2\cos\theta_{345}\cos\theta_6\right)\left(l_4\cos\theta_{34}+l_{6C}\cos\theta_{345}\cos\theta_6\right)\\+l_{6C}\left\{\sin\theta_2\sin\theta_{345}\cos\theta_6\left(\cos\theta_2\sin\theta_6+\sin\theta_2\cos\theta_{345}\cos\theta_6\right)-\sin\theta_{345}\cos\theta_{345}\cos^2\theta_6\right\}\\-l_4\left(\sin\theta_{34}\cos\theta_{345}\cos\theta_6-\sin^2\theta_2\cos\theta_{34}\sin\theta_{345}\cos\theta_6\right)\end{Bmatrix}$$

$$c_{555}=\frac{1}{2}\left\{\frac{\partial d_{55}}{\partial q_5}+\frac{\partial d_{55}}{\partial q_5}-\frac{\partial d_{55}}{\partial q_5}\right\}=\frac{1}{2}\frac{\partial d_{55}}{\partial q_5}=0$$

$$c_{665}=\frac{1}{2}\left\{\frac{\partial d_{56}}{\partial q_6}+\frac{\partial d_{56}}{\partial q_6}-\frac{\partial d_{66}}{\partial q_5}\right\}=\frac{\partial d_{56}}{\partial q_6}-\frac{1}{2}\frac{\partial d_{66}}{\partial q_5}$$

$$=m_6 {l_{6C}}^2\cos^2\theta_6\begin{bmatrix}\sin\theta_{345}\\ -\left[\left\{\left(\sin\theta_1+\cos\theta_1\right)\sin\theta_2+\cos\theta_2\right\}\sin\theta_{345}+\left(\sin\theta_1-\cos\theta_1\right)\cos\theta_{345}\right]\\ \times\left[\left\{\left(\sin\theta_1+\cos\theta_1\right)\sin\theta_2+\cos\theta_2\right\}\cos\theta_{345}-\left(\sin\theta_1-\cos\theta_1\right)\sin\theta_{345}\right]\end{bmatrix}$$

$$c_{116}=\frac{1}{2}\left\{\frac{\partial d_{61}}{\partial q_1}+\frac{\partial d_{61}}{\partial q_1}-\frac{\partial d_{11}}{\partial q_6}\right\}=\frac{\partial d_{16}}{\partial q_1}-\frac{1}{2}\frac{\partial d_{11}}{\partial q_6}$$

$$=m_6 l_{6C}\begin{bmatrix}\sin\theta_{345}\sin\theta_6\left(l_3\sin\theta_3+l_4\sin\theta_{34}+l_{6C}\sin\theta_{345}\cos\theta_6\right)\\ -\left(\sin\theta_2\cos\theta_{345}\sin\theta_6+\cos\theta_2\cos\theta_6\right)\left\{\sin\theta_2\left(l_3\cos\theta_3+l_4\cos\theta_{34}-l_{6C}\cos\theta_{345}\cos\theta_6\right)+l_{6C}\cos\theta_2\sin\theta_6\right\}\end{bmatrix}$$

$$-I_{6x}\left(\sin\theta_2\sin\theta_6-\cos\theta_2\cos\theta_{345}\cos\theta_6\right)\left(\sin\theta_2\cos\theta_6+\cos\theta_2\cos\theta_{345}\sin\theta_6\right)$$

$$+I_{6y}\left(\sin\theta_2\cos\theta_6+\cos\theta_2\cos\theta_{345}\sin\theta_6\right)\left(\sin\theta_2\sin\theta_6-\cos\theta_2\cos\theta_{345}\cos\theta_6\right)$$

$$c_{226}=\frac{1}{2}\left\{\frac{\partial d_{62}}{\partial q_2}+\frac{\partial d_{62}}{\partial q_2}-\frac{\partial d_{22}}{\partial q_6}\right\}=\frac{\partial d_{26}}{\partial q_2}-\frac{1}{2}\frac{\partial d_{22}}{\partial q_6}$$

$$=m_6 l_{6C}\left\{\cos\theta_{345}\sin\theta_6\left(l_3\cos\theta_3+l_4\cos\theta_{34}\right)-l_{6C}\sin^2\theta_{345}\cos\theta_6\sin\theta_6\right\}$$

$$+\cos\theta_6\sin\theta_6\left(I_{6x}\sin^2\theta_{345}-I_{6y}\sin^2\theta_{345}\right)$$

$$c_{336}=\frac{1}{2}\left\{\frac{\partial d_{63}}{\partial q_3}+\frac{\partial d_{63}}{\partial q_3}-\frac{\partial d_{33}}{\partial q_6}\right\}=\frac{\partial d_{36}}{\partial q_3}-\frac{1}{2}\frac{\partial d_{33}}{\partial q_6}$$

$$=m_6\left\{{l_{6C}}^2\cos\theta_6\sin\theta_6+l_3 l_{6C}\cos\theta_{45}\sin\theta_6+l_4 l_{6C}\cos\theta_5\sin\theta_6\right\}-\cos\theta_6\sin\theta_6\left(I_{6x}-I_{6y}\right)$$

$$c_{446}=\frac{1}{2}\left\{\frac{\partial d_{64}}{\partial q_4}+\frac{\partial d_{64}}{\partial q_4}-\frac{\partial d_{44}}{\partial q_6}\right\}=\frac{\partial d_{46}}{\partial q_4}-\frac{1}{2}\frac{\partial d_{44}}{\partial q_6}$$

$$=m_6\begin{bmatrix}+{l_{6C}}^2\left\{\begin{matrix}\cos\theta_6\sin\theta_6\left(\sin^2\theta_{345}-\cos\theta_2\sin\theta_{345}\right)\\ -\left(\cos\theta_2\sin\theta_6+\sin\theta_2\cos\theta_{345}\cos\theta_6\right)\left(\cos\theta_2\cos\theta_6-\sin\theta_2\cos\theta_{345}\sin\theta_6\right)\end{matrix}\right\}\\ +l_4 l_{6C}\left(\sin\theta_{34}\sin\theta_{345}\sin\theta_6+\sin^2\theta_2\cos\theta_{34}\cos\theta_{345}\sin\theta_6-\cos\theta_2\sin\theta_2\cos\theta_{34}\cos\theta_6\right)\end{bmatrix}$$

$$-\cos\theta_6\sin\theta_6\left(I_{6x}-I_{6y}\right)$$

$$c_{556}=\frac{1}{2}\left\{\frac{\partial d_{65}}{\partial q_5}+\frac{\partial d_{65}}{\partial q_5}-\frac{\partial d_{55}}{\partial q_6}\right\}=\frac{\partial d_{56}}{\partial q_5}-\frac{1}{2}\frac{\partial d_{55}}{\partial q_6}$$

$$=m_6 {l_{6C}}^2\cos\theta_6\sin\theta_6\left(\cos\theta_{345}+\sin^2\theta_{345}\right)-\cos\theta_6\sin\theta_6\left(I_{6x}-I_{6y}\right)$$

$$c_{666}=\frac{1}{2}\left\{\frac{\partial d_{66}}{\partial q_6}+\frac{\partial d_{66}}{\partial q_6}-\frac{\partial d_{66}}{\partial q_6}\right\}=\frac{1}{2}\frac{\partial d_{66}}{\partial q_6}$$

$$=-m_6 {l_{6C}}^2\cos\theta_6\sin\theta_6\left[\left\{\left(\sin\theta_1+\cos\theta_1\right)\sin\theta_2+\cos\theta_2\right\}\sin\theta_{345}+\left(\sin\theta_1-\cos\theta_1\right)\cos\theta_{345}\right]^2$$

Equation 3.14, which is about the potential energy, is a function of the joint angles and can be written as in Equation 3.24,

$$P = m_3 g\left(h_0 - l_{3C}\cos\theta_2\cos\theta_3\right) + m_4 g\left\{h_0 - \cos\theta_2\left(l_3\cos\theta_3 + l_{4C}\cos\theta_{34}\right)\right\} + m_6 g\left\{h_0 - \cos\theta_2\left(l_3\cos\theta_3 + l_4\cos\theta_{34}\right) - l_{6C}\left(\cos\theta_2\cos\theta_{345}\cos\theta_6 - \sin\theta_2\sin\theta_6\right)\right\} \quad \text{(Eq. 3.24)}$$

Thus, each element of the gravity force is

$$g_1 = \frac{\partial P}{\partial q_1} = 0$$

$$g_2 = \frac{\partial P}{\partial q_2} = m_3 g l_{3C}\sin\theta_2\cos\theta_3 + m_4 g\sin\theta_2\left(l_3\cos\theta_3 + l_{4C}\cos\theta_{34}\right) + m_6 g\left\{\sin\theta_2\left(l_3\cos\theta_3 + l_4\cos\theta_{34}\right) + l_{6C}\left(\sin\theta_2\cos\theta_{345}\cos\theta_6 + \cos\theta_2\sin\theta_6\right)\right\}$$

$$g_3 = \frac{\partial P}{\partial q_3} = m_3 g l_{3C}\cos\theta_2\sin\theta_3 + m_4 g\cos\theta_2\left(l_3\sin\theta_3 + l_{4C}\sin\theta_{34}\right) + m_6 g\left\{\cos\theta_2\left(l_3\sin\theta_3 + l_4\sin\theta_{34}\right) + l_{6C}\cos\theta_2\sin\theta_{345}\cos\theta_6\right\}$$

$$g_4 = \frac{\partial P}{\partial q_4} = m_4 g l_{4C}\cos\theta_2\sin\theta_{34} + m_6 g\left(l_4\cos\theta_2\sin\theta_{34} + l_{6C}\cos\theta_2\sin\theta_{345}\cos\theta_6\right)$$

$$g_5 = \frac{\partial P}{\partial q_5} = m_6 g l_{6C}\cos\theta_2\sin\theta_{345}\cos\theta_6$$

$$g_6 = \frac{\partial P}{\partial q_6} = m_6 g l_{6C}\left(\cos\theta_2\cos\theta_{345}\sin\theta_6 + \sin\theta_2\cos\theta_6\right)$$

Section 4 Bipedal Walking Methods

4.1 ZMP Walking

Since Miomir Vukobratović suggested the ZMP (Zero Moment Point) algorithm, it has become one of the most popular bipedal walking methods. [13] ZMP is defined as the point where the net moment of the inertial forces and the gravity forces along the axes parallel to the ground is equal to zero. If this point exists inside the area of the supporting foot during the single stance period or inside the supporting polygon during the double stance period, the robot will not fall. Figure 4.1 illustrates the ZMP concept.

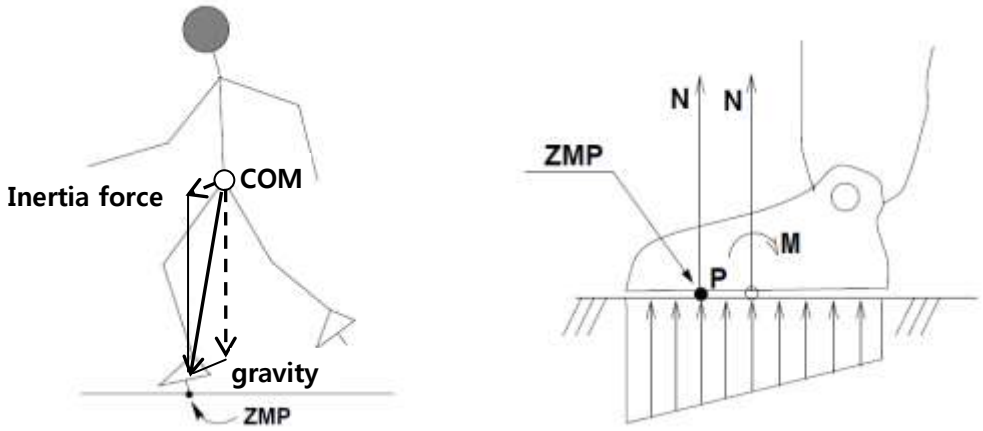

Figure 4.1 ZMP in a zero foot sole(Left), ZMP in a non-zero foot sole (Right)

The zero moment point can be calculated using D'Alambert's principle. According to D'Alambert's principle, the ZMP position vector P is subject to the constraint in Equation 4.1. Figure 4.2 is the concept diagram for ZMP.

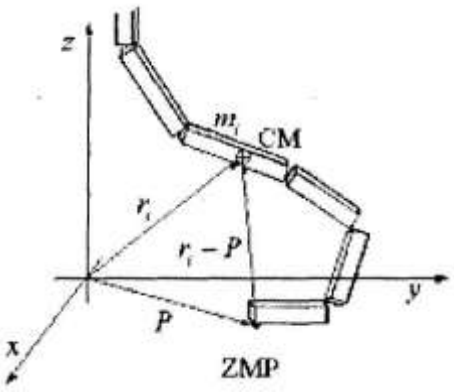

Figure 4.2 the concept diagram of ZMP

$$\sum_{i=1}^{n}\{m_i(r_i - P)\times(-\ddot{r}_i + G) - I_i\alpha_i - \omega_i \times I\omega_i\} = M_p \qquad \text{(Eq 4.1)}$$

m_i: concentrated mass at the center of mass of link *i*

r_i: position vector of the center of mass of link *i*

P : zero moment point

g : acceleration of gravity

I_i : moment of inertia

α_i : angular acceleration of link *i*

ω_i : angular velocity of link *i*

M_z : the z component of the moment at point P

Assuming that the angular acceleration and angular velocity are relatively small compared to other terms, we can approximate this equation as

$$\sum_{i=1}^{n}\{m_i(r_i - P)\times(-\ddot{r}_i + G)\} = M_p \qquad \text{(Eq 4.2)}$$

where,

$$r_i = [x_i, y_i, z_i]$$
$$P = P_{ZMP} = [x_{ZMP}, y_{ZMP}, 0]^T$$
$$G = [0, 0, -g]^T$$
$$M_p = M_{P,ZMP} = [0, 0, M_z]^T$$

From Equation 4.2 the ZMP position vector can be calculated as,

$$x_{ZMP} = \frac{\sum_{i=1}^{n} m_i(\ddot{z}_i + g)x_i - \sum_{i=1}^{n} m_i\ddot{x}_i z_i}{\sum_{i=1}^{n} m_i(\ddot{z}_i + g)}$$

$$y_{ZMP} = \frac{\sum_{i=1}^{n} m_i(\ddot{z}_i + g)y_i - \sum_{i=1}^{n} m_i\ddot{y}_i z_i}{\sum_{i=1}^{n} m_i(\ddot{z}_i + g)} \qquad \text{(Eq 4.3)}$$

4.2 Intuitive Walking Method with Sinusoidal Foot Movement

In the robot competitions such as Robocup, Robo-One and Robogames, there are a large number of miniature bipedal humanoid robots such as those shown in figure 4.3. The majority of these robots do not use academic walking methods such as ZMP. Instead, many humanoid robot hobbyists have utilized sinusoidal foot trajectories for many years with great success. Their walking algorithms command the trajectory of the feet to follow sine waves in the x, y and z directions. Once the three directional sine waves are combined, the robot begins to walk. The amplitudes, frequencies and phases are tweaked by trial and error. Although, most of these hobbyists do not use academic walking methods, their robots walk and run with great success.

The full-sized bipedal humanoid robot, CHARLI also uses this kind of sinusoidal foot trajectory planning. However, this research focuses on investigating why this method is successful and what relationship exists between the sinusoidal foot movement and the ZMP. Unlike hobbyist humanoid robots, CHARLI's walking algorithm can be said to be based on the ZMP method as well, because its sinusoidal foot trajectories are generated based on ZMP theory.

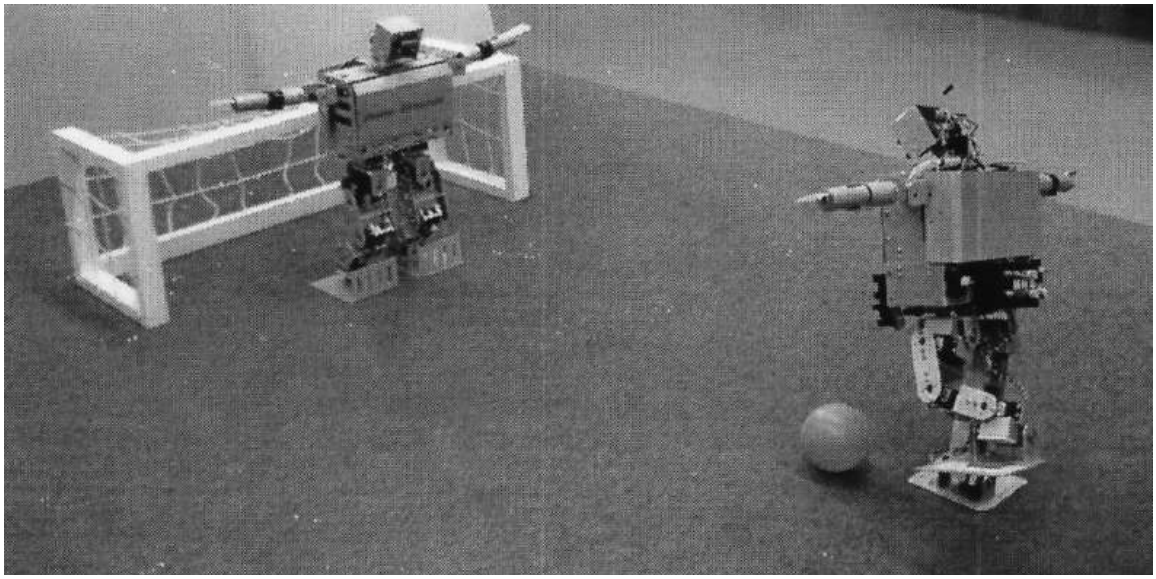

Figure 4.3 RoboCup competion [32]

4.3 Gate Generation

Gate generation based on the ZMP walking method starts from Equation 4.3 which shows the spatial relationship between ZMP and each mass.

$$x_{ZMP} = \frac{\sum_{i=1}^{n} m_i(\ddot{z}_i + g)x_i - \sum_{i=1}^{n} m_i \ddot{x}_i z_i}{\sum_{i=1}^{n} m_i(\ddot{z}_i + g)}$$

$$y_{ZMP} = \frac{\sum_{i=1}^{n} m_i(\ddot{z}_i + g)y_i - \sum_{i=1}^{n} m_i \ddot{y}_i z_i}{\sum_{i=1}^{n} m_i(\ddot{z}_i + g)} \qquad \text{(Eq. 4.3)}$$

The multiple particles system has to be used to calculate this Equation 4.3. However, it requires many calculations which make real-time computation hard. Therefore, CHARLI uses an inverted pendulum model to control and estimate ZMP instead of multiple particles. This allows for fast computation and easy estimation as well. [33]

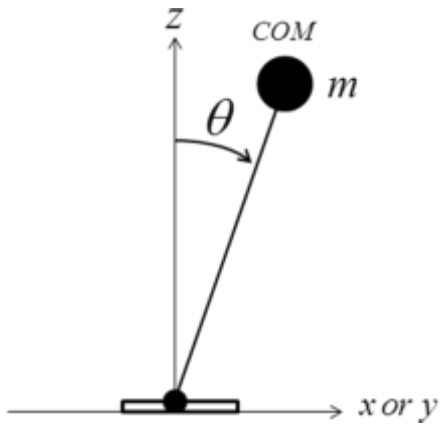

Figure 4.4 Inverted Pendulum Model

In the inverted pendulum model, all masses in Equation 4.3 can be thought of as one concentrated mass located at the center of mass, so the position values can be written as,

$$[x_i, y_i, z_i] = [x_{COM}, y_{COM}, z_{COM}] \qquad \text{(Eq. 4.4)}$$

Also, if we assume θ is so small ($\theta << 1$) that z directional differential term can be ignored. Thus, the equations of motion can be simplified as Equation 4.5.

$$x_{ZMP} = x_{COM} - \frac{z_{COM}}{g}\ddot{x}_{COM}$$
$$y_{ZMP} = y_{COM} - \frac{z_{COM}}{g}\ddot{y}_{COM} \qquad \text{(Eq. 4.5)}$$

These equations of motion give us a clue why simple sinusoidal foot movement works well for bipedal robot's walking, as mentioned in Section 4.2. The COM movement can be said to be the opposite movement of the feet, because they are in relative movement to each other. So the COM trajectories are,

$$x_{COM}(t) = -x_{foot}(t)$$
$$y_{COM}(t) = -y_{foot}(t) + y_{offset} \qquad \text{(Eq. 4.6)}$$

If both the feet and COM trajectories follow a sine function as shown below,

$$x_{COM}(t) = A_{x,COM}\sin(\omega t + \phi_x)$$
$$y_{COM}(t) = A_{y,COM}\sin(\omega t + \phi_y) \qquad \text{(Eq. 4.7)}$$

where, $A_{x,COM}, A_{y,COM}$: amplitudes of COM trajectories
ω : natural frequency of COM trajectory
ϕ_x, ϕ_y : phases of COM trajectory

the ZMP trajectory can be obtained from the equations of motion.

$$x_{ZMP}(t) = \left(1 + \frac{\omega^2}{\omega_n^2}\right)A_{x,COM}\sin(\omega t + \phi_x) = \left(1 + \frac{\omega^2}{\omega_n^2}\right)x_{COM}(t)$$
$$y_{ZMP}(t) = \left(1 + \frac{\omega^2}{\omega_n^2}\right)A_{y,COM}\sin(\omega t + \phi_y) = \left(1 + \frac{\omega^2}{\omega_n^2}\right)y_{COM}(t) \qquad \text{(Eq. 4.8)}$$

where, ω_n is the natural frequency of the pendulum $\omega_n = \sqrt{\frac{g}{z_{COM}}}$

Equation 4.8 shows the ZMP trajectories have the same form as that COM trajectories, when the COM trajectories are sinusoidal functions. The only difference is the amplitudes. The relationship between the amplitudes is,

$$A_{x,ZMP} = \left\{1+\left(\omega/\omega_n\right)^2\right\} A_{x,COM}$$
$$A_{y,ZMP} = \left\{1+\left(\omega/\omega_n\right)^2\right\} A_{y,COM} \qquad \text{(Eq. 4.9)}$$

Equation 4.9 tells us several features about bipedal walking. First, the ZMP amplitude of ZMP gets larger as the robot moves faster. Thus, if the robot is required to walk fast, its COM amplitudes should be small. Second, if the frequency is relatively small compared to the robot's natural frequency, such that ω/ω_n approaches zero, the ZMP trajectories are almost the same as the COM trajectories. This scenario describes the static walking case. Third, a low COM position makes the ZMP amplitude smaller, so a low COM can increase stability.

Based on these equations, simple sinusoidal functions were used to generate a gait. Figure 4.5 shows the trajectory of CHARLI's feet with respect to the COM position.

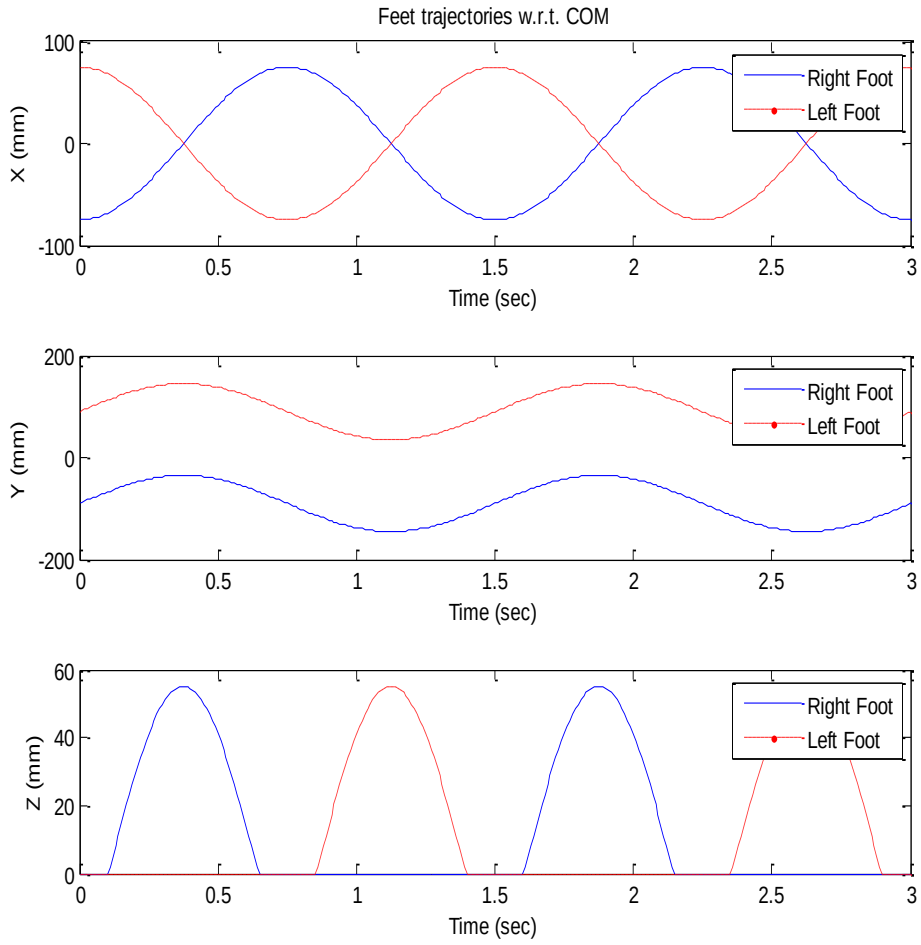

Figure 4.5 The feet trajectories with respect to COM position

Figure 4.6 shows the feet and COM movement with respect to the global coordinate.

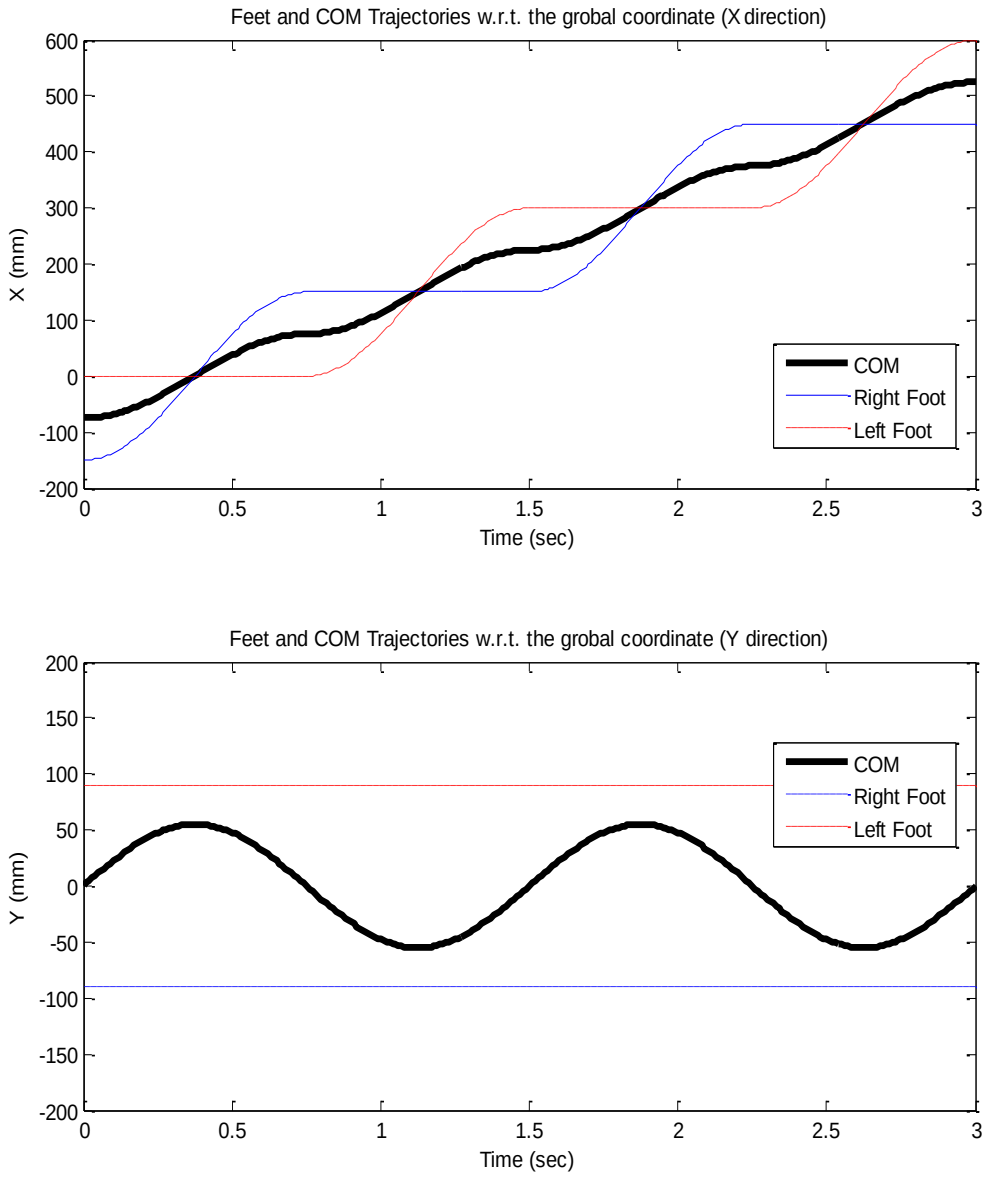

Figure 4.6 the feet and COM trajectories with respect to the global coordinate

By combining the x and y position of COM and the ZMP calculated using Equation 4.3, we can obtain Figure 4.7 The rectangular shape of Figure 4.6 shows the footprints and the dotted lines represent ZMP in the single stance status.

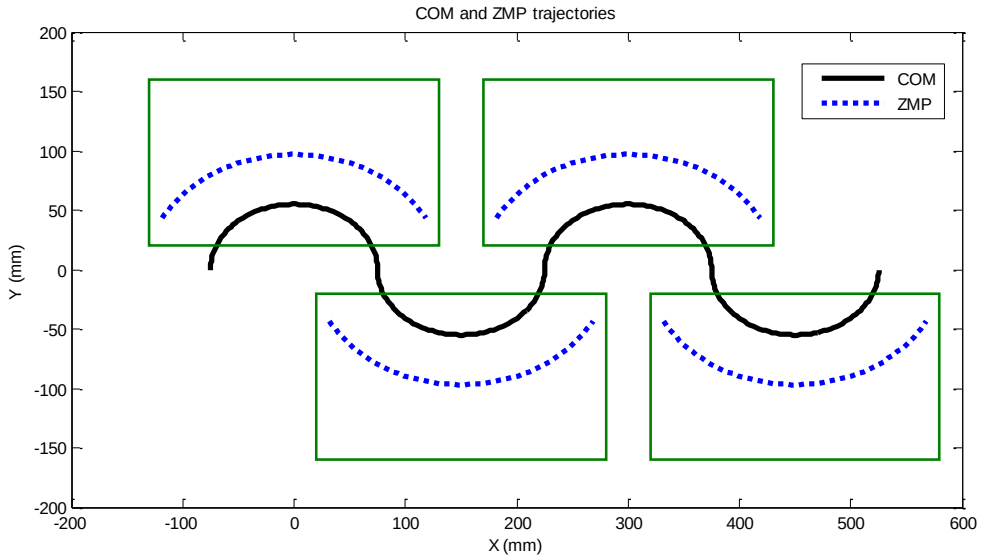

Figure 4.7 COM and ZMP trajectories in x-y plane with respect to the global coordinate (forward walking)

In sum, we can control the feet trajectories and know the relationship between the feet trajectories and ZMP. In other words, we can estimate ZMP and control it through the control of feet trajectories.

Furthermore, adding one more sinusoidal curve to the yaw angle of feet allows CHARLI to make turn. Figure 4.8 shows how to generate the angle.

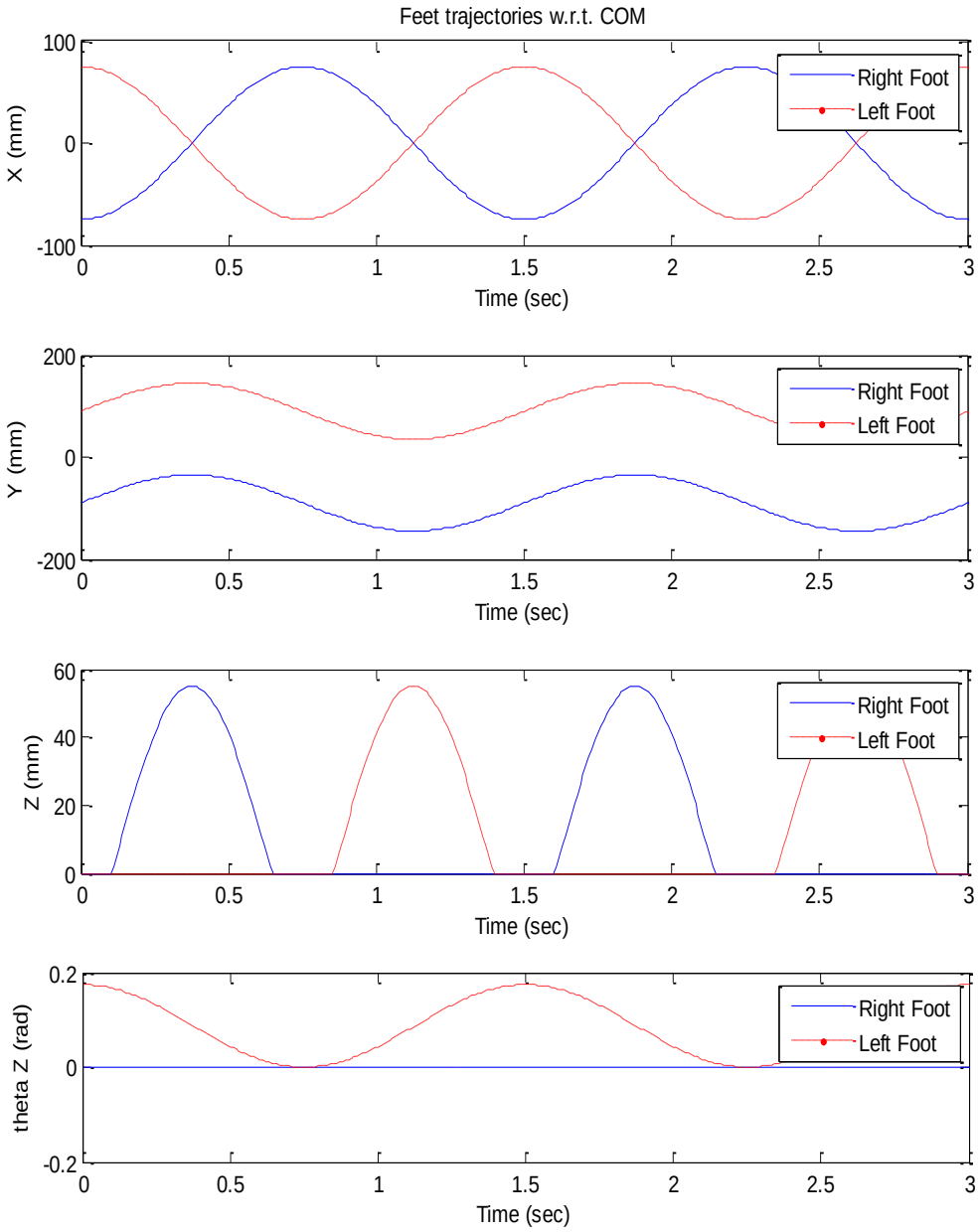

Figure 4.8 the feet and COM trajectories with respect to the global coordinate

However, the feet trajectories made by one sinusoidal function are not good enough to make smooth walking pattern. It should be made by combinations of more sinusoidal functions of which frequencies are two or four times bigger than main sinusoidal function.

The key point of X directional movement is to make left and right foot move together in double stance status. If both leg move against each other in double stance, the actuators of each leg will make forces against each other, which causes an actuator failure.

Figure 4.9 shows the x directional feet trajectories, when two more sinusoidal functions are added. It shows right and left leg move together during double stance period, 0.25sec~0.5sec, 1.0sec~1.25sec, 1.75sec~2.0sec, 2.5sec~2.75sec.

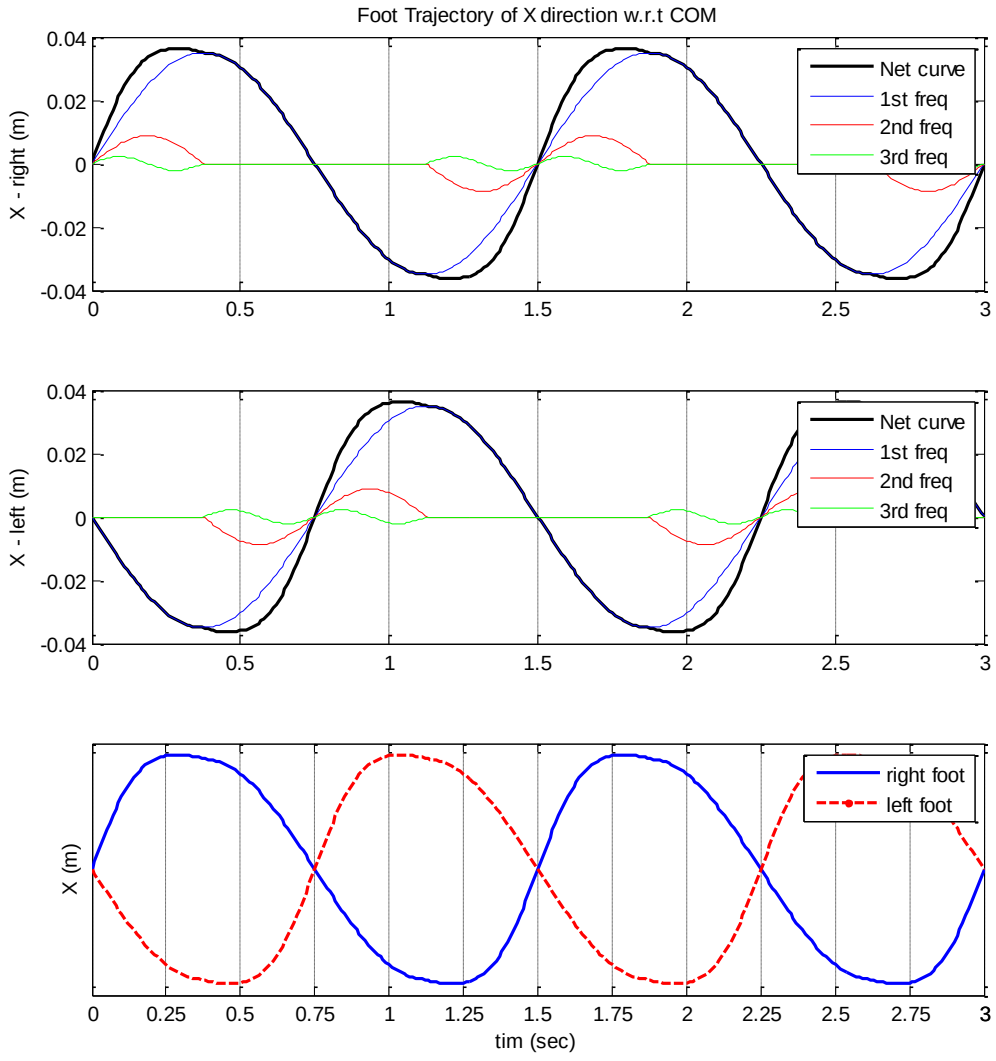

Figure 4.9 The X directional feet trajectories adding two more sinusoidal curves (Right leg (top), Left leg (middle), combination of two legs(down))

Unlike X directional movement, Y directional sinusoidal curves of both legs always move together. However, if the hip roll actuator of the stance leg cannot resist the weight of upper body and the other swing leg in the single stance status, the swing leg will hit the stance leg. Adding one more sinusoidal curve can solve this problem. Figure 4.10 show how to add one more sinusoidal curve to avoid this risk. However, if the actuator is strong enough, this function may not be useful.

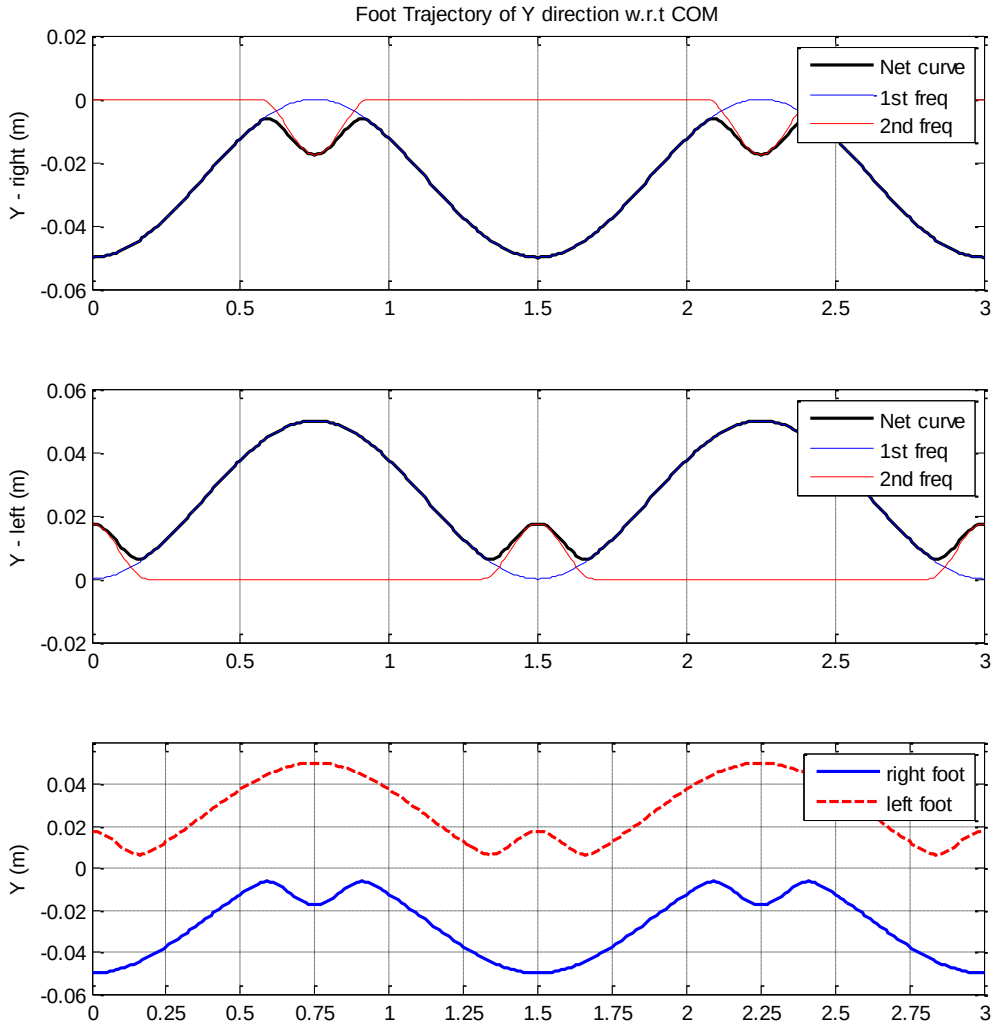

Figure 4.10 The Y directional feet trajectories adding one more sinusoidal curve (Right leg (top), Left leg (middle), combination of two legs(down))

The main issue of Z directional movement is the shock absorption. If there are not any physical errors during walking, we don't have to worry about the shock, when the leg strikes the ground. However, realistically, there are a lot of disturbances to make errors, so the shock would happen. For this reason, it will be good choice to make a movement which can absorb shocks.
Figure 4.11 shows how to add the second and the third sinusoidal curve to absorb shocks. When the leg hits the ground, which means the end of single status, the both legs lift up together. Then, the hitting shock can be absorbed by this movement.

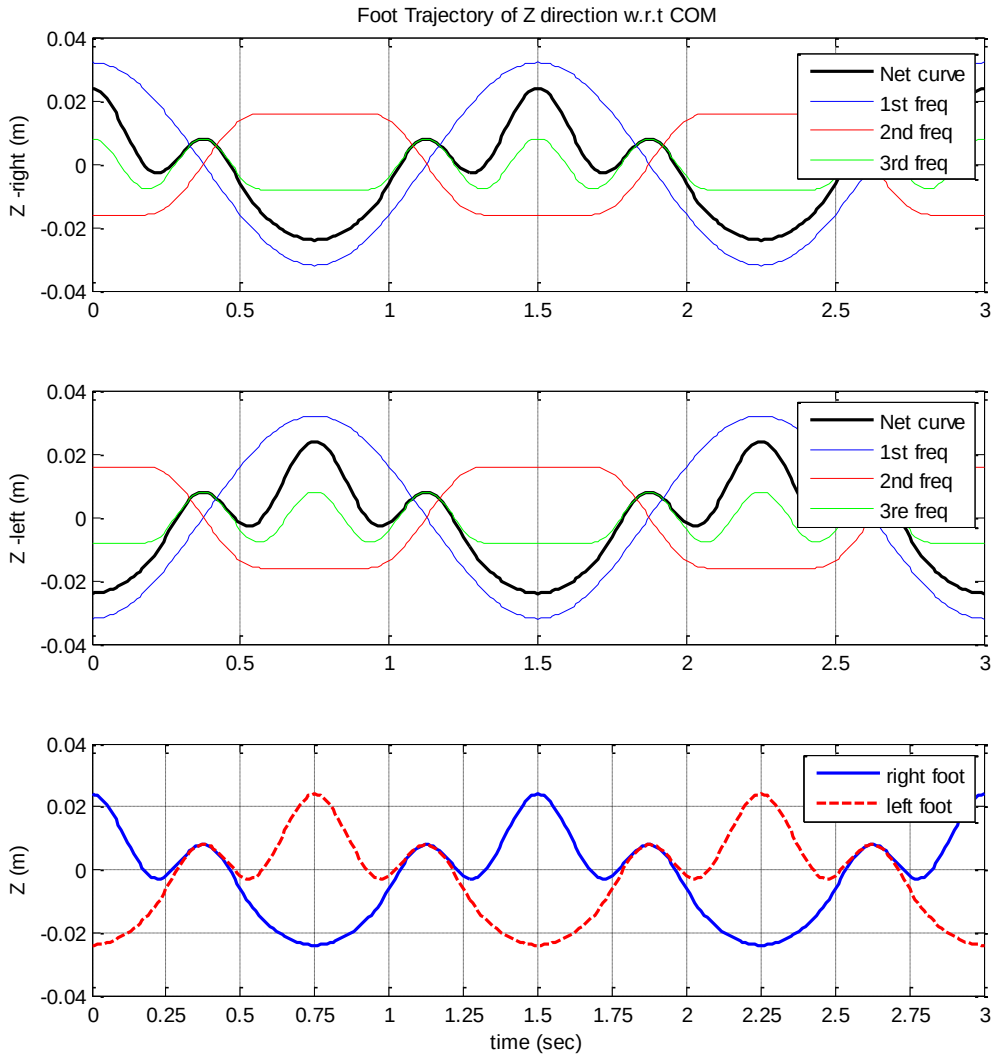

Figure 4.11 The Z directional feet trajectories adding two more sinusoidal curves (Right leg (top), Left leg (middle), combination of two legs(down))

4.4 Stabilization

Although ZMP is controllable, it is often insufficient for large unpredictable disturbances during walking. In the event of uneven terrain, the actual foot angle would be different from the expected angle. The result is unexpected acceleration and disturbance of the COM position which could move the ZMP outside of the feet. Disturbances could also come externally such as a push or collision with another object. Thus, a robot must be capable of compensating for physical disturbances.
To compensate for disturbances and correct the position of the COM, CHARLI has a feedback loop as shown in Figure 4.12 The compensator is based on sensing the angular velocity from inertial measurement unit. (IMU). The feedback loop adjusts the desired angles for each joint based on the IMU readings. Since the data is given as angular velocity, the compensator acts as a differential (D) controller. During normal walking the angular velocity readings are small but rapidly increase in the event of a disturbance so a controller based on these readings is very effective in sensing and compensating or disturbances. Appropriate gains are found through experimentation and tuning.

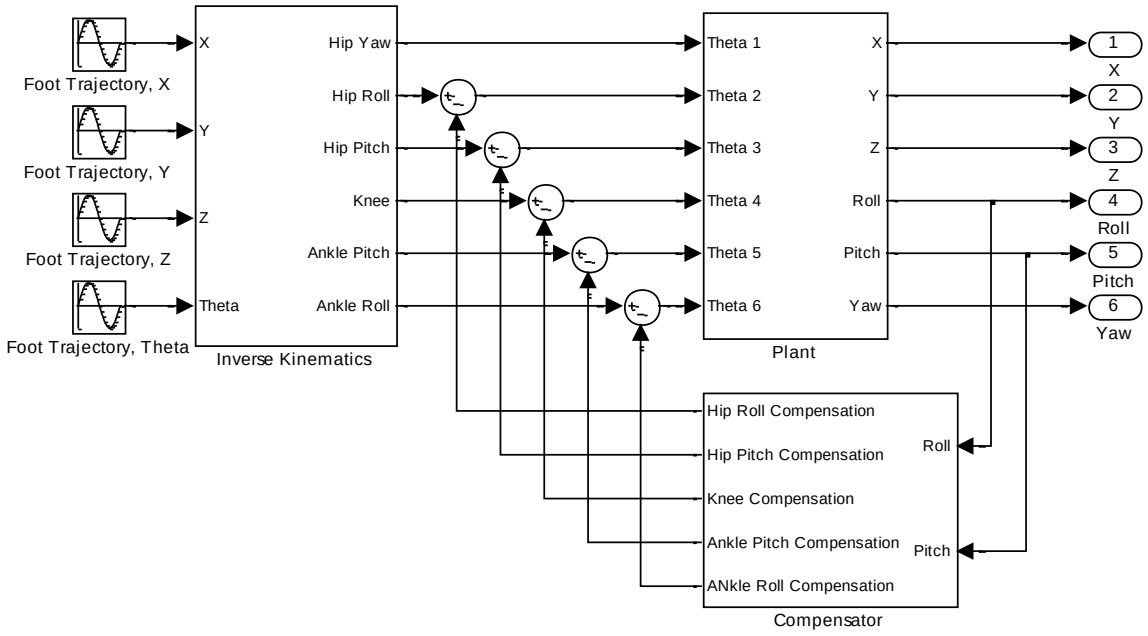

Figure 4.12 Block Diagram for CHARLI's position control

Section 5 Simulation for Bipedal Walking

A simulation of the dynamic performances of a full-sized humanoid robot is one of the crucial processes of its development, because all major factors are coupled each other and hard to estimate intuitively, so they must be estimated using simulation before being fabricated. Therefore, a successful simulation is one of the key elements of a successful robot. In this chapter, the simulation model and its results will be introduced.

5.1 Developing a Simulation Model

The simulation model for bipedal walking was made based on the gate generation introduced in Chapter 4. Figure 5.1 shows the concentrated mass and link model used for CHARLI's walking.

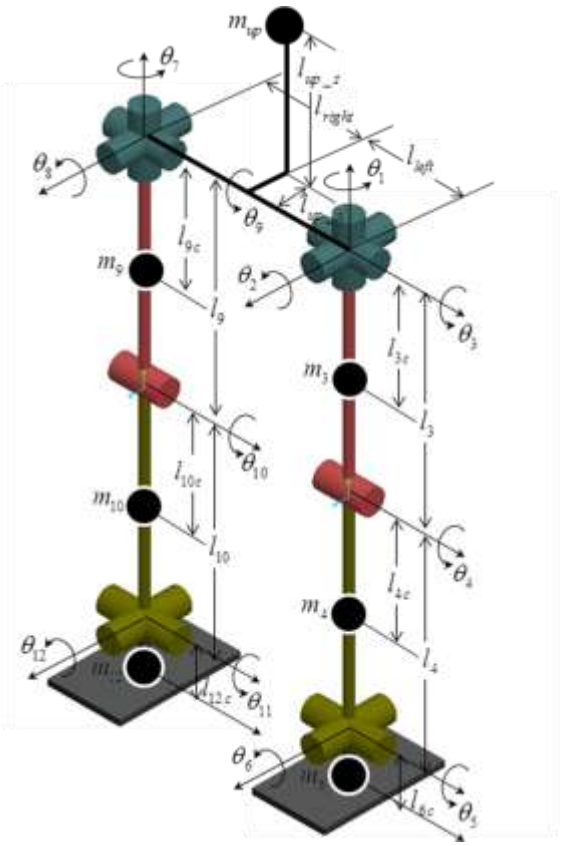

Figure 5.1 The simulation model consisted of links and concentrated masses for CHARLI's bipedal walking

The weights of the concentrated masses and respective quantities used for CHARLI's simulations are shown in Table 5.1. Also, Table 5.2 shows the moment of inertia of each concentrated mass. All products of inertias are less than 10 percent of their moment of inertias, so they are disregarded in the walking simulation.

Table 5.1 The weight of each mass

Name		Mass (kg)	Quantity	total (kg)
Thigh		1.729	2	3.458
Shin		0.783	2	1.566
Foot		0.886	2	1.772
Upper Body	Torso	3.565	1	3.565
	Upper arm	0.372	2	0.744
	Forearm	0.411	2	0.822
	Head	0.212	1	0.212
	sub total	-	-	5.343
Total				12.139

Table 5.2 The moment of inertia of each mass

Name		Inertia at COM (kg m^2)		
		Ixx	Iyy	Izz
Thigh		0.020246	0.021065	0.001386
Shin		0.011036	0.011152	0.000296
Foot		0.001189	0.003119	0.003056
Upper Body	Torso	0.076047	0.069303	0.018555
	Upperarm	0.000725	0.000726	0.000184
	Forearm	0.002315	0.002329	0.000125
	Head	0.000395	0.000463	0.000181
	Total	0.327499	0.264866	0.076876

Figures from 5.2 to 5.5 show the geometrical shapes of each mass and the type of joints.

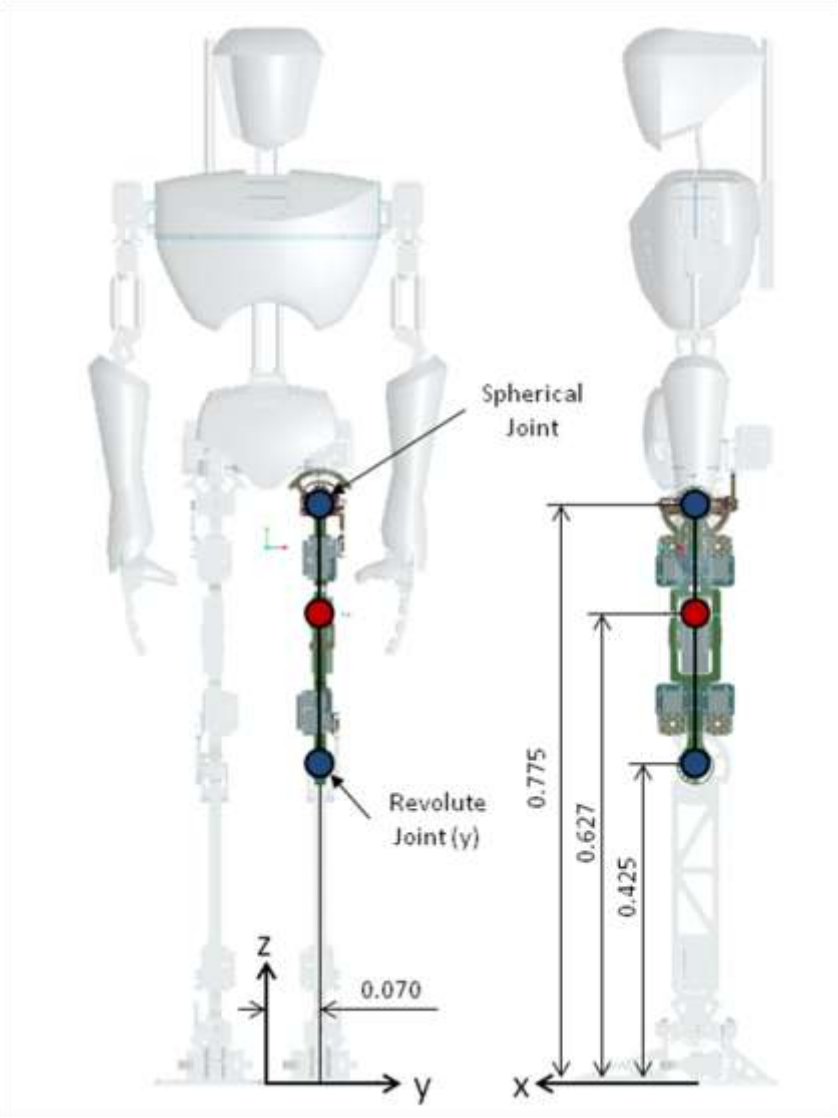

Figure 5.2 The geometrical shapes and the joint type of the thigh

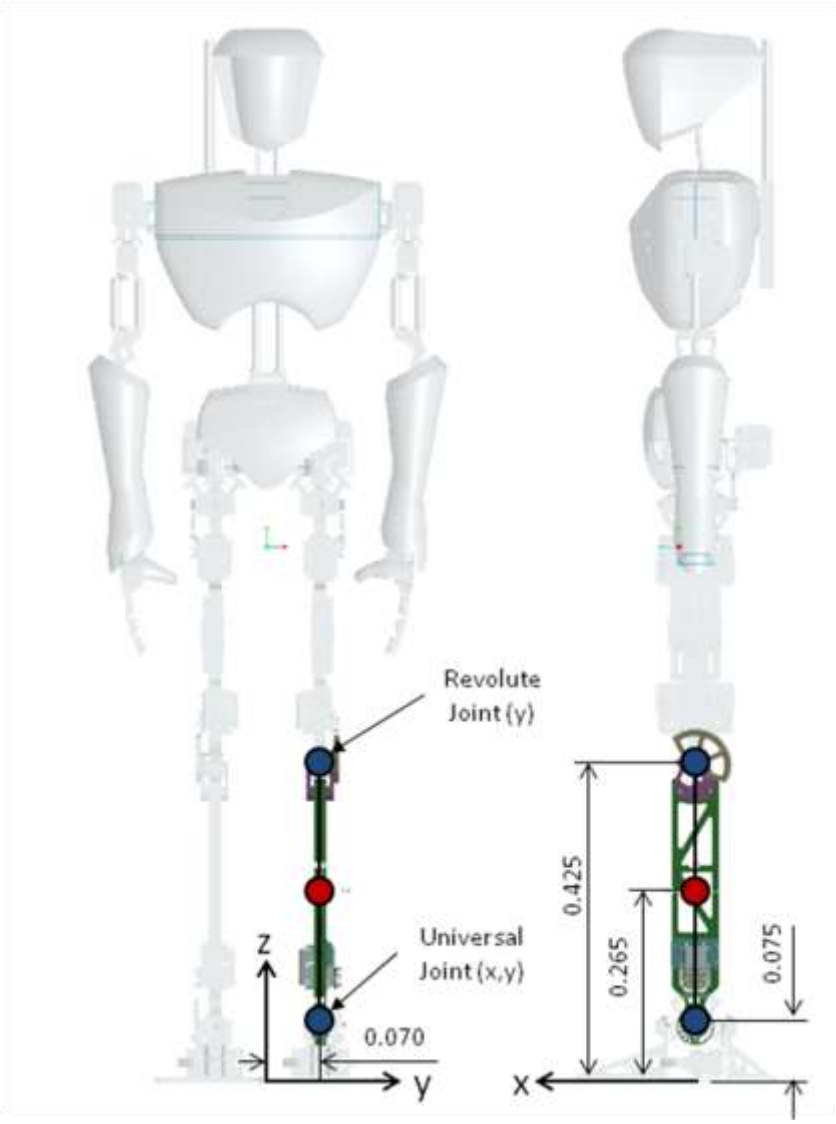

Figure 5.3 The geometrical shapes and the joint type of the shin

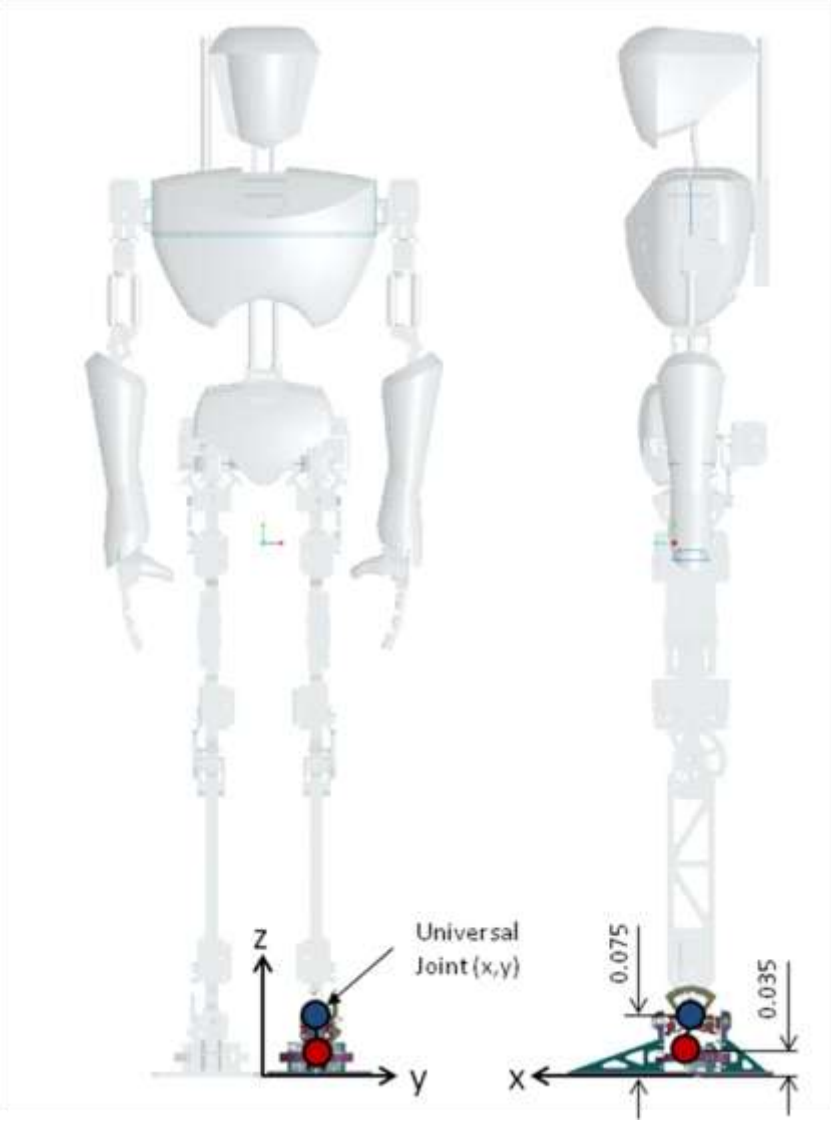

Figure 5.4 The geometrical shapes and the joint type of the foot

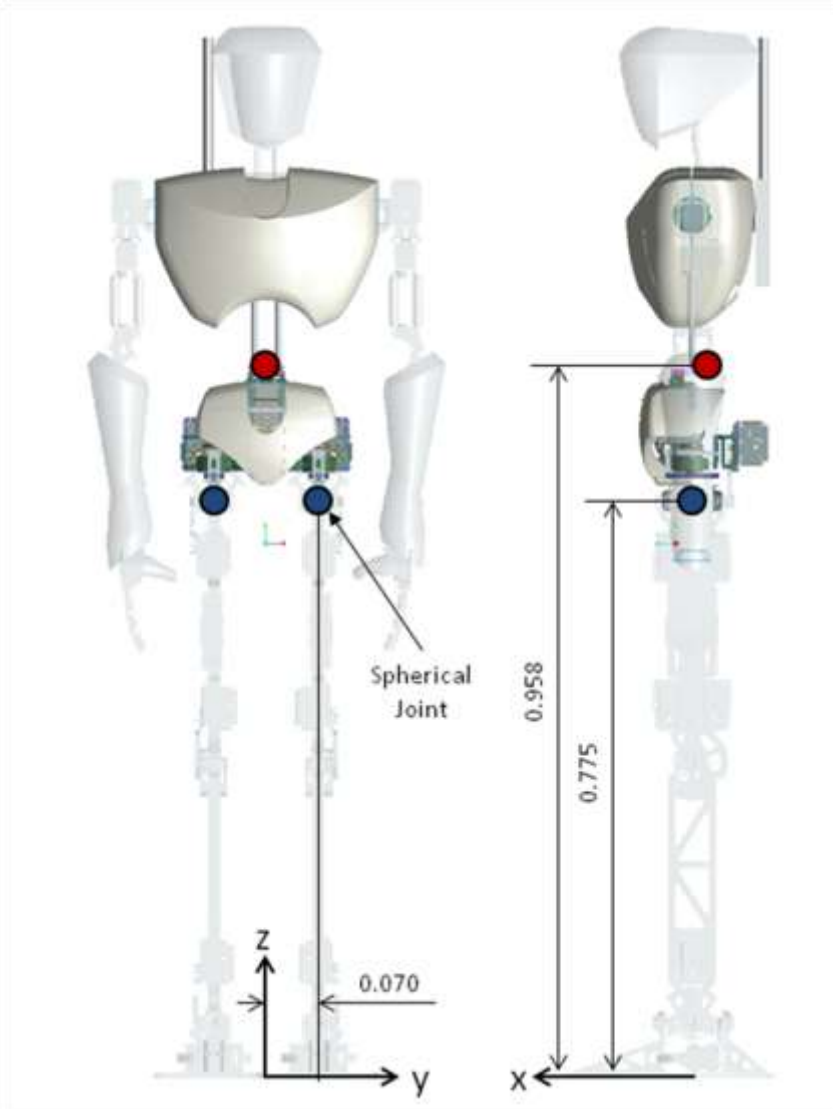

Figure 5.5 The geometrical shapes and the joint type of the upper body

5.2 Simulation for Bipedal walking method

One of the main goals of simulation is to figure out the appropriate parameter values such as the amplitudes of each sinusoidal curve, walking frequency and step size. The term 'appropriate' could mean many things, but mostly it means 'to not fall down during walking' in this chapter. In other word, it can be said whether ZMP is located in the feet area or not.

MATLAB was used for the bipedal walking simulations and Figure 5.6 shows the feet trajectories used for the bipedal walking simulation.

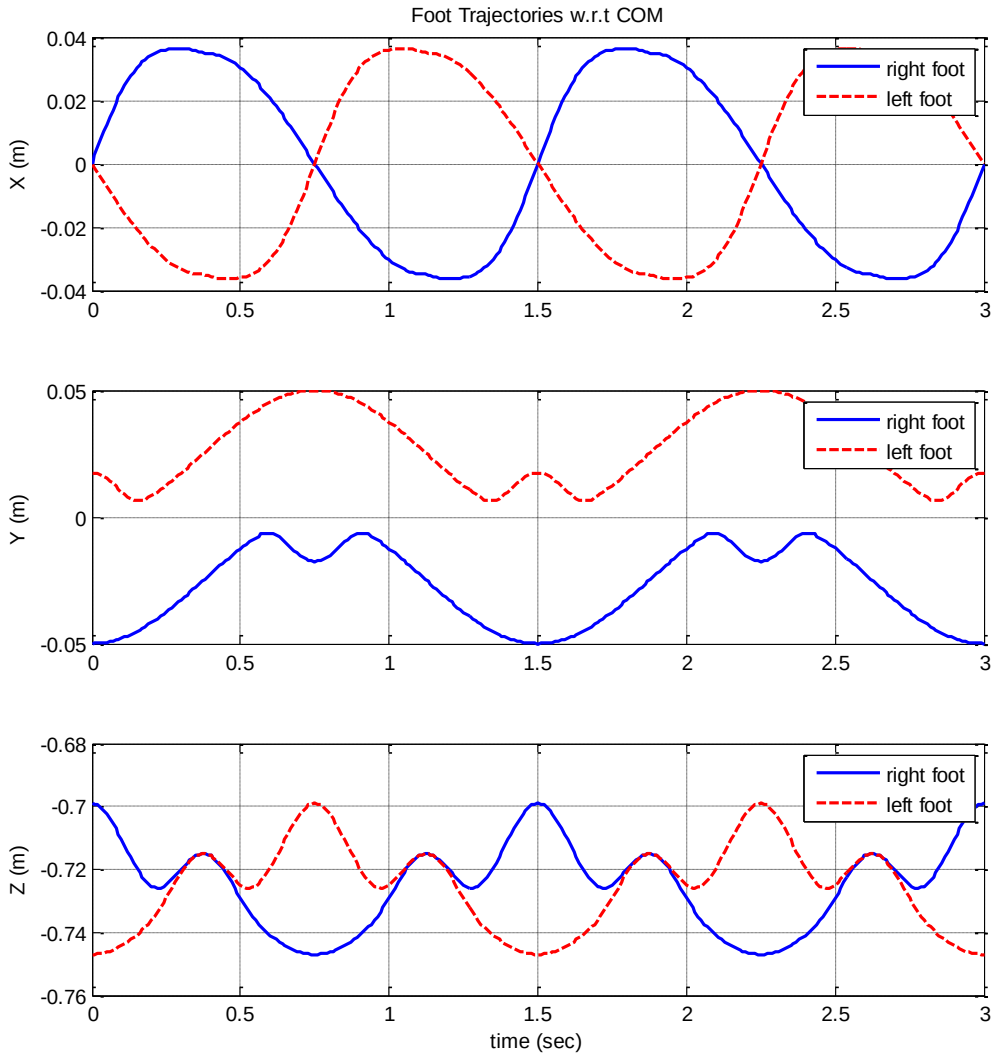

Figure 5.6 Feet trajectories used for the bipedal walking simulation
(X direction (top), Y direction (middle), Z direction (down))

Based on the feet trajectories, the trajectory of the origin of CHARLI's body can be calculated by the bipedal walking simulation. The result is shown in Figure 5.7.

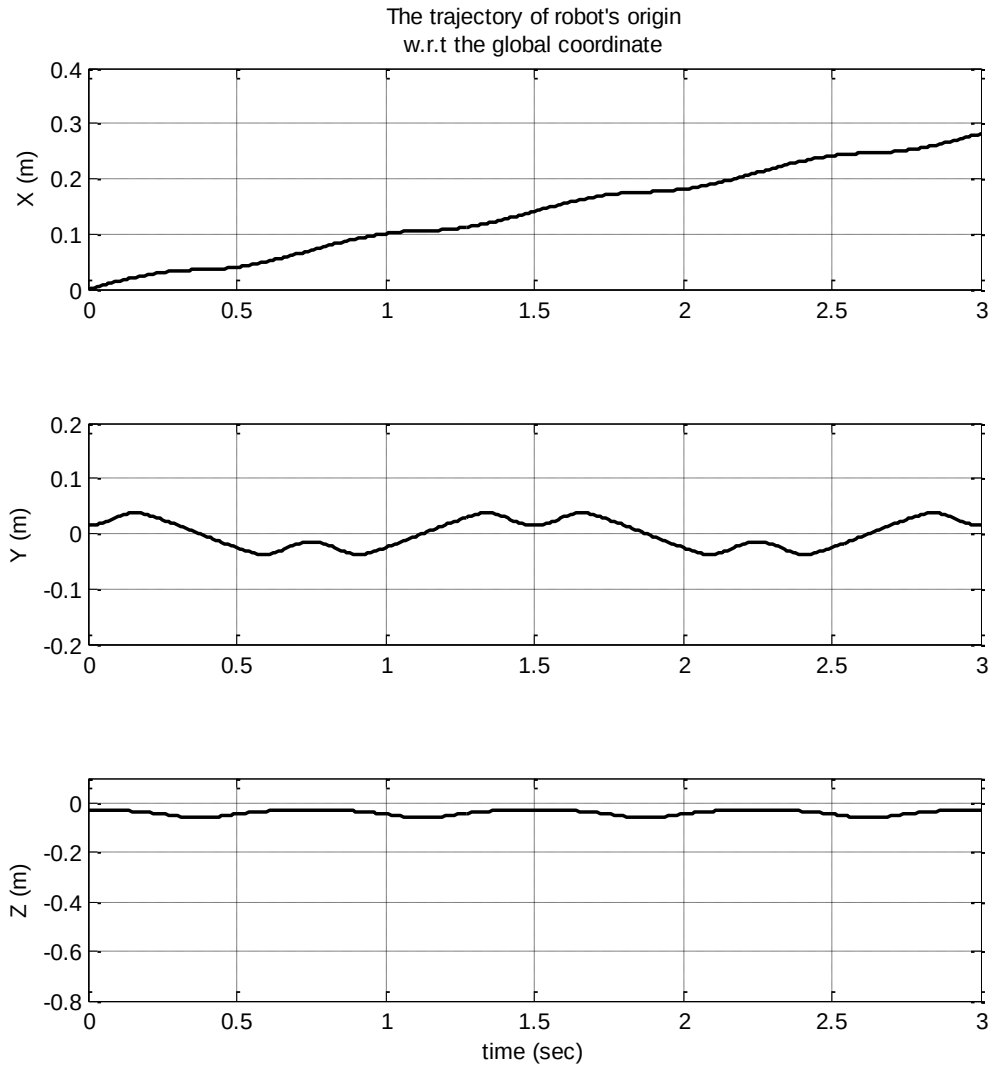

Figure 5.7 The trajectories of CHARLI's origin with respect to the global coordinate (X direction (top), Y direction (middle), Z direction (down))

The next step is to figure out the trajectories of each mass. The angle of each joint can be obtained by the inverse kinematics of the feet trajectories. Then, the trajectories of each mass can be calculated by the forward kinematics of the angle of joints which is figured out from the inverse kinematics. Figure 5.8 and 5.9 show the trajectories of each mass.

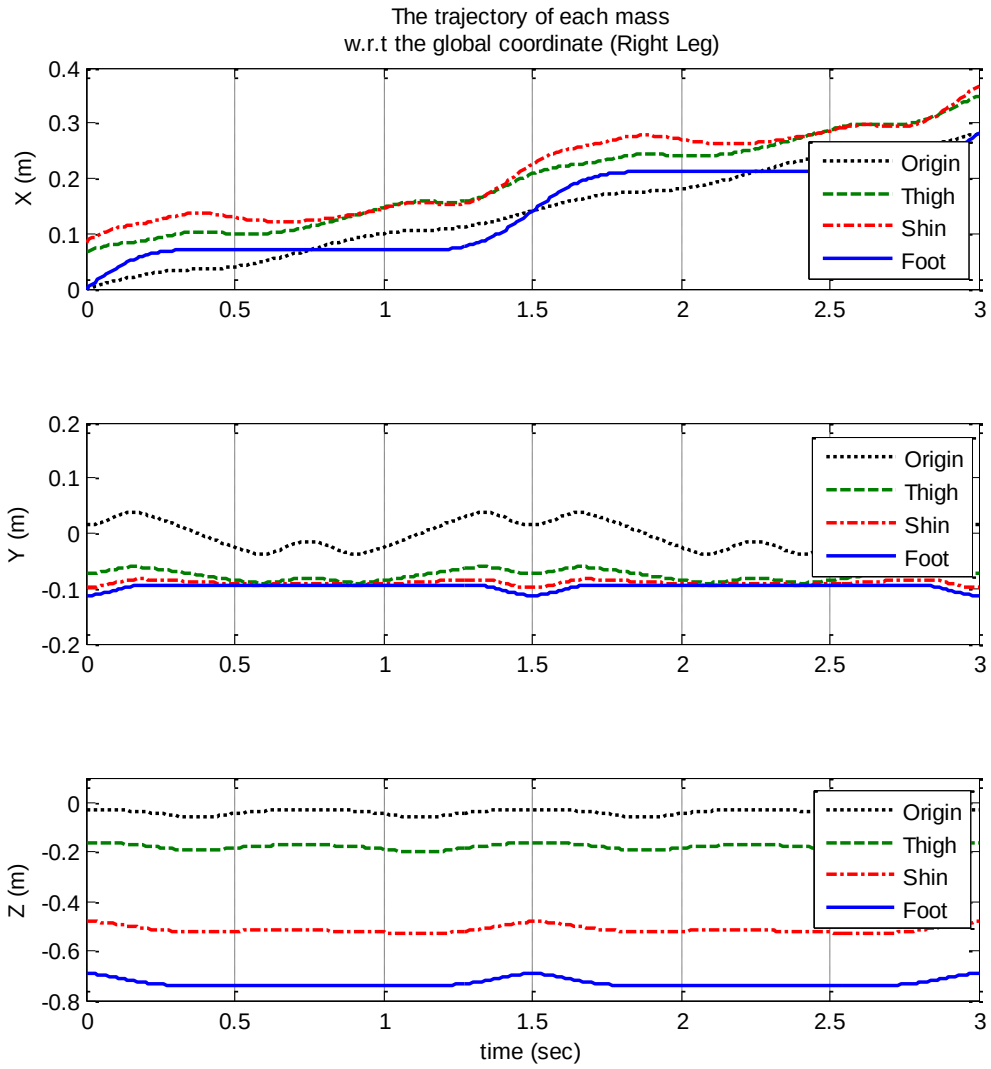

Figure 5.8 The trajectories of each mass of right leg with respect to the global coordinate (X direction (top), Y direction (middle), Z direction (down))

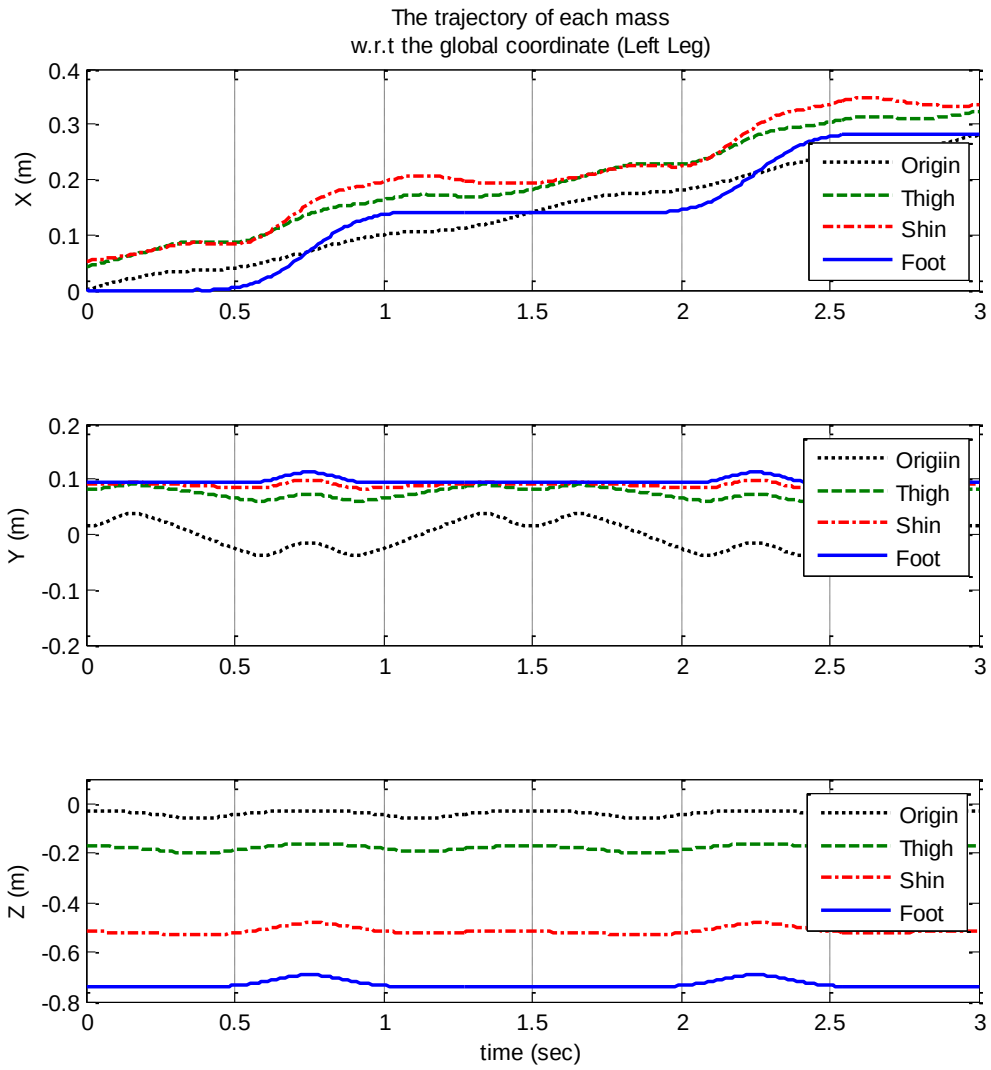

Figure 5.9 The trajectories of each mass of left leg with respect to the global coordinate (X direction (top), Y direction (middle), Z direction (down))

The trajectories of the COM can be calculated by the summation of positions of all masses. Equation 5.1 shows how to calculate it. Figure 5.10 shows its result.

$$X_{com} = \frac{\sum_{i=1}^{n}(x_i m_i)}{m_{total}}$$

$$Y_{com} = \frac{\sum_{i=1}^{n}(y_i m_i)}{m_{total}} \qquad \text{(Eq. 5.1)}$$

$$Z_{com} = \frac{\sum_{i=1}^{n}(z_i m_i)}{m_{total}}$$

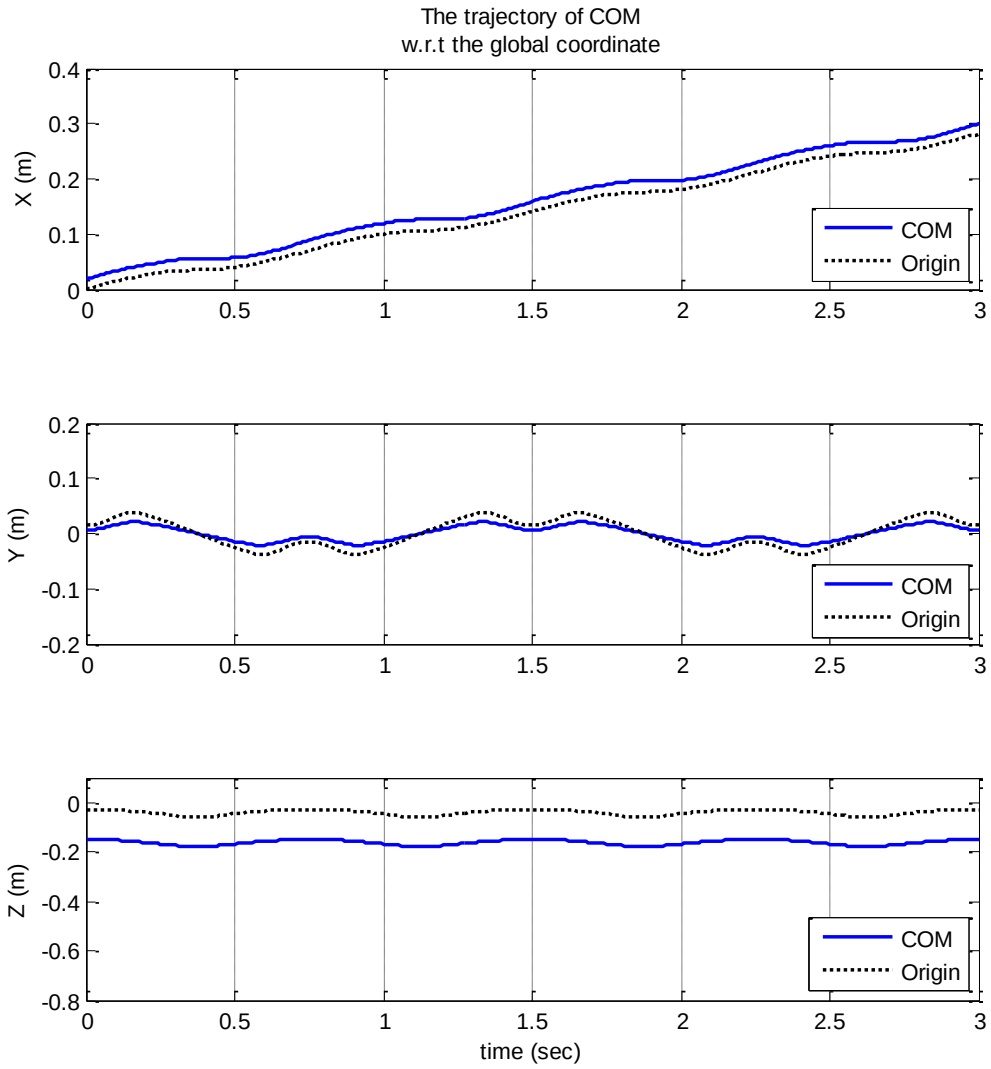

Figure 5.10 The trajectories of COM with respect to the global coordinate
(X direction (top), Y direction (middle), Z direction (down))

Figure 5.11 and 5.12 shows the trajectory of COM and origin in XY plane and XZ plane respectively.

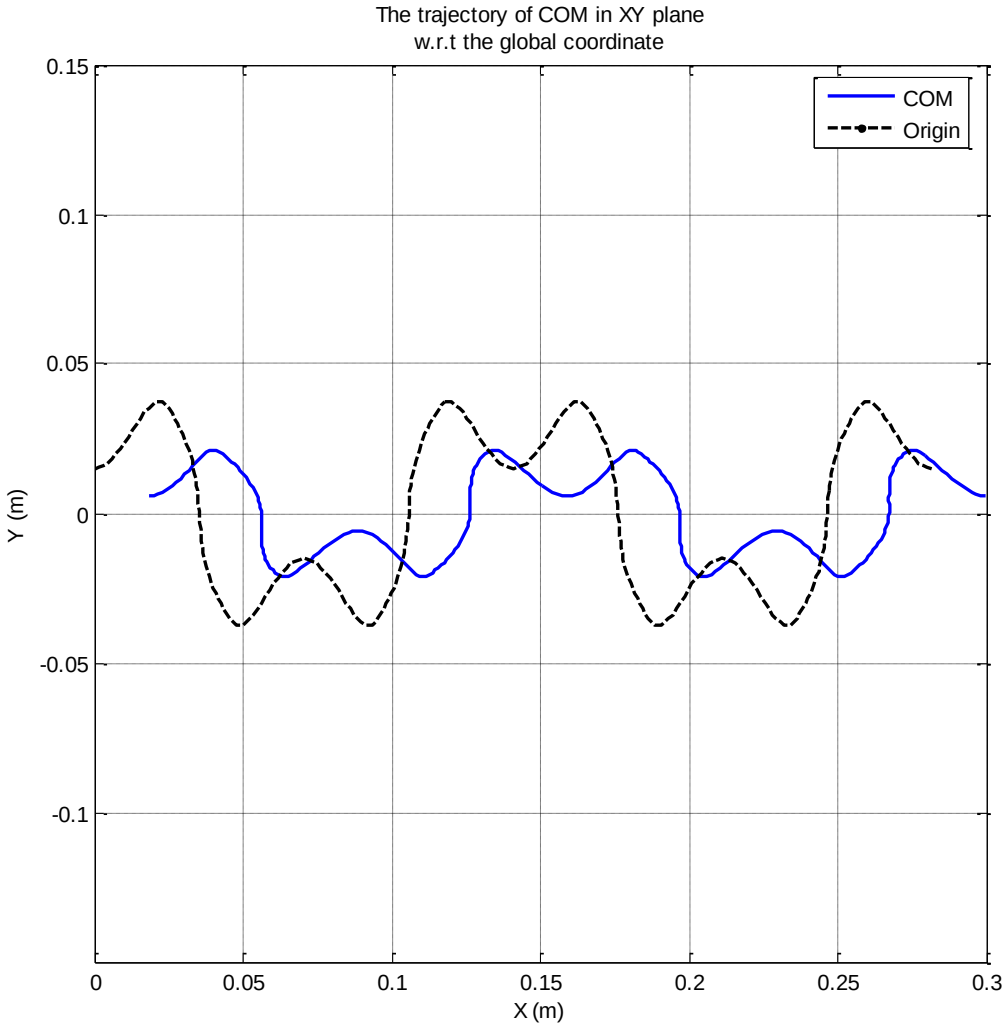

Figure 5.11 The trajectories of COM and ZMP in XY plane

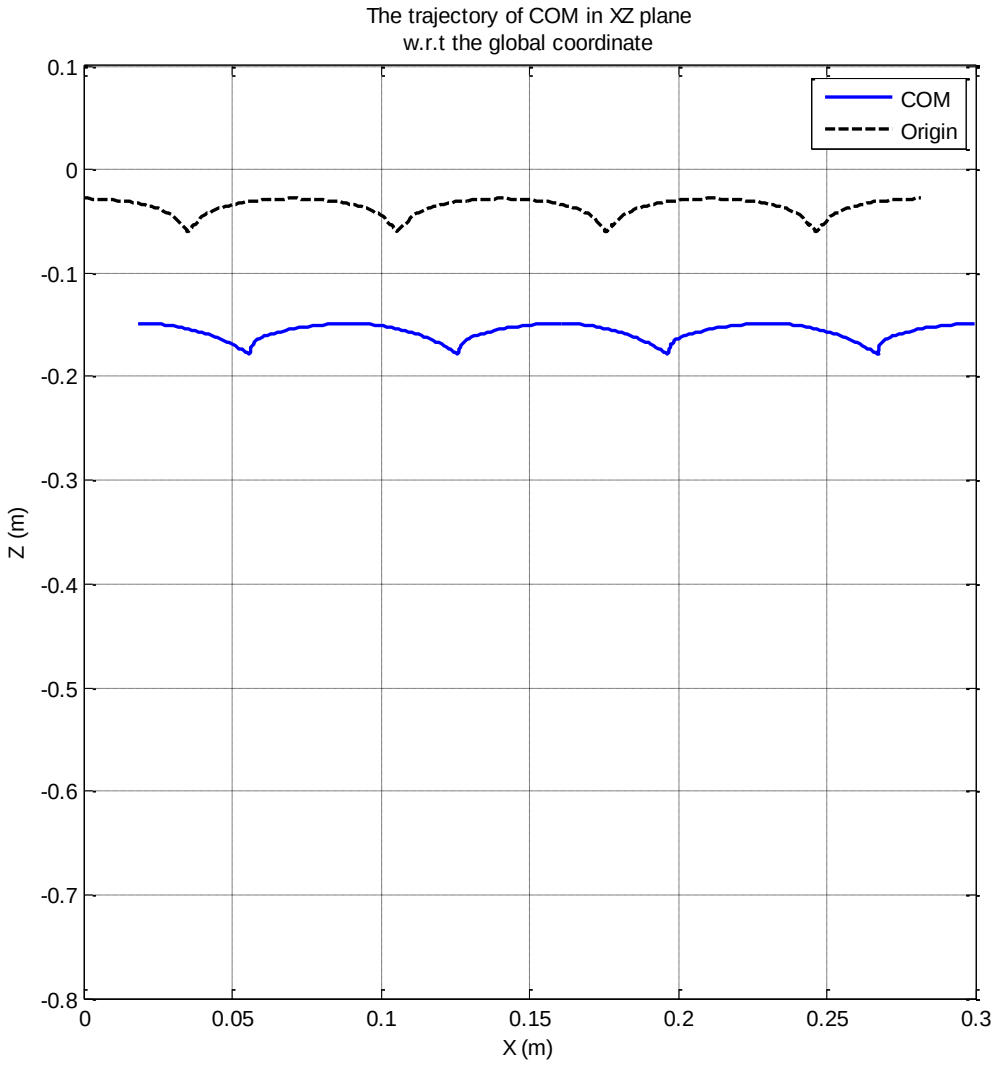

Figure 5.12 The trajectories of COM and ZMP in XZ plane

This result can be shown in 3D space like Figure 5.13.

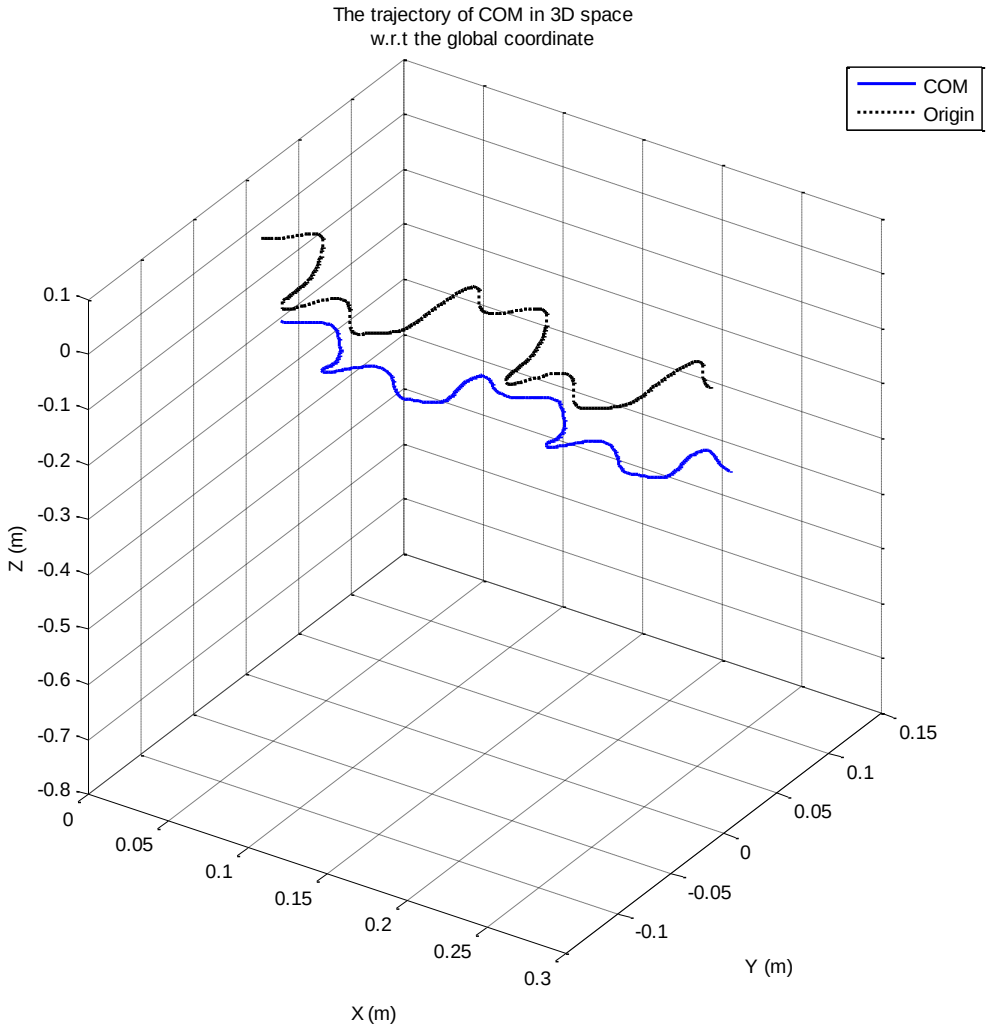

Figure 5.13 The trajectories of COM and ZMP in 3D space.

Based on the trajectories of the COM, the trajectories of the ZMP can be obtained by Equation 4.3. Figure 5.14 shows the trajectory of the COM and the ZMP in XY plane. The rectangular shape of this figure shows the footprints. In this simulation, the second sinusoidal curve in the Y direction was eliminated, because it forces the ZMP outside of the feet area.

In summary, we can expect these walking values would make CHARLI walk without falling, because the ZMP is located in the feet area.

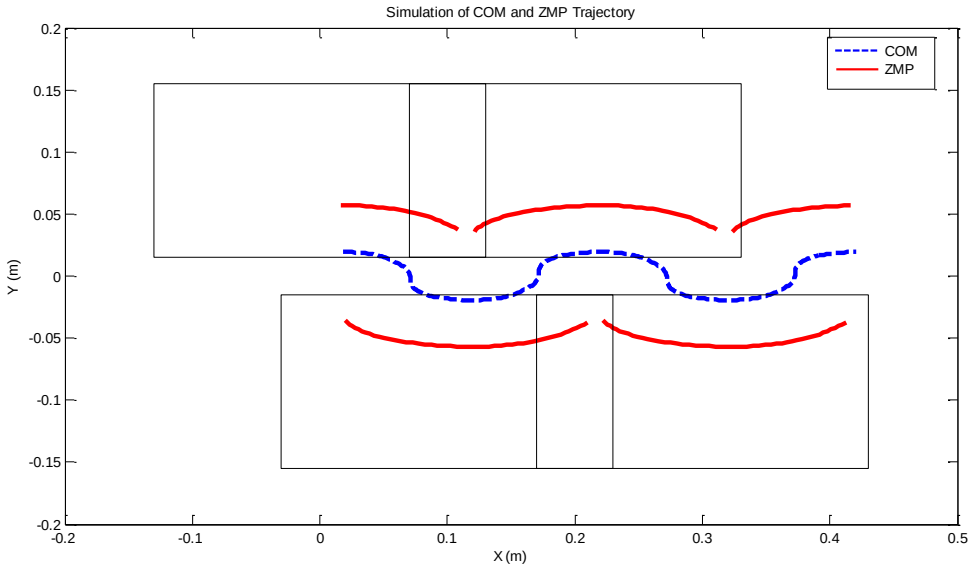

Figure 5.14 COM and ZMP trajectories in XY plane
(Forward walking)

5.3 Simulation for Dynamic Performances

The dynamic simulation is no less important than the bipedal walking simulation. Its main purpose is to figure out the torque requirements of the joints to walk with a certain speed. In other words, the bipedal walking simulation is for figuring out whether a robot falls down or not, while the dynamic simulation is for figuring out how much torque the joints need.

The dynamic simulation starts with calculating angular velocity, and angular acceleration of each joint. They can be obtained by the differentiation of the joint angle which is calculated by inverse kinematics. Figures from 5.15 to 5.19 show the angular velocity, and angular acceleration of each joint.

.

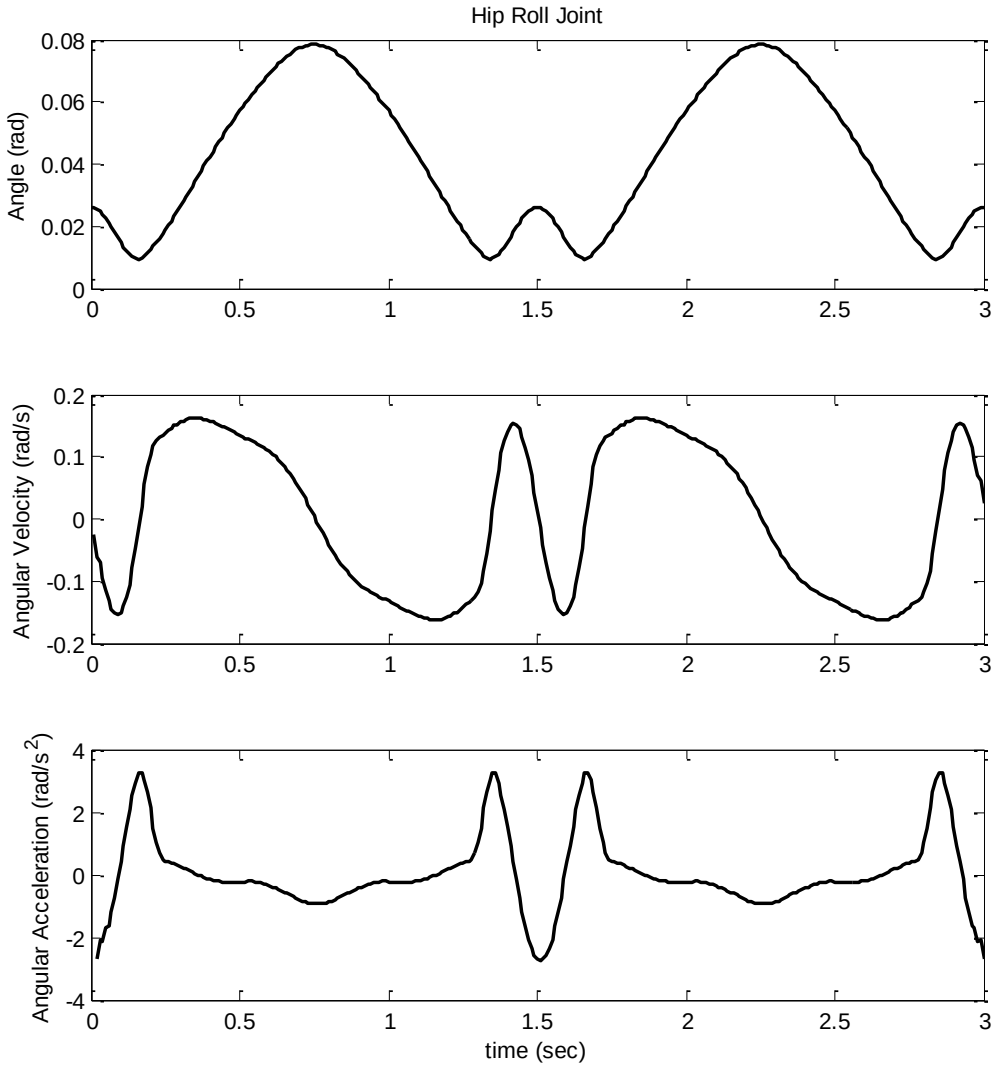

Figure 5.15 Angle (top), Angular velocity (middle) and Angular acceleration (down) of Hip Roll joint

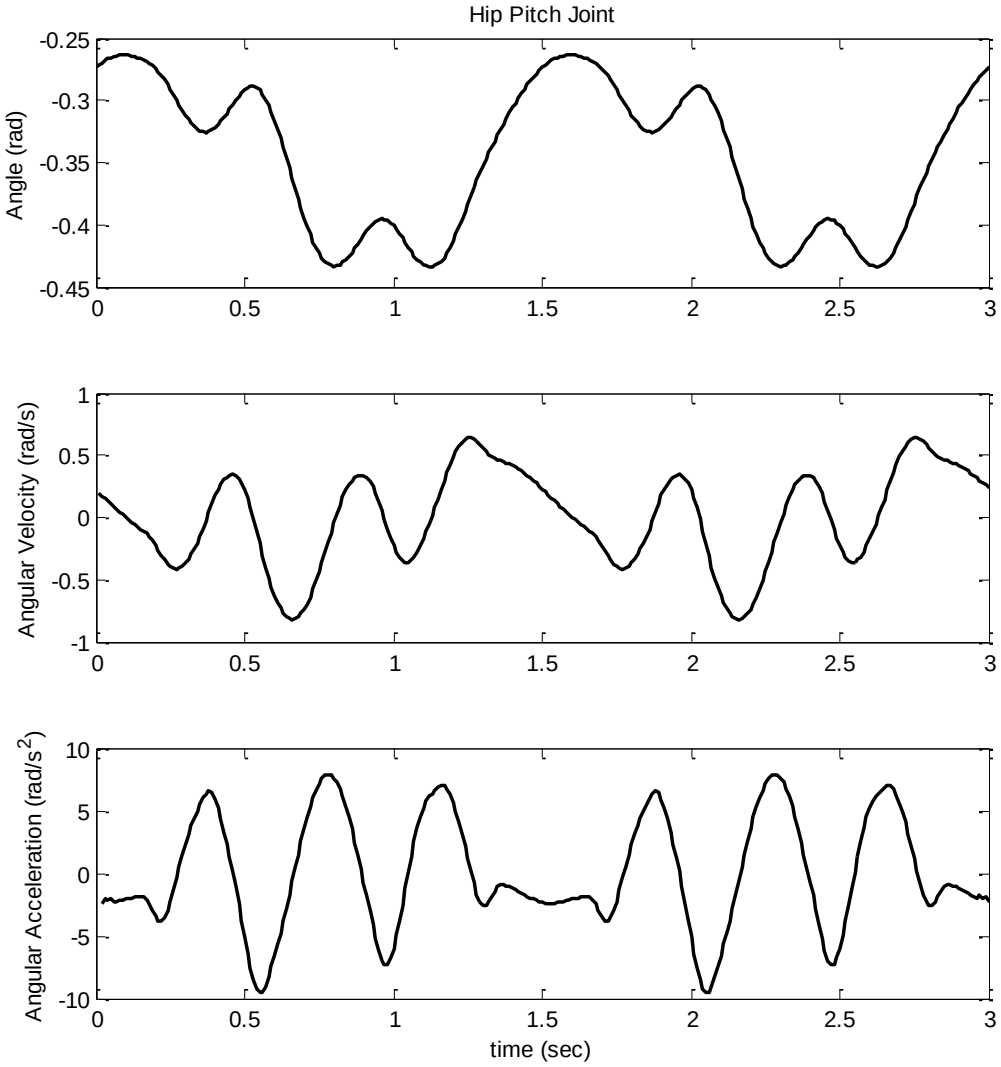

Figure 5.16 Angle (top), Angular velocity (middle) and Angular acceleration (down) of Hip Pitch joint

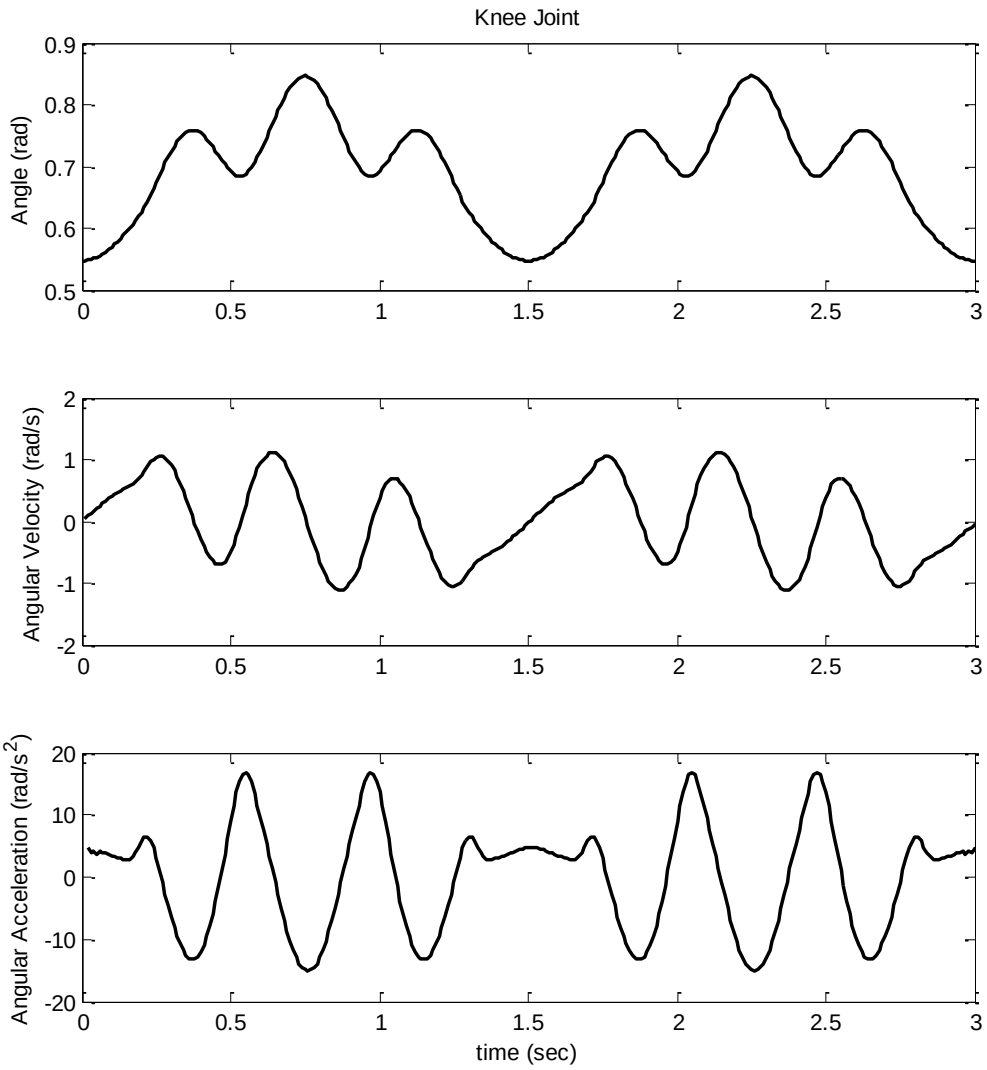

Figure 5.17 Angle (top), Angular velocity (middle) and Angular acceleration (down) of Knee joint

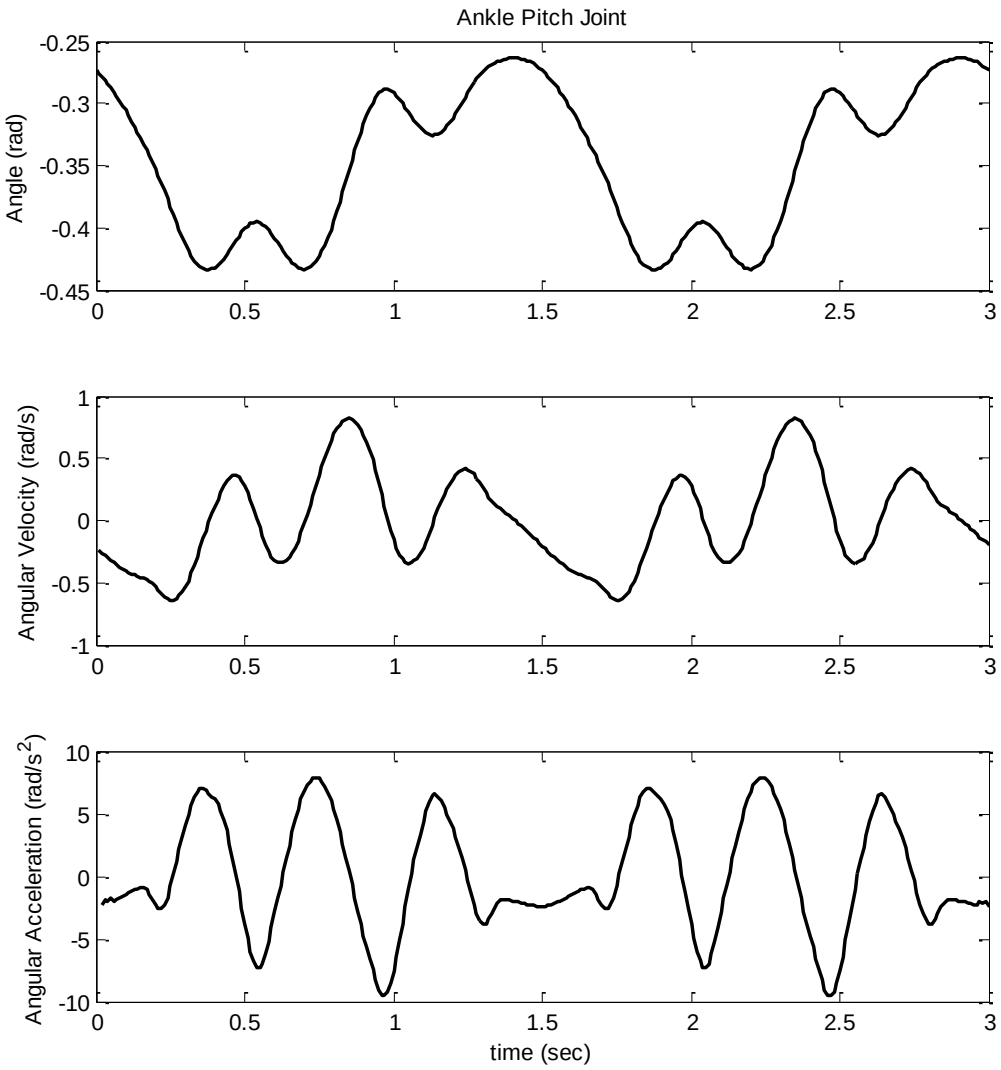

Figure 5.18 Angle (top), Angular velocity (middle) and Angular acceleration (down) of Ankle Pitch joint

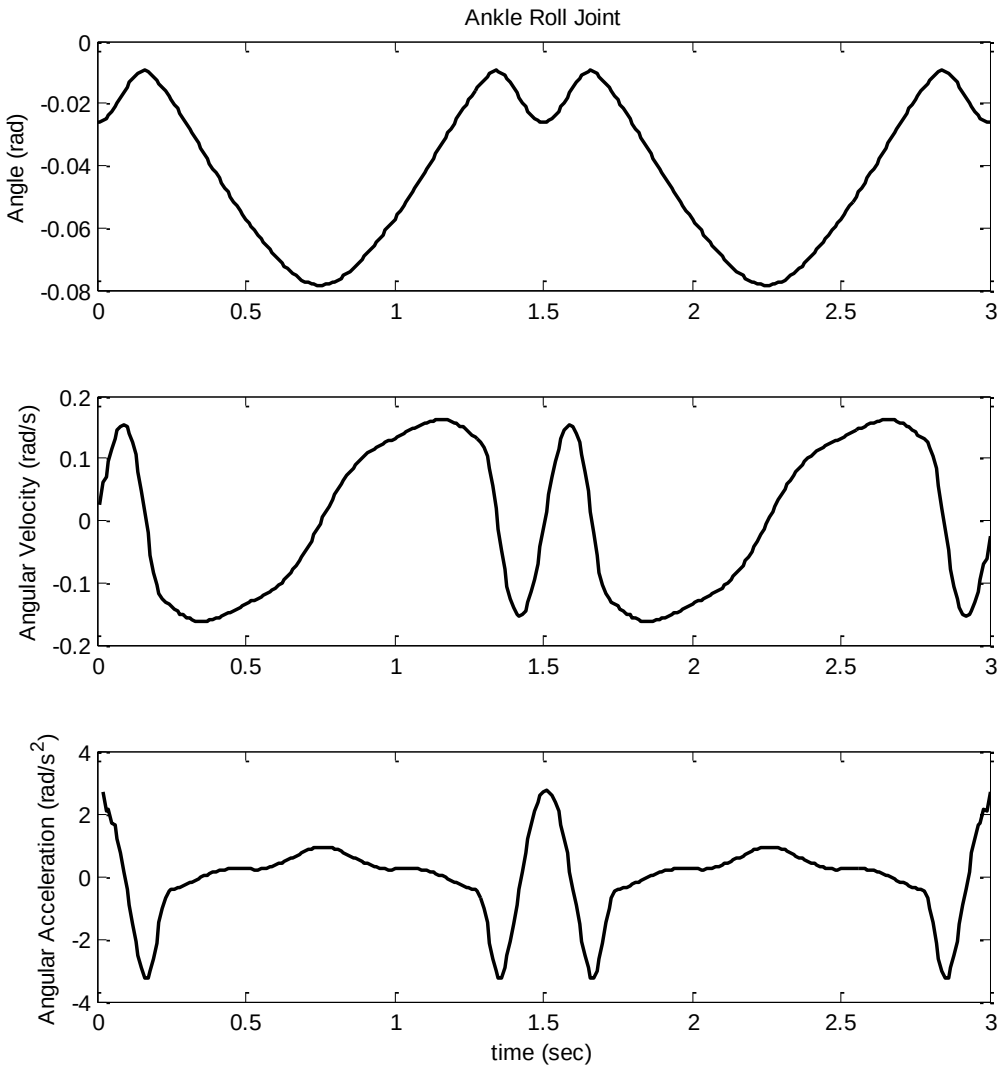

Figure 5.19 Angle (top), Angular velocity (middle) and Angular acceleration (down) of Ankle Roll joint

The torque of each joint can be calculated using Equation 3.23 and the simulation results of the angular position, angular velocity and angular acceleration. Figure 5.20 shows how much torque each joint needs in certain walking values. Figure 5.21 shows its absolute values to see the amount only.

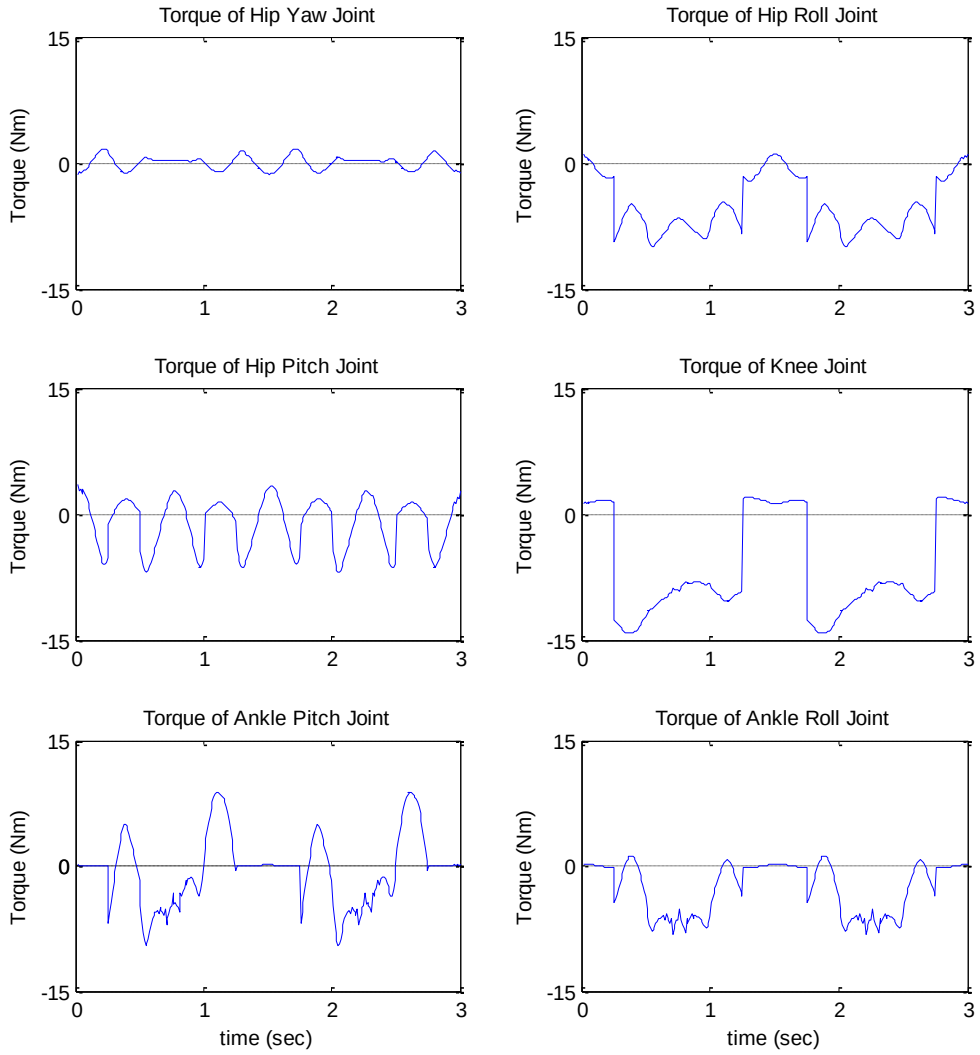

Figure 5.20 The simulation results of required torque of each joint

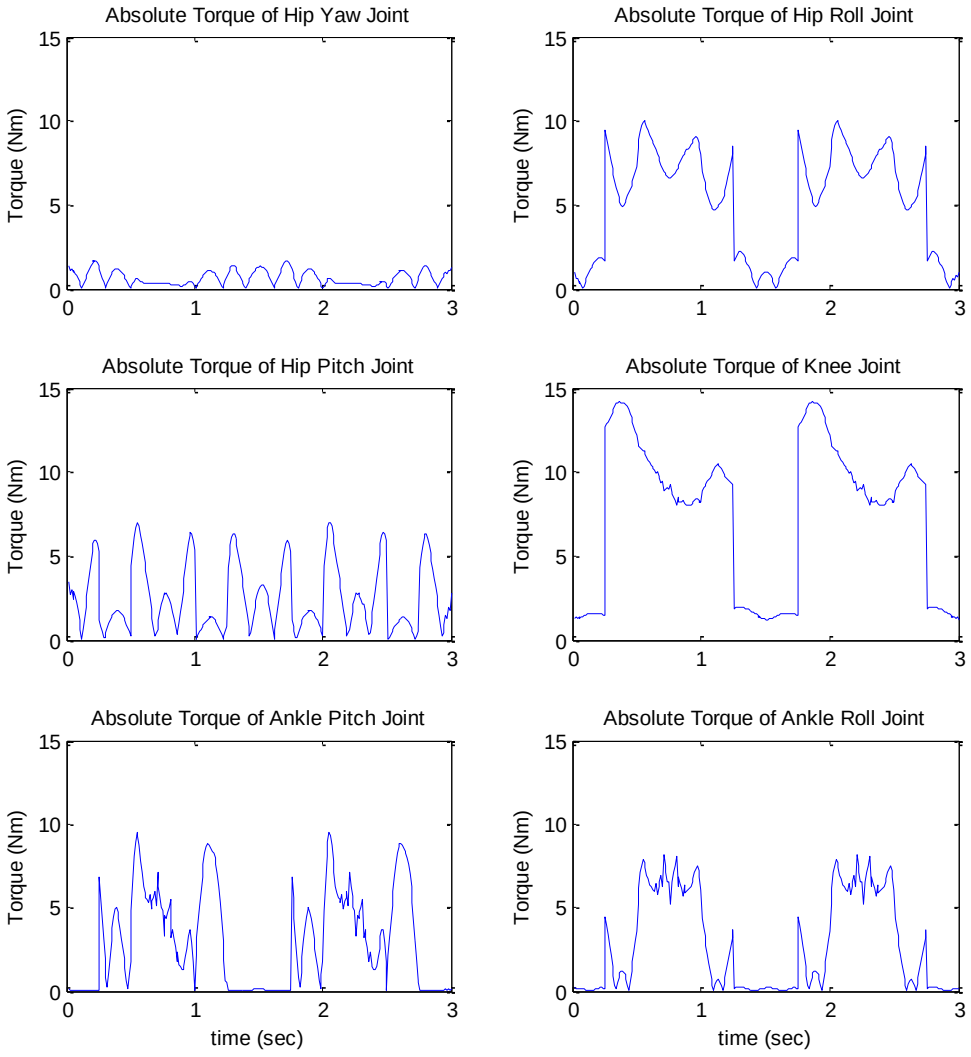

Figure 5.21 The simulation results of required torque amount of each joint

5.4 Discussion

Based on given foot trajectories, the joint angles can be calculated through solving the inverse kinematics while the joint positions are calculated from solving the forward kinematics. We can then obtain all leg movements and estimate the walking status.

Figure 5.22 shows the leg movement when the first sinusoidal curves only are used. Otherwise, Figure 5.23 shows the leg movement with other sub-sinusoidal curves. It shows how sub-sinusoidal curves contribute to make walking more naturally and how it absorbs a shock.

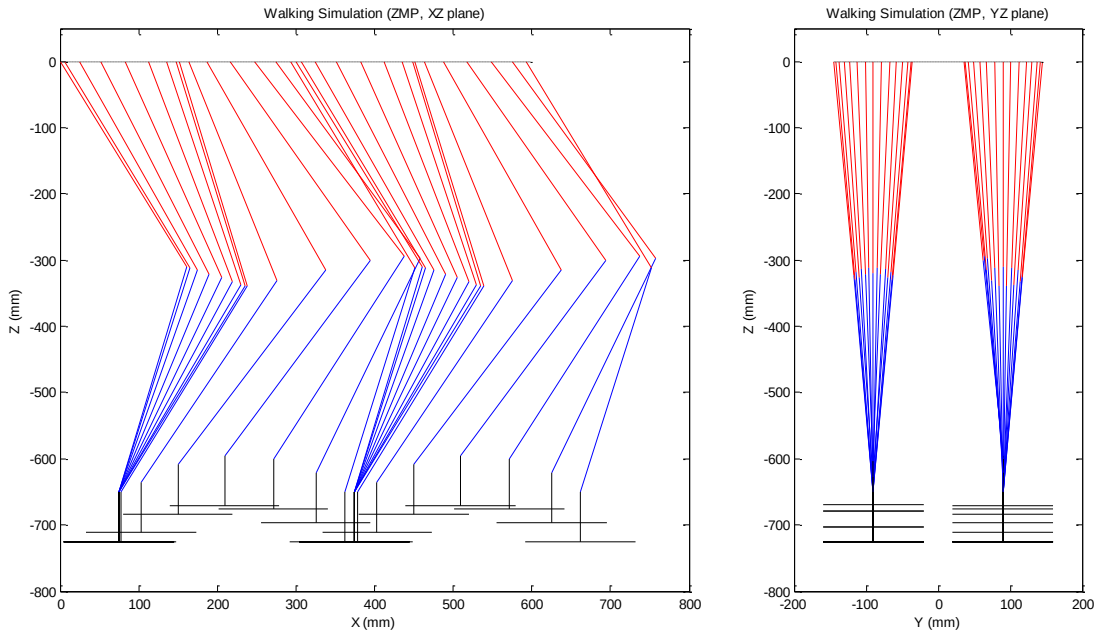

Figure 5.22 Leg Movement with only first sinusoidal curve (XZ plane (left), YX plane (right))

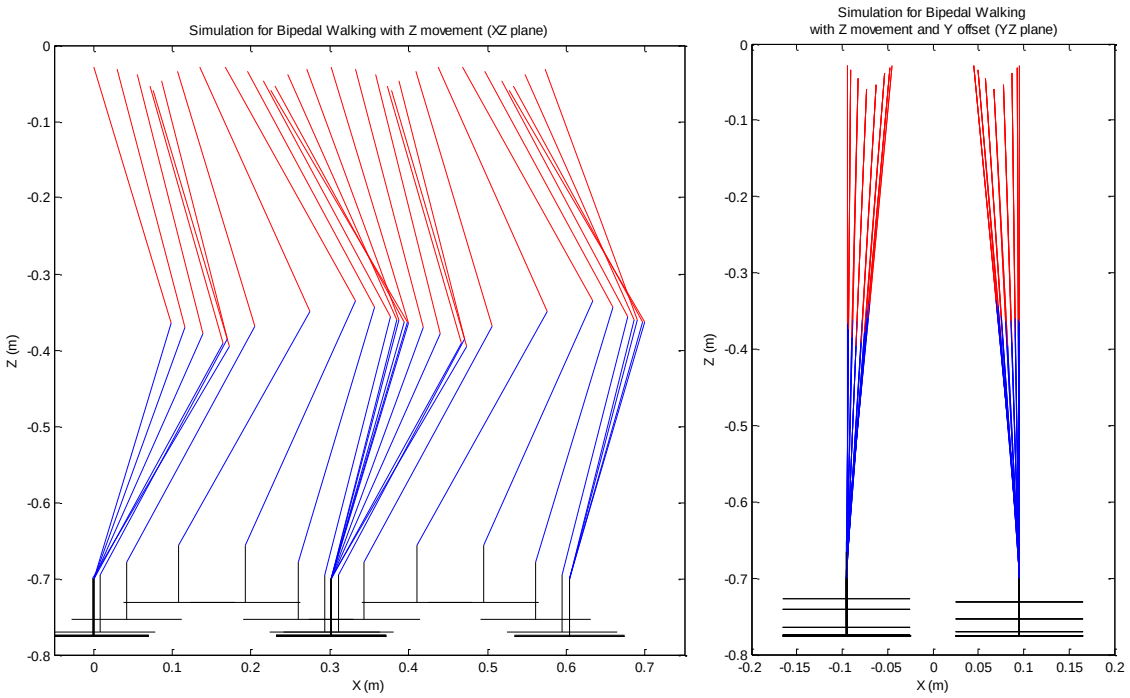

Figure 5.23 Leg Movement with sub-sinusoidal curves (XZ plane (left), YX plane (right))

In this chapter, both simulation results allow us to know where the ZMP is located and how much torque is required. Also, the angular position, angular velocity and angular acceleration of each joint can be calculated though the walking simulation. All the data is essentially needed for the development of a full-sized humanoid robot.

For example, the angle values let designers know the ranges of motion so that they can avoid interference of parts against each other. Also, the angular velocity values and torque requirement are basic information to select appropriate actuators.

Most of all, the simulation helps developers to make tradeoffs between all these coupled design values, such as the weight and length of each frame, walking speed, step size and even the budget to purchase actuators. Therefore, this kind of simulation should be done before the development to ensure it succeeds.

Section 6 Development of Full-sized Humanoid Robots

One of the main challenges in the development of full-size humanoid robots is designing joints for the lower body which can produce sufficient torque to handle the required static and dynamic loads. This is difficult because the actuators for these joints need to be compact enough to be packaged in the constrained space within the robot. To solve this problem, most full-size robots use DC servomotors with harmonic drives for actuation and gear reduction; however, this approach makes them heavy and expensive. The main goal of the mechanical design of CHARLI was to reduce the robot's weight effectively without utilizing conservative actuation or gear reduction system. A light-weight design allows the use of smaller actuators – resulting in further weight reduction and decreased costs.

6.1 Development of CHARLI-L

6.1.1 Design Concept of CHARLI-L

In this section, the design of the full-sized bipedal humanoid robot, CHARLI-L, is presented. CHARLI-L's light-weight design is achieved through the use of spring assisted parallel four-bar linkages with synchronized actuation in the lower body. This mechanism reduces the torque requirements of the individual actuators, which enables the use of off-the-shelf components to further reduce costs.

The use of four-bar linkages for bipedal robots has been suggested before. Arnaud Hamon et. al. presented a cross four-bar linkage design for the knee joint to take advantage of the spring force [34]. The results from their simulation showed that the spring could be used to make the system more energy efficient. J. McKendry et. al. developed a new kinematic mechanism for a bipedal robot which consists of several four-bar linkages with a single actuator [35]. Their design, however, used three legs to stabilize the body. Hyeung-Sik Choi, et. al.[36] and Thomas Buschmann et. al. [37] used four-bar linkages to translate linear actuation to rotational motion for a joint in a bipedal robot.

CHARLI-2 uses a parallel four-bar linkage for its leg. CHARLI-L's leg design consists of three main parts: a parallel four-bar linkage, a synchronized actuator, and a tensional spring. Among the three, the parallel four-bar linkage is the key element that holds the structure together.

Unlike conventional full-size humanoid robots, CHARLI-L does not use gear reduction mechanisms such as harmonic drives. Instead, multiple distributed actuators are used to reduce weight. Synchronization of the actuators allows for smaller and lower torque actuators to be utilized with off-the-shelf components. While dual inline actuators could accomplish the same goal, the parallel four-bar linkage proves a compact solution. Figure

6.1 shows the parallel four-bar linkage used in CHARLI-L's leg with the orientation of the actuators.

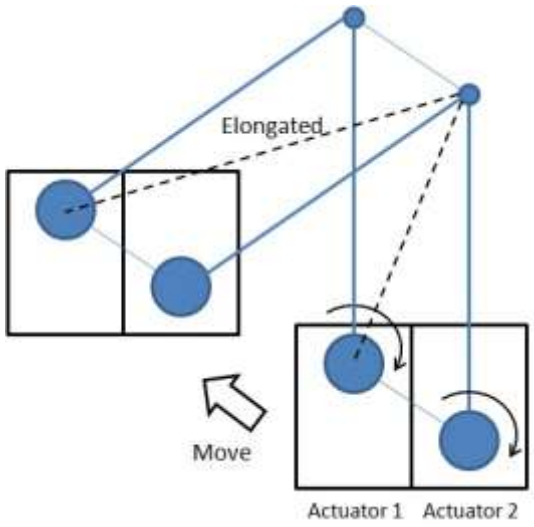

Figure 6.1 The concept diagram of spring assisted parallel 4-bar linkage with synchronized actuation

Assuming the two actuators move simultaneously with identical torque, the overall torque is doubled.

The parallel four-bar linkage offers two additional advantages. First, the required degrees of freedom (DOF) in the leg can be reduced, decreasing the number of actuators and overall weight. Most bipedal robots use a serial chain configuration of 6-DOF in each leg to realize general motion. With the assumption that the robot only walks on flat surfaces, however, the foot can be constrained to be parallel to the ground, enabling a walking gate with only 5-DOF. Using one parallel four-bar linkage for the thigh and one for the shin, CHARLI-L's hip joint is constrained to be parallel to the ankle joint. As a result, only 5 actuator sets (5-DOF) are necessary to generate a walking pattern.

The second advantage of the parallel four-bar linkage approach is the additional torque which can be provided using a tensional spring. Figure 6.1 illustrates how the length of one diagonal line of the parallelogram elongates when the four-bar linkage moves (in the direction of the arrow.) If a tensional spring is installed along this diagonal line, it will stretch and create a tensile force as the linkage moves. This tensile force contributes to moving the link to the initial position. When CHARLI-L's leg supports the upper body during walking, the resulting tensile force reduces the required torque of the actuators as shown in figure 6.2.

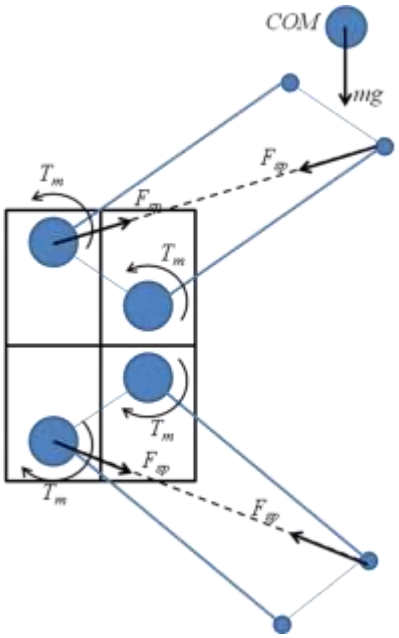

Figure 6.2 Diagram of CHARLI-L's Leg

6.1.2 Mechanical Design of CHARLI-L

Due to the parallel four-bar linkage mechanism of the leg, CHARLI-L does not require hip or ankle actuators for pitch control. This allows forward and backward walking using only two sets of knee actuators. Figure 6.3 shows the torque requirements for one knee joint as the center of mass moves downward. When the COM is closer to the ground the knee joint requires more torque to resist the upper body due to the longer moment arm.

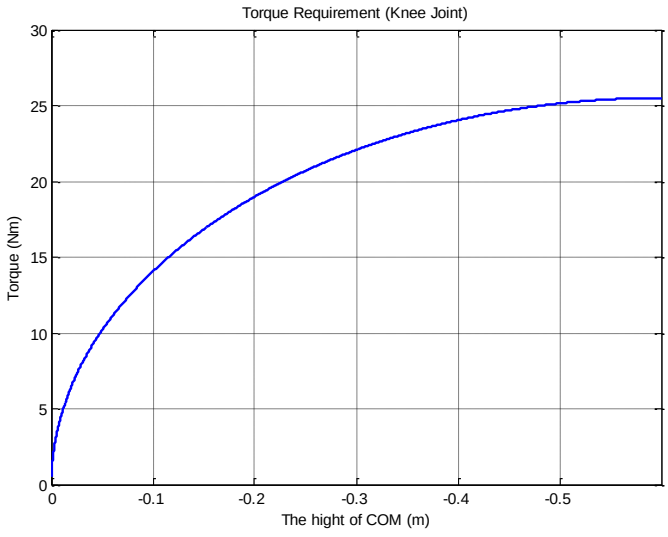

Figure 6.3 Torque Requirement for the Knee Joint

CHARLI-L uses Dynamixel EX-106+ motors for the knee actuators due to their effective power to weight ratio and affordable price. The built-in synchronization function of the EX-106+ provides an easy and reliable method to actuate two motors in tandem. The maximum holding torque of one actuator is only 10Nm. Thus, the maximum holding torque using the synchronization function is only 20Nm. The simulation results in figure 4 show that the knee joint requires more than 25Nm to stand up. During walking, the moment arm fluctuates in the range of 0.35m to 0.6m requiring, at minimum, 21Nm torque. As a result, CHARLI-L cannot walk using synchronized EX-106+ actuators alone.

To remedy this problem without resorting to heavier, higher torque actuators, a tension spring is used in a clever configuration to reduce the torque requirements of the actuators. Figure 6.4 shows the diagram of the parallel four-bar linkage with the tensional spring between the two facing joints.

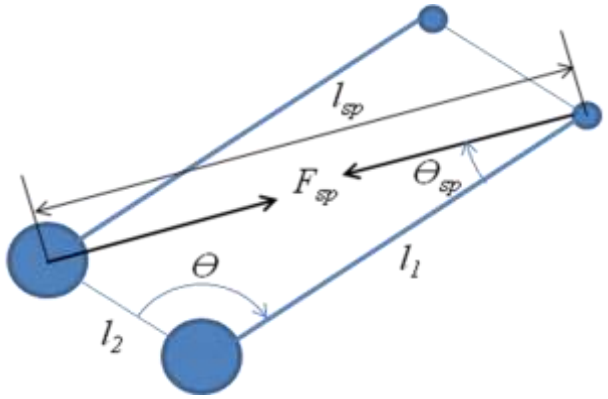

Figure 6.4 Diagram of Four-bar Linkage with Spring Force

Figure 6.5 shows the actuator's torque requirements for the knee joint using a tensional spring. A spring constant of 980N/m was selected; this is effectively doubled because one parallel four-bar linkage has two springs installed for symmetry. The dashed blue line is the required torque of the knee joint without tensional springs, as in Figure 6.5, and the dotted red line is the torque generated by the spring. The black line shows the reduced net torque of the knee joint with the spring. The maximum required torque of the joint is approximately 15Nm using the spring; this is 5Nm less than maximum torque of synchronized actuators. A bigger spring constant could be selected to further reduce the actuator's toque requirement but it would result in additional torque requirements when CHARLI-L lifts a leg. The spring constant also affects the actuator's velocity and damping, so a 25% reduction in torque was chosen as a design margin and a spring constant of 980N/m was chosen based on this criteria.

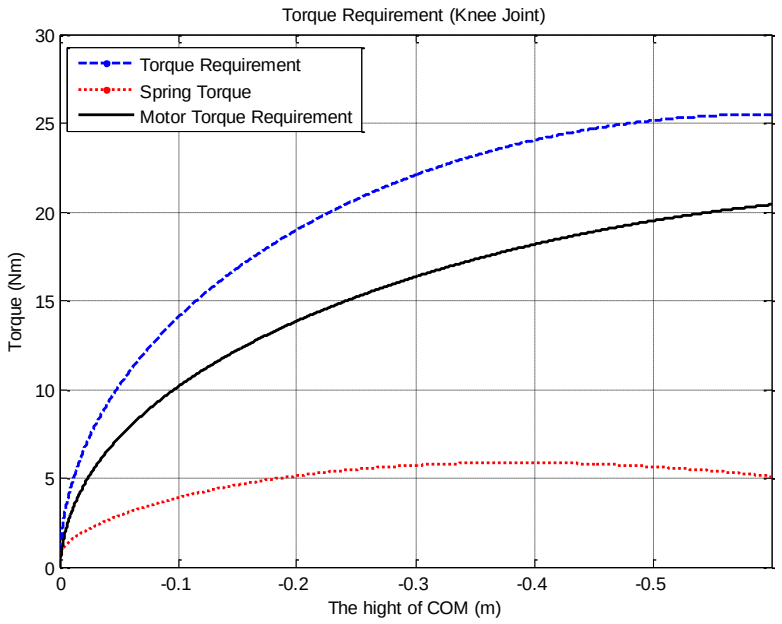

Figure 6.5 Torque graph for the Knee Joint with Tensional Springs

Figure 6.6 CHARLI-L's leg (left: 3D CAD model, right: real assembled part)

Figure 6.6 shows the CAD model and fabricated assembly of CHARLI-L's leg. Figure 6.7 shows the full CAD model of CHARLI-L. The actuators for the pitch direction are located in the knee area, while the hip and ankle actuators are used for the roll direction only. The total weight of the lower body is 6.3kg with the actuators weighing a total of 2.7kg - 43% of the overall weight. The proposed mechanism significantly reduced the weight of the robot compared to other humanoid robots in the same class. For example, the weight of one servo actuator module producing 80Nm maximum torque is approximately 2kg including a harmonic drive. If a robot uses 12 such actuators in the lower body, the total weight of the actuators will exceed 20kg. This is the primary reason why full-size humanoid robots are so heavy. The weight of the lower body is normally around 30kg. CHARLI-L's lower body is only one fifth of the weight of robots in the same class.

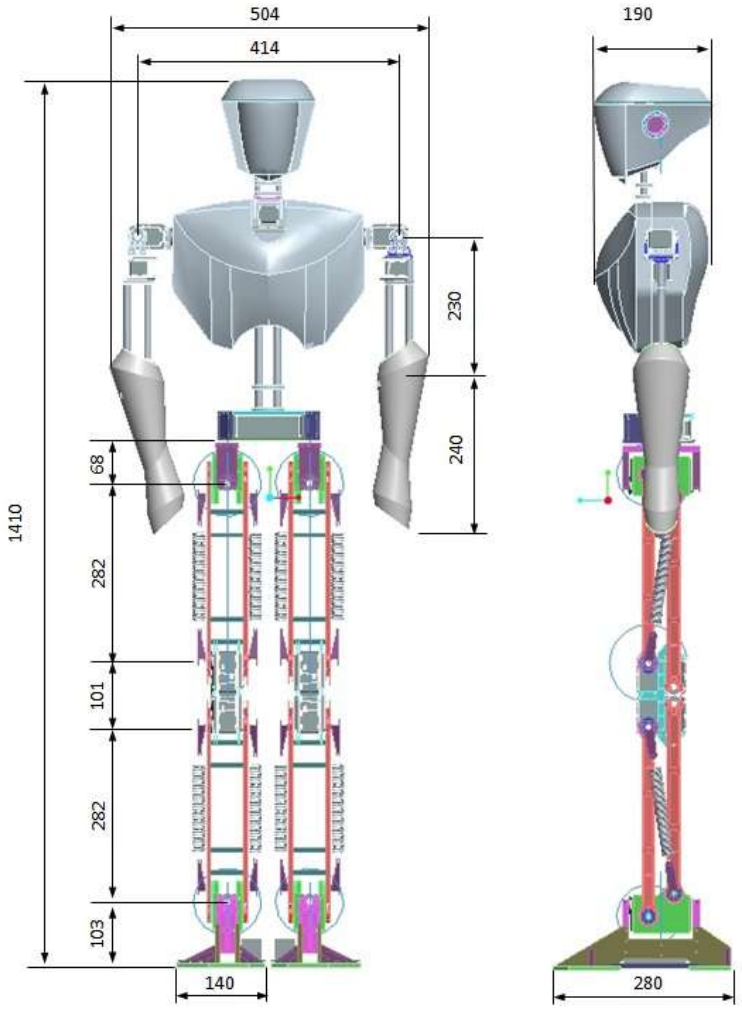

Figure 6.7 3D CAD model of CHARLI-L with overall dimensions

6.1.3 Electronics for CHARLI-L

Figure 6.8 shows the major related electronic components for CHARLI-L. All high-level processing and control is performed on a Compulabs fit-PC2 Intel Atom-based PC running GNU/Linux. The PC communicates with the Dynamixel motors using a ROBOTIS USB2Dynamixel serial USB to RS485 converter. For vision processing, a single Philips SPC1300NC webcam provides images to the main controller via streaming I/O. CHARLI-L's primary feedback sensor for stabilization and locomotion is a MicroStrain 3DM-GX3-25. This high precision IMU streams gyro and acceleration data to the fit-PC via USB. Electric power is supplied by four separate Lithium-Polymer battery packs; a 2200mAh 18.5V battery pack each for the two legs, one 2200mAh 18.5V battery pack for the upper body, and a separate 1100mAh 11.1V battery pack for the electronics and sensors. Having a separate power source for the electronics and sensors is important for providing clean power which is isolated from the noise of the electromechanical actuators.

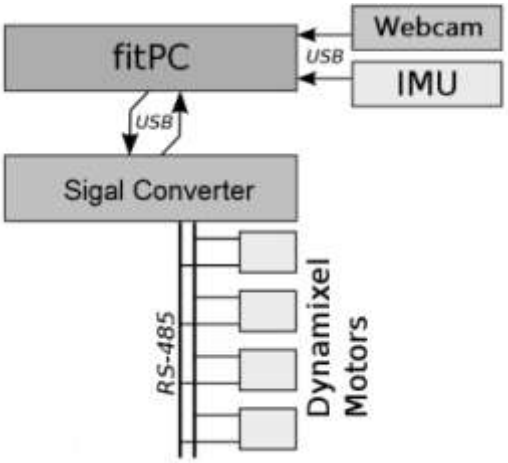

Figure 6.8 Electronic Architecture of CHARLI-L

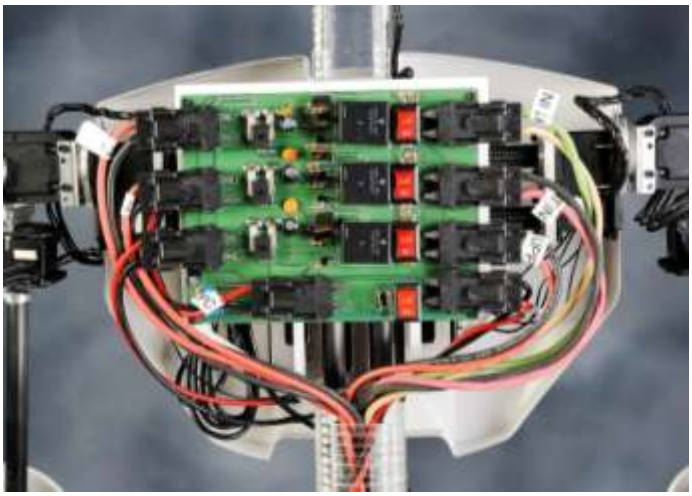

Figure 6.9 Electronic of CHARLI-L

6.2 Development of CHARLI-2

6.2.1 Design Concept of CHARLI-2

Through the success of CHARLI-L, I obtained a great amount of data and experience related to full-size humanoid robots. CHARLI-L served as a valuable platform to investigate bipedal walking, however, it was not designed for human-like walking. Therefore, CHARLI-2 was designed and fabricated to realize human-like walking.

A human-like walking gait requires at least 6 DOF per leg. In this regard, the four-bar linkage system is inadequate, since it enables only 5 DOF per leg assuming that the foot sole is always parallel to the ground during walking. Humans do not walk like this. Thus, a new concept was needed to increase the actuating torque, so a gear reduction mechanism was chosen for the design of CHARLI-2. Figure 6.10 shows the concept of the gear reduction mechanism. Synchronized dual actuators rotate separate pinion gears which rotate one main gear at the joint. In this configuration the individual torques of the two actuators combine to double the overall torque. Additionally, the actuator's overall torque is increased by the gear reduction ratio. Thus, the total joint torque will be double the actuator torque multiplied by the gear ratio.

To reduce the actuators' torque requirement, the moment of inertia should be minimized. That is, in addition to overall weight, weight distribution is also crucial for bipedal robot's walking. Thus, CHARLI-2 was carefully designed to minimize the moment of inertia.

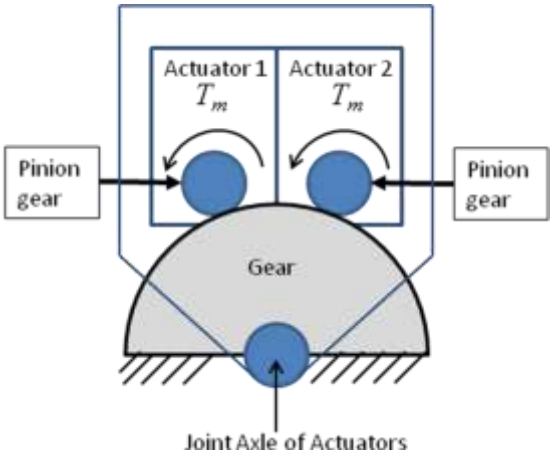

Figure 6.10 The concept diagram of gear reduction mechanism with synchronized actuation

6.2.2 Mechanical Design of CHARLI-2

Figure 6.11 shows CHARLI-L's gear reduction mechanisms. Based on the simulation results, the torque requirements were estimated and the configuration of actuators and gear reduction ratio were chosen. The hip roll, hip pitch and knee joints are actuated using synchronized motors. The hip yaw, ankle roll and ankle pitch use single actuators. The gear reduction ratio is 1:3.

As discussed previously, mass distribution is a crucial design point for minimizing the moment of inertia. For this reason CHARLI-2's batteries are installed in the thighs, and the shins and feet are designed to be as light as possible. As a result, CHARLI-2's center of mass is located close to the hip joint as shown in Figure 6.12. Additionally, the overall weight is 5% lighter than CHARLI-L. Figure 6.13 shows the full CAD model of CHARLI-2.

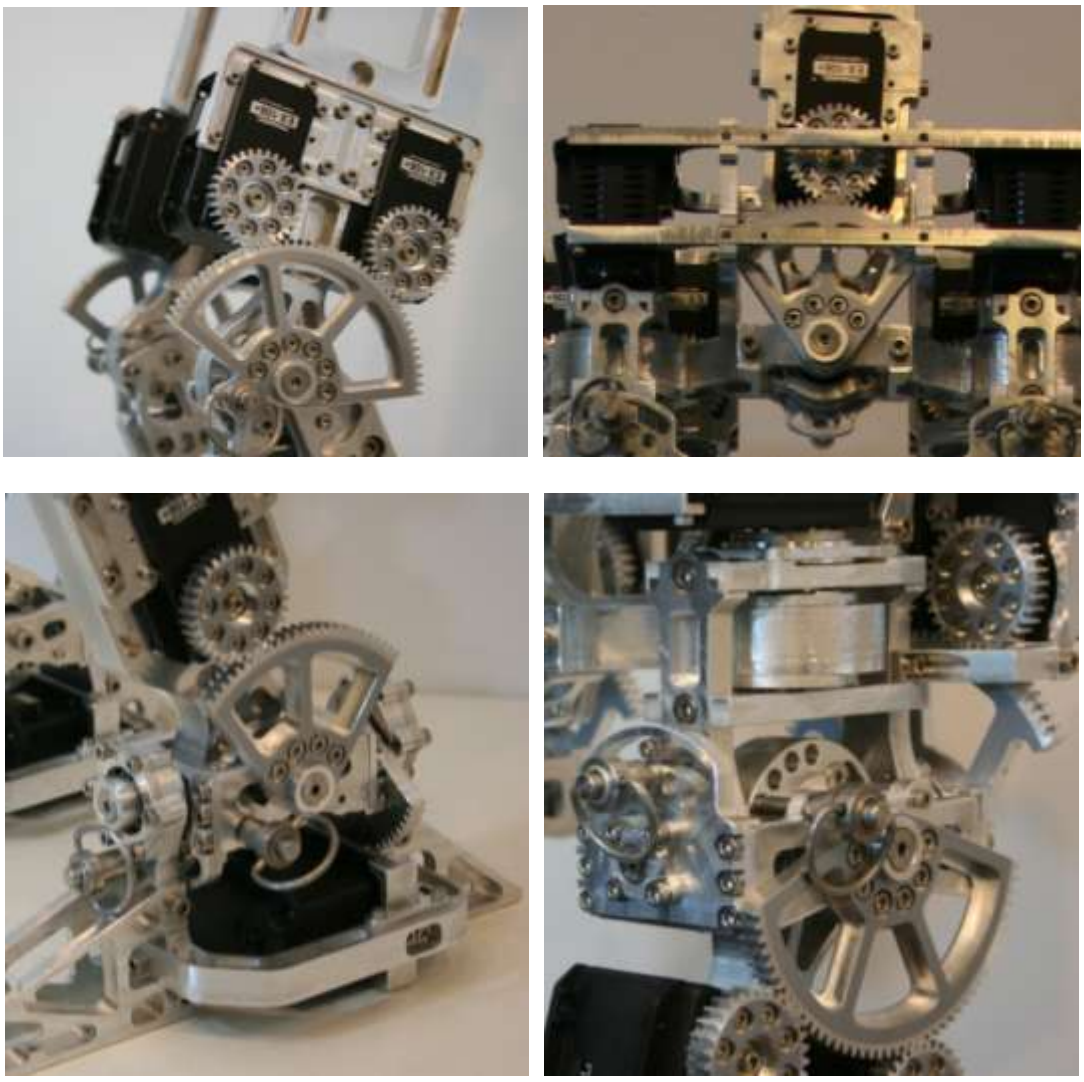

Figure 6.11 Gear reduction mechanisms
(upper left: Knee, upper right:Waist, lower left: Ankle, lower right: Hip)

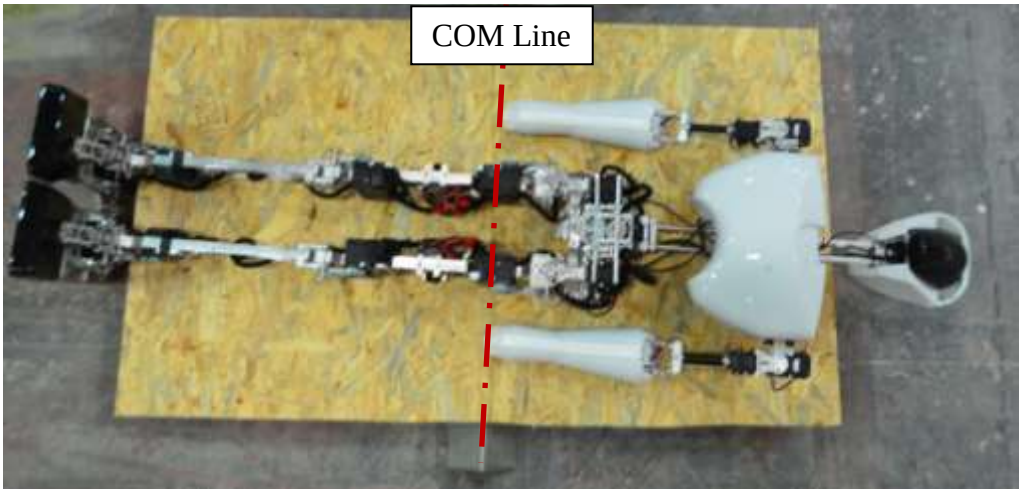

Figure 6.12 Measuring the COM height of CHARLI-2

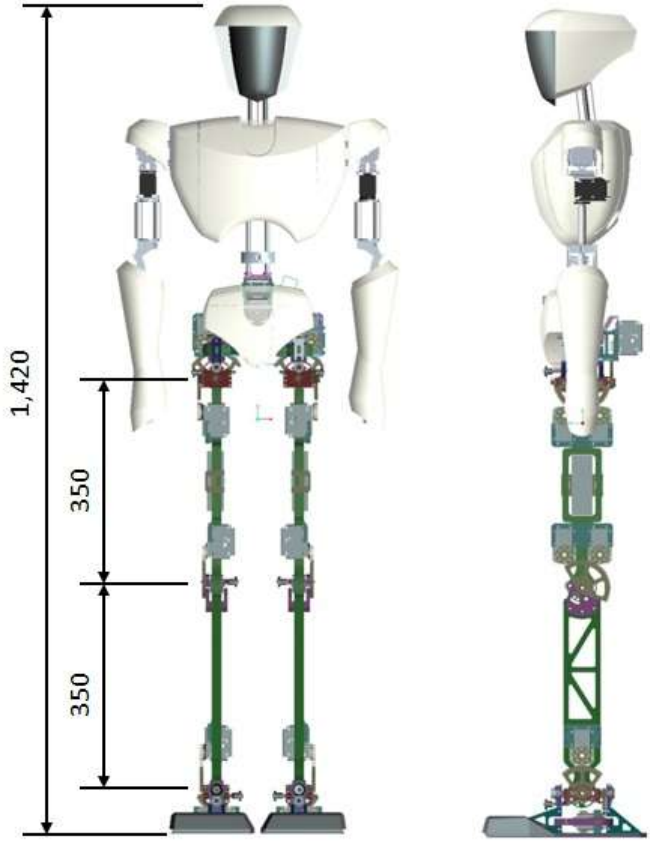

Figure 6.13 3D CAD model of CHARLI-2 with overall dimensions

6.2.3 Electronics for CHARLI-2

Figure 6.14 shows the major related electronic components for CHARLI-2. As in CHARLI-L, all high-level processing and control is performed on a Compulabs fit-PC2i Intel Atom-based PC running GNU/Linux. A ROBOTIS Co. CM-730 sub-controller board acts as the communication relay between the Dynamixel actuators and the fit-PC, providing services for both sensor acquisition and actuator control. This improved design allows a faster control loop than CHARLI-L. For vision processing, a single Logitech C905 webcam provides images to the main controller via streaming I/O. CHARLI-2's primary feedback sensor for stabilization and locomotion is a MicroStrain 3DM-GX3-25. Electric power is supplied by four separate Lithium-Polymer battery packs; a 2250mAh 14.8V battery pack each for the two legs, one 1000mAh 14.8V battery pack for the upper body, and a separate 1300mAh 11.1V battery pack for the electronics and sensors. Having a separate power source for the electronics and sensors was important to provide clean power, not influenced by the noise of the electromechanical actuators.

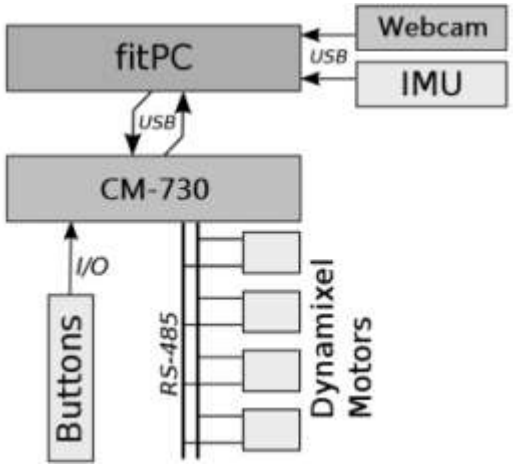

Figure 6.14 Electronic Architecture of CHARLI-2

Figure 6.15 Electronic of CHARLI-2

6.3 Comparison between CHARLI-L and CHARLI-2

As mentioned above, CHARLI-2 is the upgraded version of CHARLI-L. Accordingly, several technical items have been improved or changed.

In terms of the mechanical design, CHARLI-2 was given more DOF than CHARLI-L. The main purpose of CHARLI-2 is to investigate human-like walking, so it was designed with 6 DOF in each leg and an additional waist joint. Furthermore, CHARLI-2 uses a gear train system for each leg joint to increase the actuating torque. For CHARLI-L, I tried to minimize the height of the COM, but CHARLI-2's COM is located higher, near the hip joint.

In terms of the electronic design, CHARLI-2 has an additional processor (the CM-730 made by ROBOTIS Co) to increase computing speed and relay commands from USB to RS485. The Logitech C905 camera replaced the Philips SPC1300NC, because the Logitech C905 cam provides higher quality images. Table 6.1 shows the specifications for both robots which are displayed in figure 5.16.

Table 6.1 The specification of CHARLI-L and CHARLI-2

		CHARLI-L	CHALRI-2
Height (mm)		1410	1410
Weight (kg)		12.7	12.1
DOF	Leg	5 x 2	6 x 2
	Arm	4 x 2	4 x 2
	Head	3	2
	Waist	-	1
	Total	21	23
Actuator (Dynamixel)	Leg	EX-106+ x 18	EX-106+ x 18
	Arm	RX-64 x 4, RX-28 x 4	RX-64 x 4, RX-28 x 4
	Head	RX -28 x 3	RX -28 x 2
	Waist	-	EX-106+ x 1
Sensor	IMU	MicroStrain,3DM-GX3-25	MicroStrain 3DM-GX3-25
	Camera	Philips SPC1300NC	Logitech C905
Control System	HW	FitPC2	FitPC-2i, CM-730
	SW	MATLAB, Ubuntu, C++	Ubuntu, C++
Power	Actuator	LiPo 2200mAh 18.5V x3	LiPo 2250mAh 14.8V x 2 LiPo 1000mAh 14.8V x 1
	Computing	LiPo 1100mAh 11.1V x1	LiPo 1300mAh 11.1V x 1

6.4 Fabrication of Full-sized Humanoid Robots

Building a robot needs a lot of machines. First of all, if the parts of a robot are made by a metal, milling machine is required to fabricate it. CHARLI's parts were mainly made by aluminum alloy 6062 and 5053, so CNC machining center, Bridgeport GX-480, was mainly used for CHARLI's fabrication. Figure 6.16 shows CNC machining center and its tools.

Figure 6.16 CNC Machining Center; Model: Bridgeport GX-480 (Top)
Tools: Endmills and Chucks (Bottom)

CNC machining center is operated by G-code which has information of a tool path. The G-code can be made with CAD-CAM programs. Thus, NX7-Manufacturing program, which is well known as CAD-CAM program, was used to make G-code. Figure 6.17 shows how to make G-code using NX7-Manufacturing program. The bottom figure shows the tool path simulation performed by NX7-Manufacturing program.

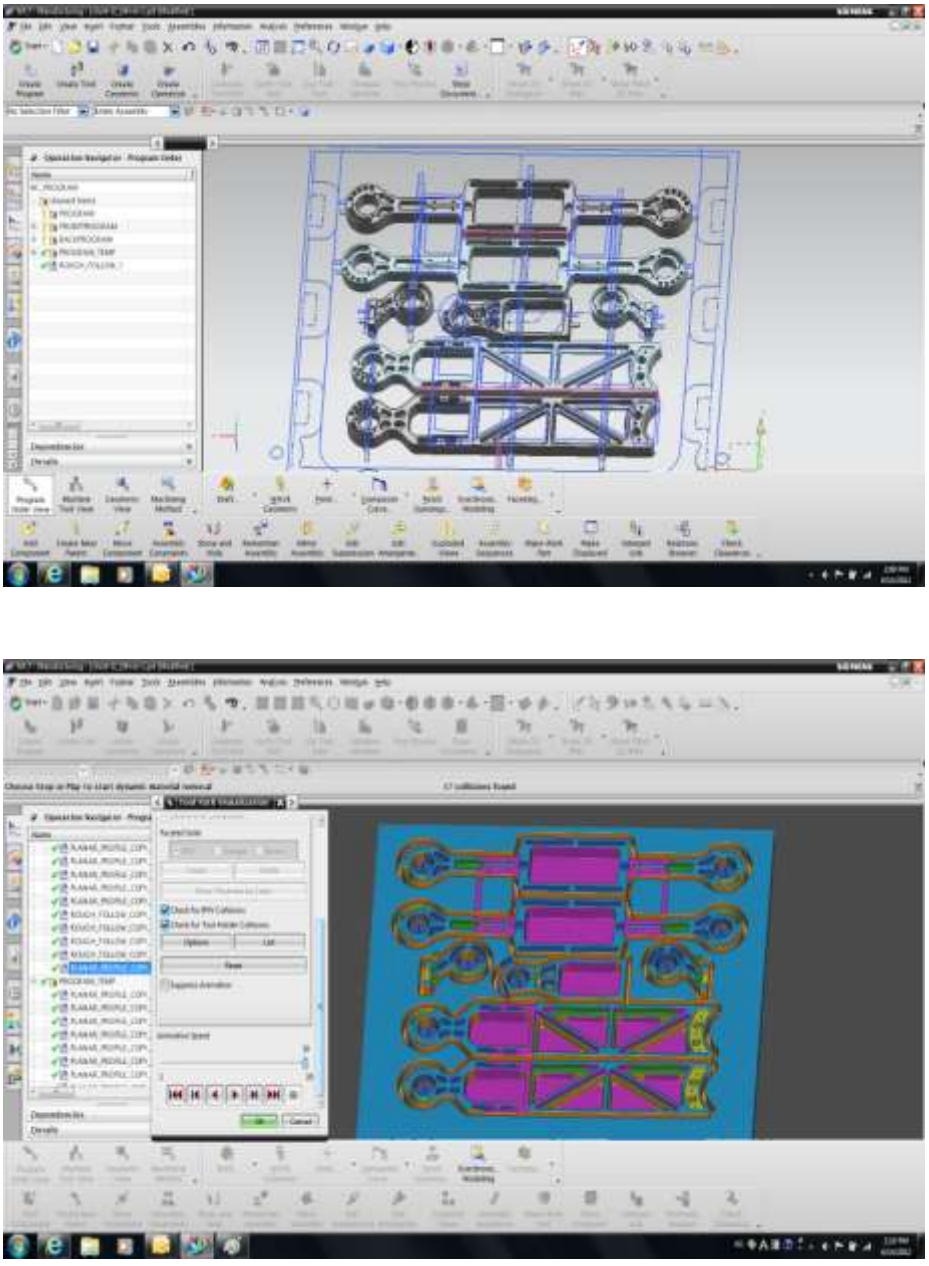

Figure 6.17 Making a tool path using NX7-Manufacturing (Top)
Tool path simulation using NX7-Manufacturing (Bottom)

Figure 6.18 shows the aluminum alloy plate cut by CNC machining center. After taking parts out from the aluminum alloy plate, most parts are needed to get post processing to make it better. Figure 6.19 shows the other machines used for post processing.

Figure 6.18 Aluminum alloy plate cut by CNC machining center

Figure 6.19 Drilling machines and Bend Saw

Figure 6.20 shows the assembled aluminum parts after post processing.

Figure 6.20 Assembled Aluminum parts

Fabricating CHARLI's cover is done by vacuum forming. The molds were made by CNC machining center like other aluminum parts. Then, thin plastic covers were made though vacuum forming process. Figure 6.21 shows the vacuum forming machine, cover molds and plastic covers.

Figure 6.21 Vacuum Forming Machine, Model: Formech Midi (Top)
Cover Molds and Plastic Covers (Bottom)

Figure 6.22 shows the laser cutter, VLS3.60, which was used for making acrylic parts forming CHARLI's spine.

Figure 6.22 Laser cutter, Model VLS3.60

CHARLI-L and CHARLI-2 could be built though all these manufacturing processes. Figure 6.23 shows the appearance of the both robots.

Figure 6.23 The appearances of CHARLI-L (Left) and CHARLI-2 (Right)

Section 7 Experiments

7.1 Bipedal Walking Tests

7.1.1 Test for Walking Ability

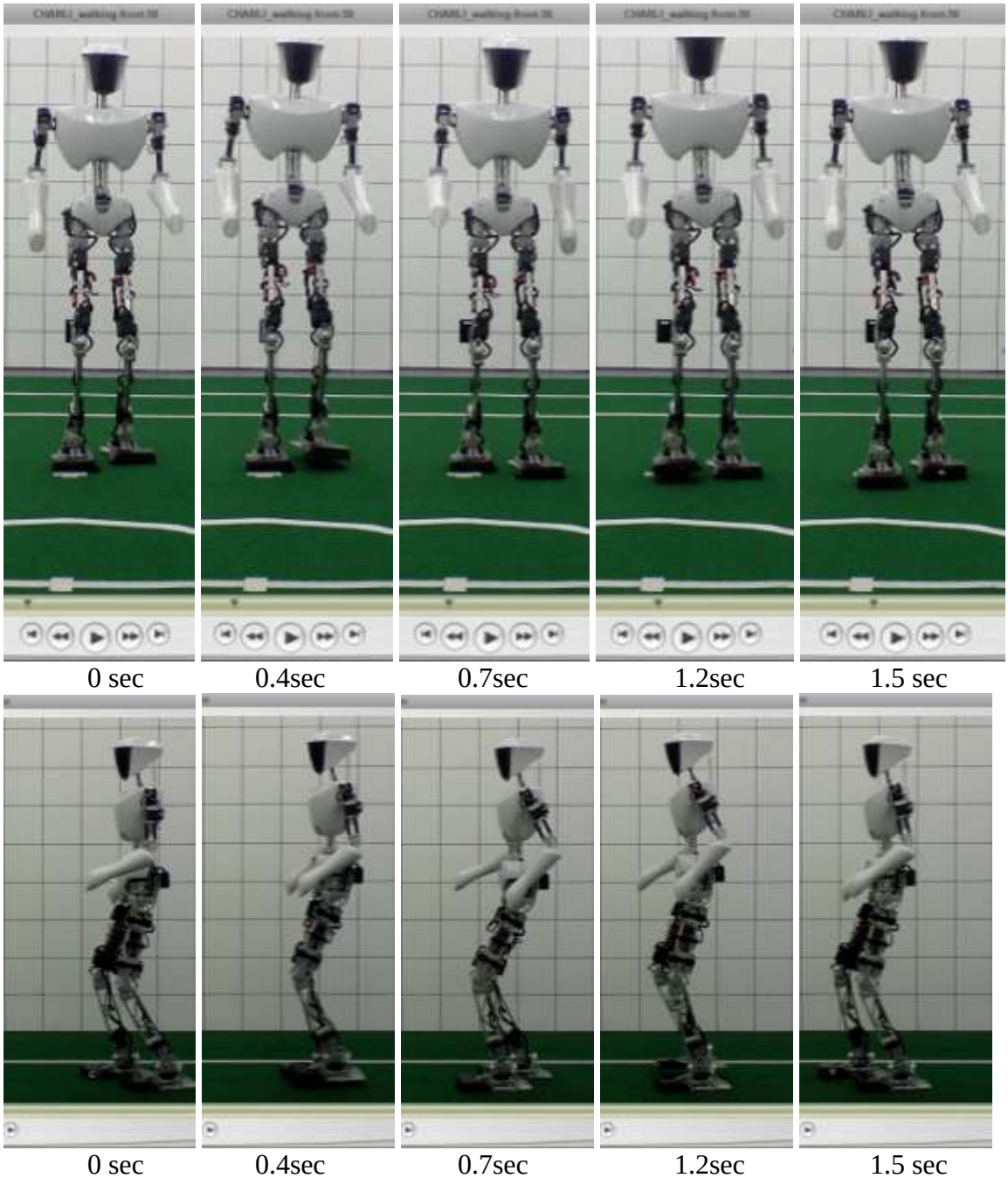

Figure 7.1 Walking Test (ZMP method, Forward walking, 0.2m/s)
Front view (yz plane, Top), Side view (xz plane, Bottom)

Figure 7.1 shows CHARLI-2's forward walking status with a velocity of 0.2m/s. Its walking status was stable and step size was accurate. The error of the step size was less than 5 percent of designated step size. To check its stability, The angle and angular velocity data of CHARLI's body was measured by the MicroStrain 3DM-GX3-25 IMU sensor mounted to CHARLI's lower abdomen. Figure 7.2 shows the angle and angular velocity during forward walking with a velocity of 0.2 m/s. As shown in Figure 7.2, the angles and angular velocities remained stable during the forward walking test. Both pitch and roll angles move within $\pm 3^{\circ}$.

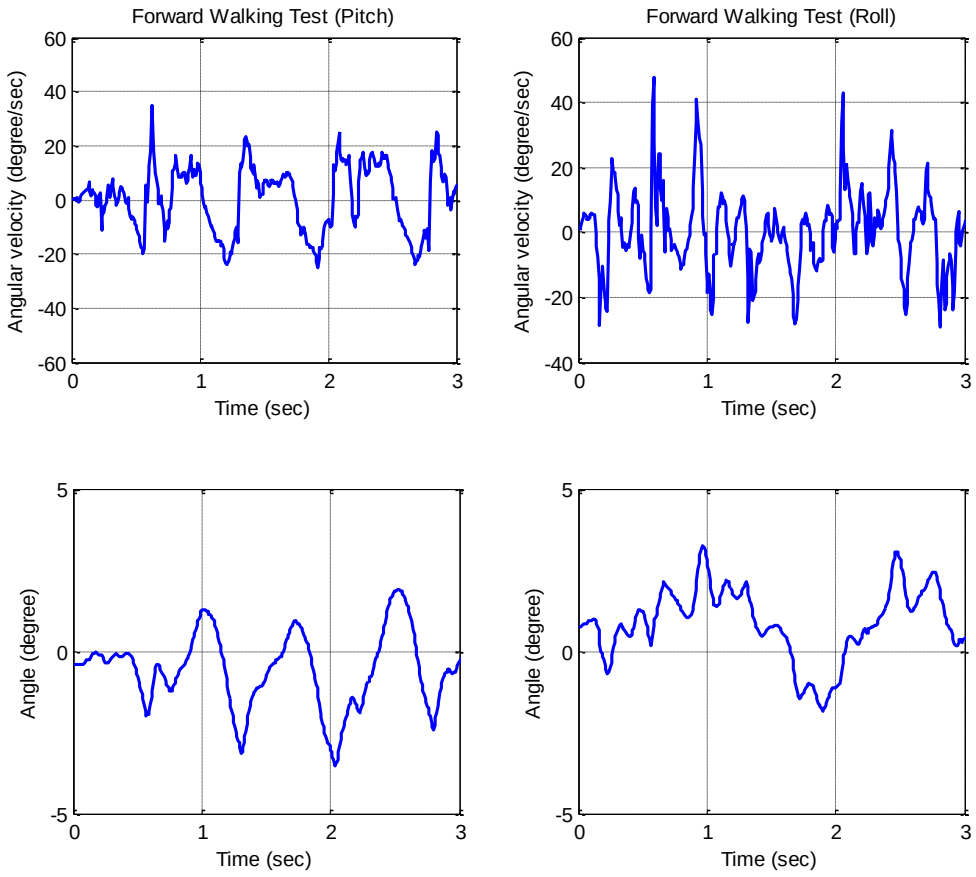

Figure 7.2 The measured angle and angular velocity data of CHARLI's body during forward walking
Angular velocity in pitch direction (top left)
Angular velocity in roll direction (top right)
Angle in pitch direction (Bottom left)
Angle in roll direction (Bottom right)

7.1.2 Test for Tracking COM Trajectory

ZMP trajectory of CHARLI should be examined to quantify how well it performs. Measuring forces of the foot plate or ankle is the most common method of examining ZMP of a humanoid robot. However, one of the main goals of the CHARLI project is to minimize the use of sensors to reduce cost and complexity. The reason why the intuitive walking method utilizing sinusoidal function is proposed in this paper is to make a full-sized humanoid robot without sensing ZMP. Therefore, another method was needed to examine CHARLI's ZMP trajectory, because CHARLI does not have any sensing ability to measure its ZMP.

Measuring COM trajectory could be a good alternative to the ZMP measurement. As mentioned in Chapter 4, COM and ZMP are related, and the ZMP can be calculated though Equation 4.3.

COM position can be calculated though Equation 5.1. This means that if we know the position and weight of each link, we can calculate the COM position. 3D CAD programs can calculate the weight of each part and assembly with little error. Thus, once the positions of each link are measured, COM position can be calculated. For testing purposes, the positions of each link were measured using a motion capture test.

Figure 7.3 shows the motion capture test equipment of the Locomotion Research Laboratory at Virginia Tech, directed by Dr. Thurmon Lockhart.

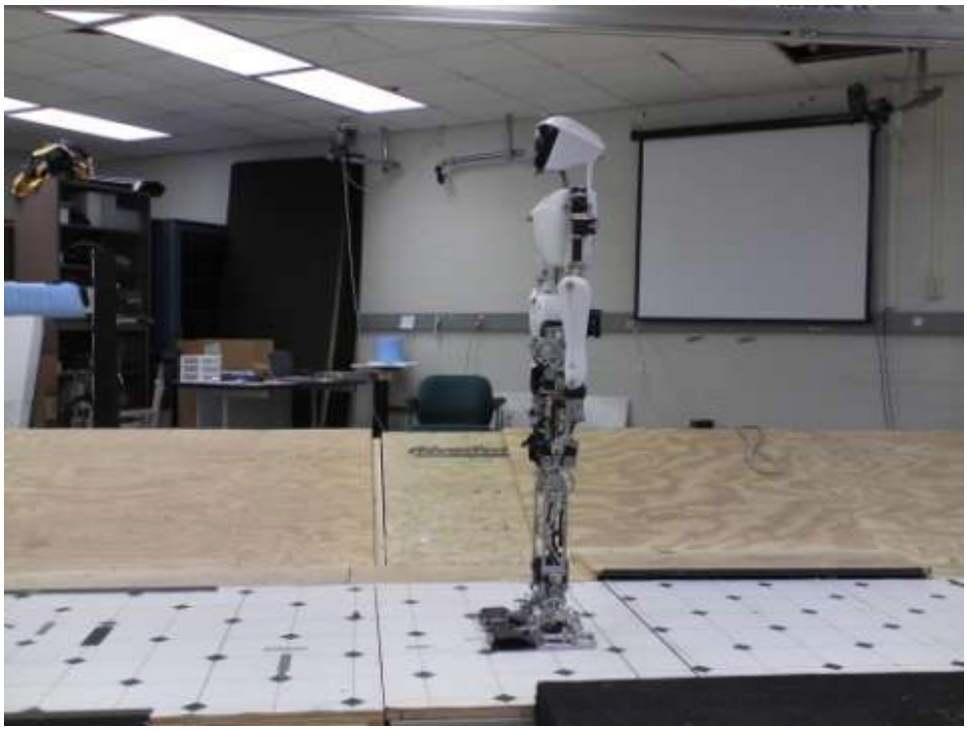

Figure 7.3 The motion capture test equipment of Locomotion Research Laboratory at Virginia Tech directed by Dr. Thurmon Lockhart

Figure 7.4 depicts the attachment of markers to CHARLI. These markers can reflect infrared light, and 6 high speed infrared cameras capture these makers. The images of the markers transfer to a computer, which calculates the position of each marker.

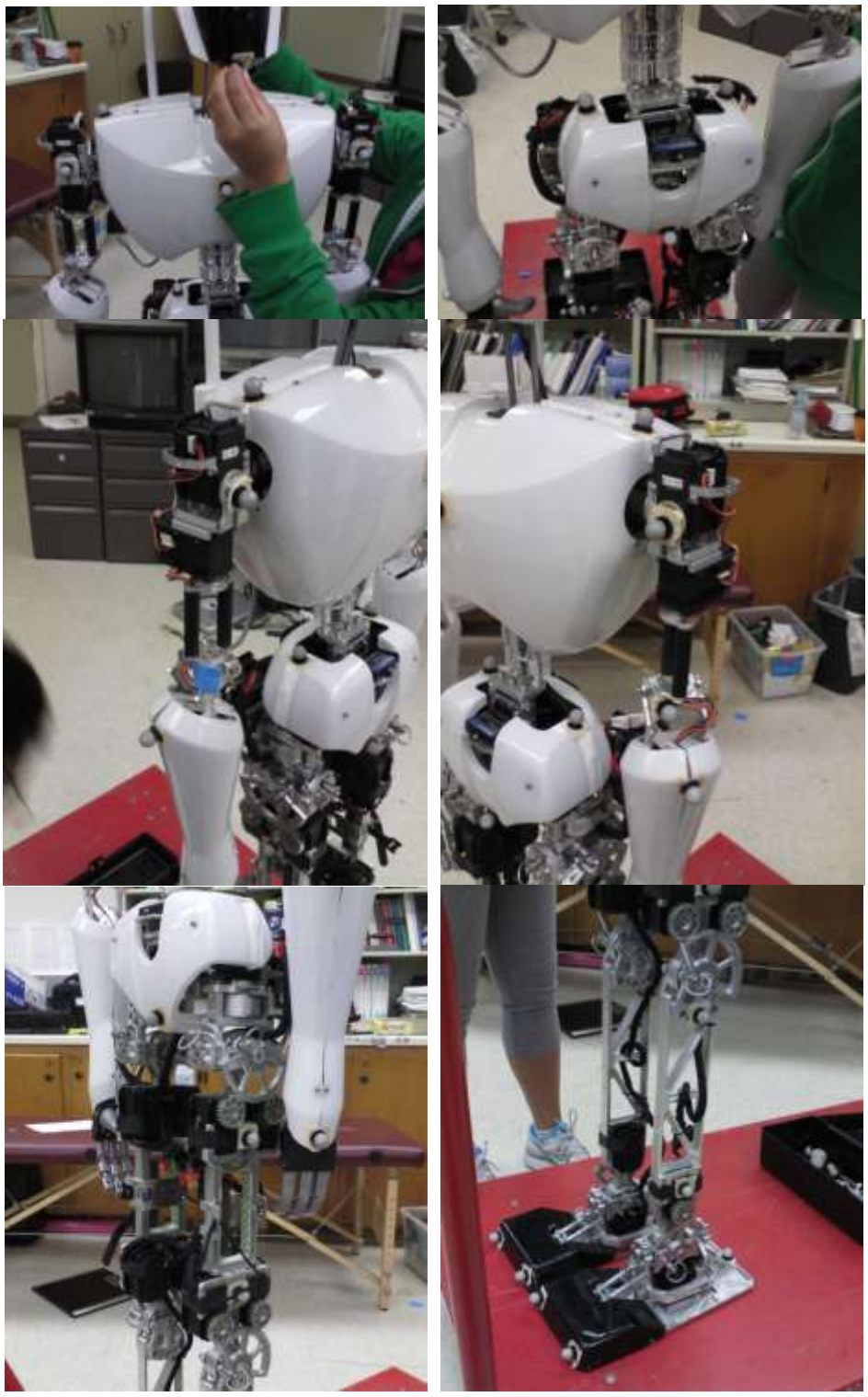

Figure 7.4 Attaching Markers reflecting Infra-red light

Figure 7.5 shows captured motion data. Figure 7.6 shows clips from a movie generated from captured motion data during forward waking.

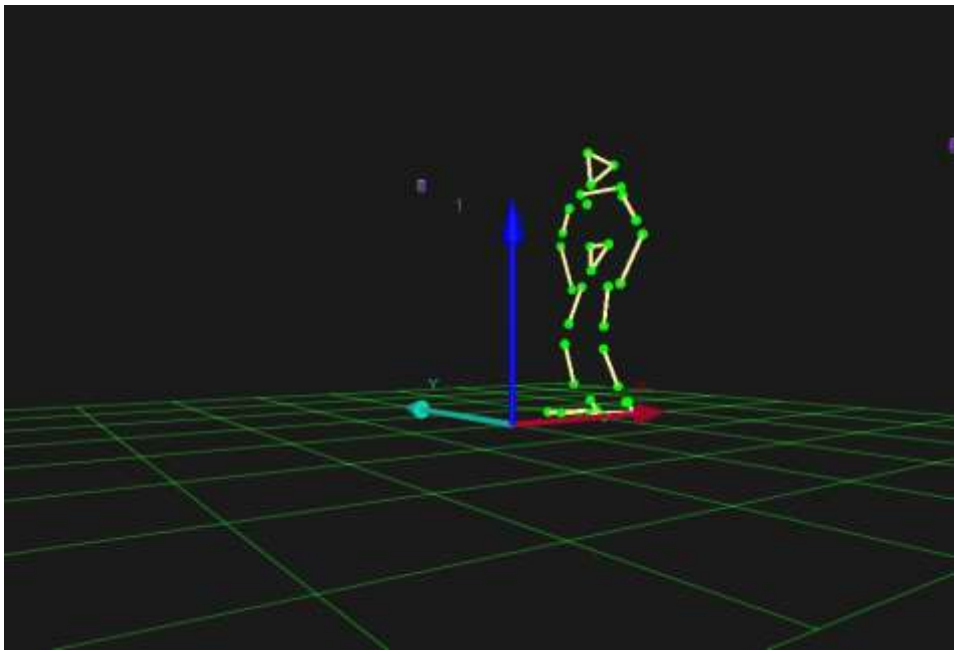

Figure 7.5 Captured motion data (iso view)

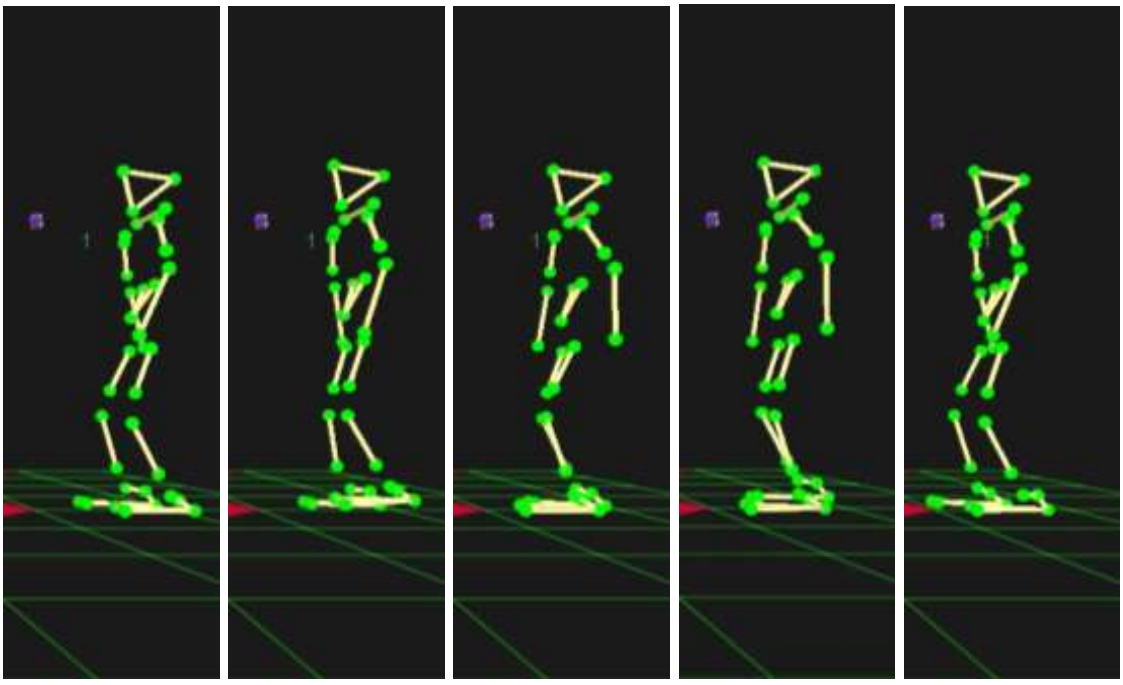

Figure 7.6 Movie made by captured motion data during forward walking (0.15 m/s)

Figures from 7.7 to 7.10 show the position of marker, and their relative locations to the center of mass of each link.

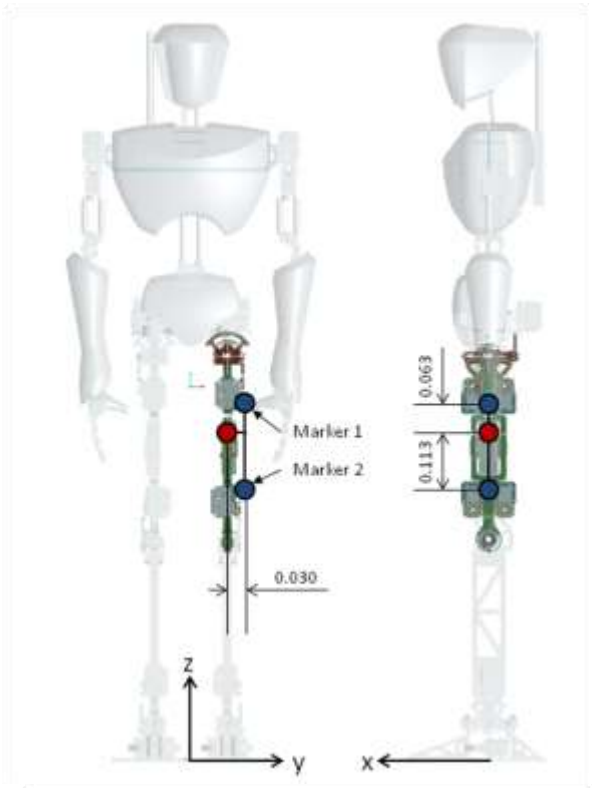

Thigh

Mass: 1.729kg

Marker1: (0, 100, 690) mm

Marker2: (0, 100, 514) mm

COM: Left(0, 70, 627) mm

$$= \left(\frac{113M_{1x}+63M_{3x}}{176}, \frac{113M_{1y}+63M_{2y}}{176}-30, \frac{113M_{1z}+63M_{2z}}{176}\right)$$

COM: Right(0, -70, 627) mm

$$= \left(\frac{113M_{1x}+63M_{4x}}{176}, \frac{113M_{1y}+63M_{4y}}{176}+30, \frac{113M_{1z}+63M_{4z}}{176}\right)$$

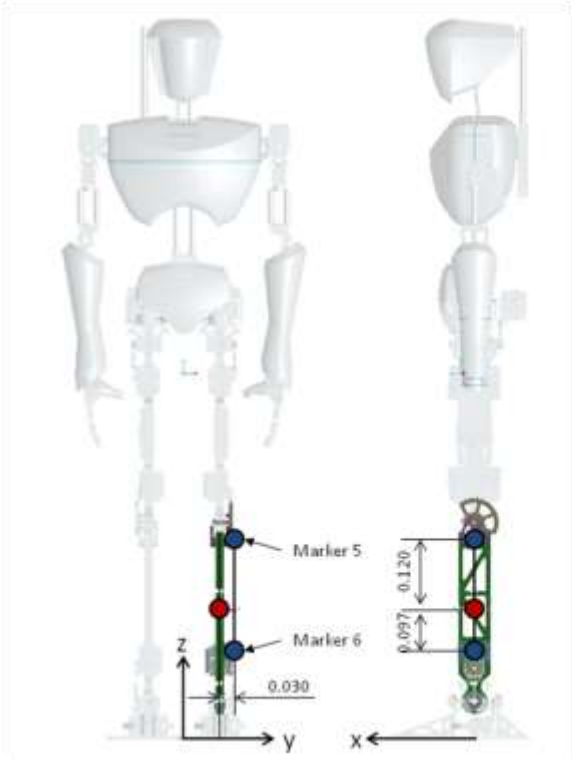

Shin

Mass: 0.783kg

Marker5: (0, 100, 385) mm

Marker6: (0, 100, 168) mm

COM: Left(0, 71, 265) mm

$$= \left(\frac{97M_{5x}+120M_{6x}}{217}, \frac{97M_{5y}+120M_{6y}}{217}-30, \frac{97M_{5z}+120M_{6z}}{217}\right)$$

COM: Right(0, -71, 265) mm

$$= \left(\frac{97M_{5x}+120M_{6x}}{217}, \frac{97M_{5y}+120M_{6y}}{217}+30, \frac{97M_{5z}+120M_{6z}}{217}\right)$$

Figure 7.7 The Position of Marker and its relationship with COM, (Thigh (top), Shin (Bottom))

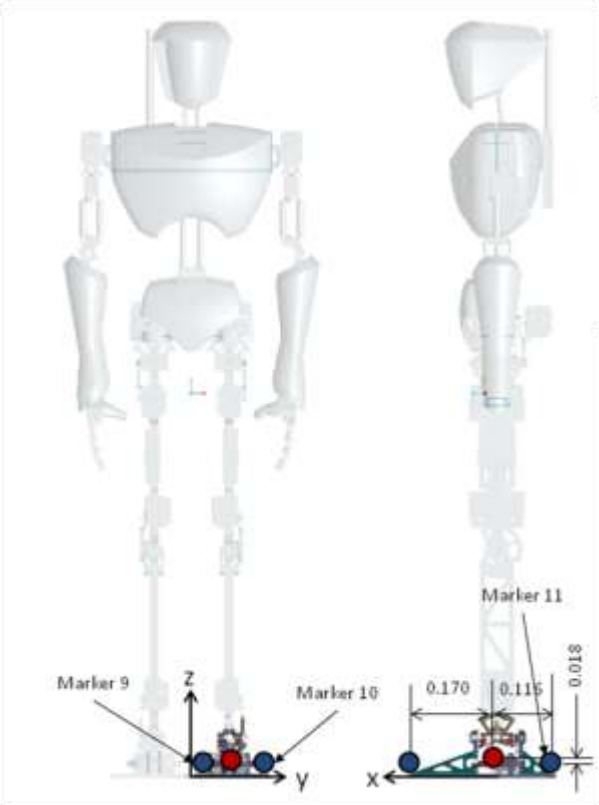

Feet

Mass: 0.886kg

Marker9: (176, 20, 17) mm

Marker10: (176, 132, 17) mm

Marker11: (-110, 70, 17) mm

COM: Left(6, 73, 35) mm

$$=\left(\frac{58M_{9x}+58M_{10x}+170M_{11x}}{286},\frac{M_{9y}+M_{10y}+2M_{11y}}{4},\frac{58M_{9z}+58M_{10z}+170M_{11z}}{286}+18\right)$$

COM: Right(6 , -73, 35) mm

$$=\left(\frac{58M_{12x}+58M_{13x}+170M_{14x}}{286},\frac{M_{12y}+M_{13y}+2M_{14y}}{4},\frac{58M_{12z}+58M_{13z}+170M_{14z}}{286}+18\right)$$

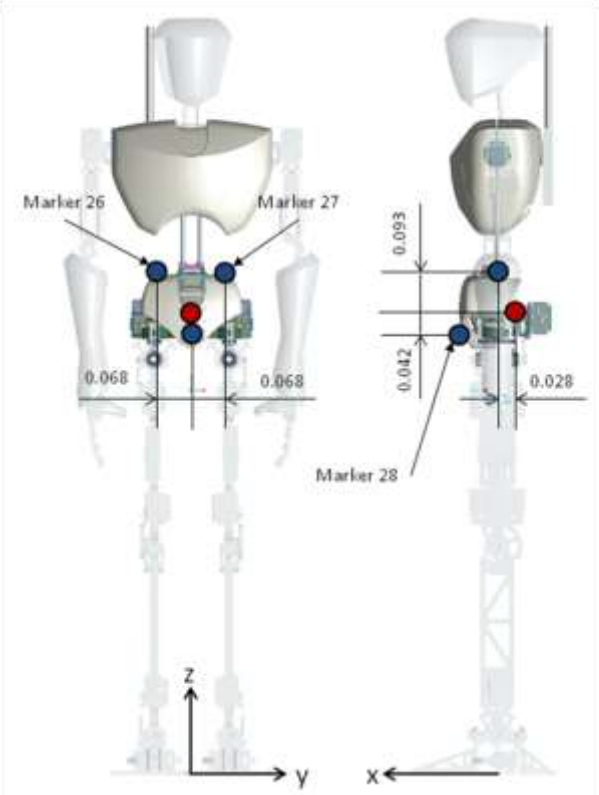

Pelvis

Mass: 1.798kg

Marker26: (0, -68, 940) mm

Marker27: (0, 68, 940) mm

Marker28: (65, 0, 805) mm

COM: (- 28, 0, 847) mm

$$=\left(\frac{M_{26x}+M_{27x}}{2}-28,\frac{M_{26y}+M_{27y}+2M_{28y}}{4},\frac{42M_{26z}+42M_{27z}+186M_{28z}}{270}\right)$$

Figure 7.8 The Position of Marker and its relationship with COM, (Foot (top), Pelvis (Bottom))

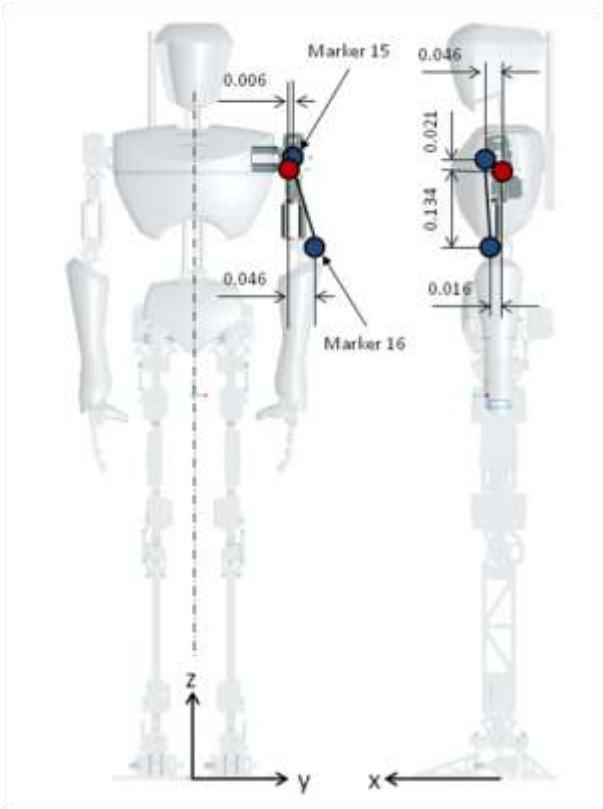

Upper arm

Mass: 0.372kg

Marker15: (40, 187,1,155) mm

Marker16: (10, 214,1,000) mm

COM: Left(-6, 184, 1,134) mm

$$=\left(\frac{134M_{15x}+21M_{16x}}{155}-42,\frac{134M_{15y}+21M_{16y}}{155}-11,\frac{134M_{15z}+21M_{16z}}{155}\right)$$

COM: Right(-6, -184, 1,134) mm

$$=\left(\frac{134M_{17x}+21M_{18x}}{155}-42,\frac{134M_{17y}+21M_{18y}}{155}+11,\frac{134M_{17z}+21M_{18z}}{155}\right)$$

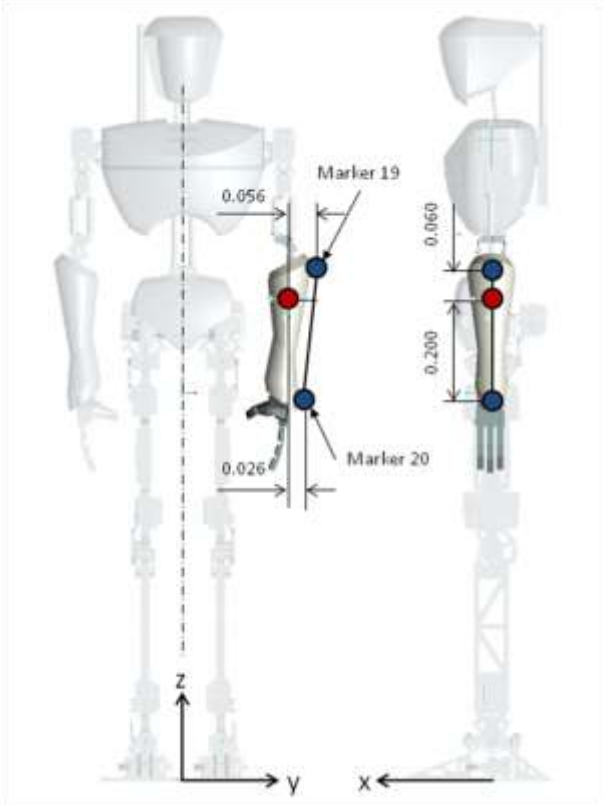

Forearm

Mass: 0.411kg

Marker19: (0, 252, 949) mm

Marker20: (0, 222, 689) mm

COM: Left(0, 196, 889) mm

$$=\left(\frac{20M_{19x}+6M_{20x}}{26},\frac{20M_{19y}+6M_{20y}}{26}-49,\frac{20M_{19z}+6M_{20z}}{26}\right)$$

COM: Right(0, -196, 889) mm

$$=\left(\frac{20M_{21x}+6M_{22x}}{26},\frac{20M_{21y}+6M_{22y}}{26}+49,\frac{20M_{21z}+6M_{22z}}{26}\right)$$

Figure 7.9 The Position of Marker and its relationship with COM,
(Upper arm (top), Forearm (Bottom))

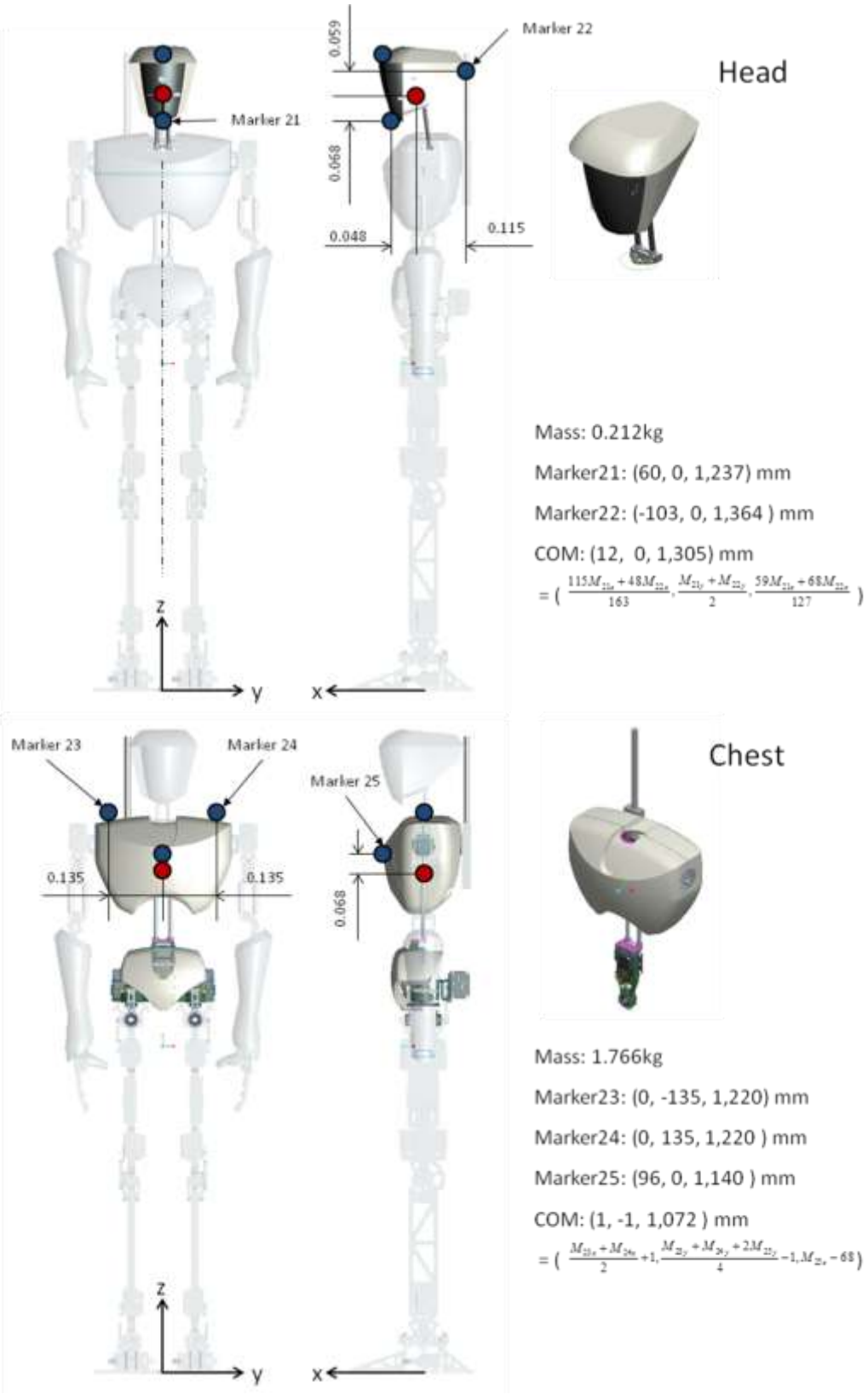

Figure 7.10 The Position of Marker and its relationship with COM, (head (top), Chest (Bottom))

Once the position data of markers are measured through the motion capture test, the positions of COM of each link can be calculated by the equations shown in Figures from 7.7 to 7.10. Then the position of COM of a body also can be calculated by Equation 5.1, based on the positions of COM of each link.
Figure 7.11 shows measured COM trajectories of a body compared with reference COM trajectories. It shows CHARLI's COM trajectories closely follow the planed reference trajectories. The errors of positions were less than 12mm, 10mm and 7mm in the x, y and z direction respectively.

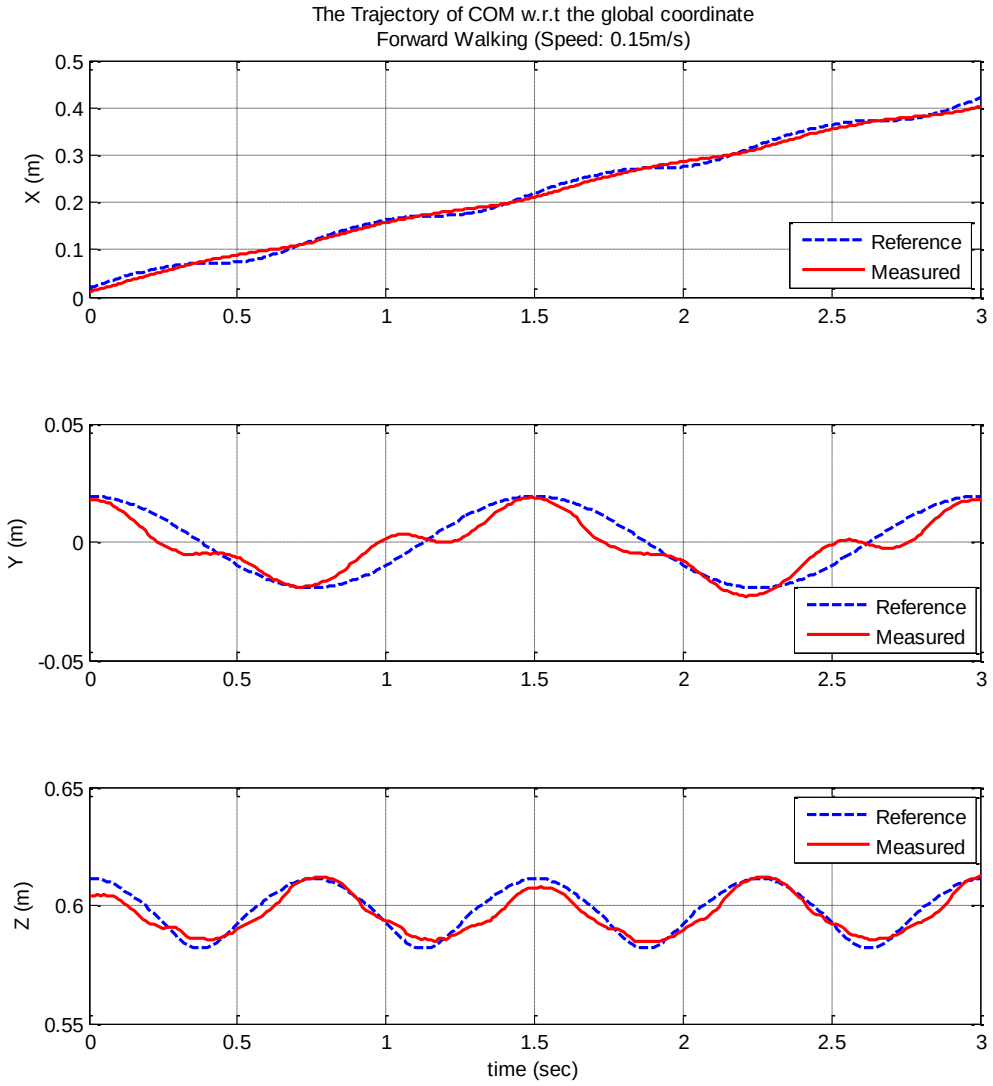

Figure 7.11 The trajectories of reference COM and measured COM
(X direction (top), Y direction (middle), Z direction (Bottom))

Figure 7.12 shows measured COM trajectories of a body compared with reference COM trajectories in XY and XZ plane.

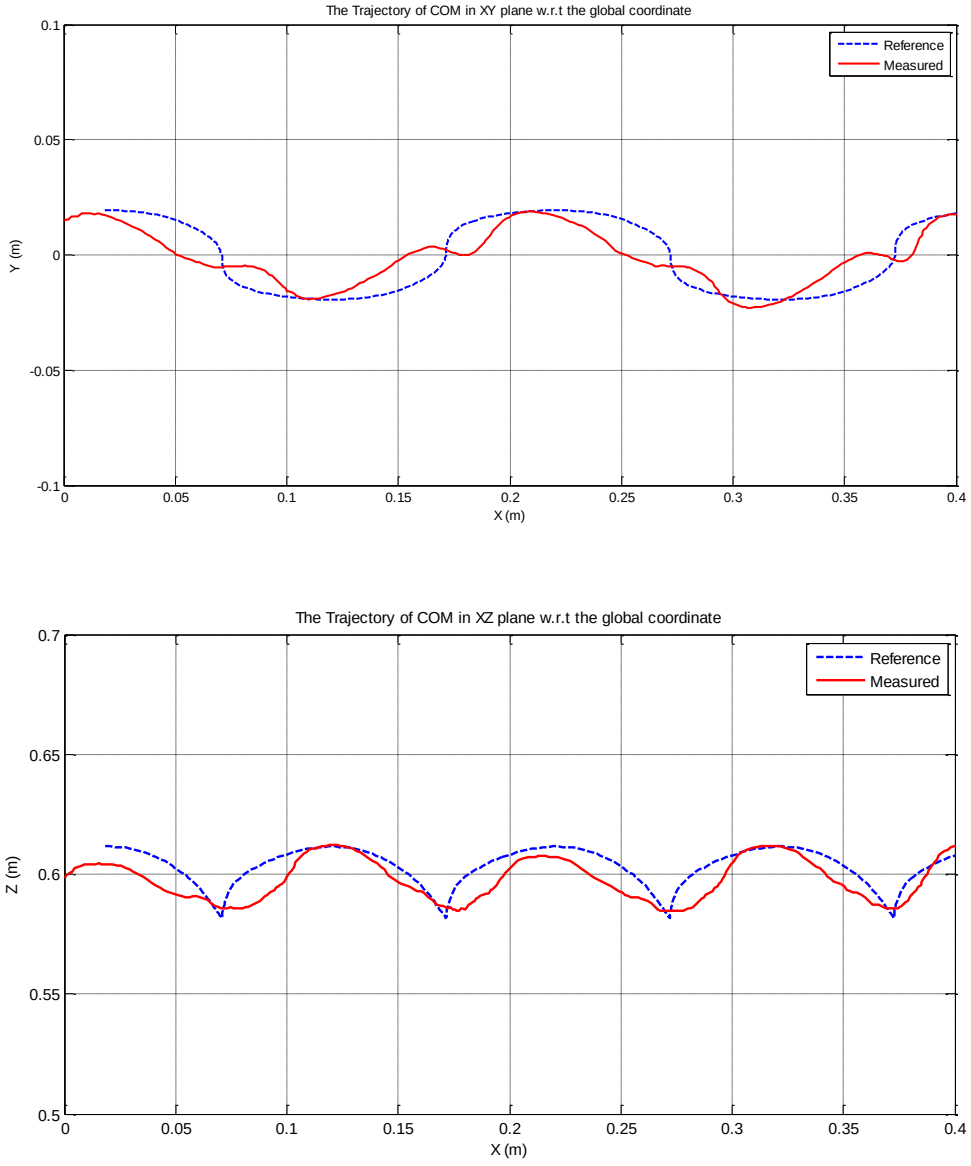

Figure 7.12 The trajectories of reference COM and measured COM (XY plane (top), XZ plane (Bottom))

Figure 7.13 shows measured COM trajectories of a body compared with reference COM trajectories in 3D space.

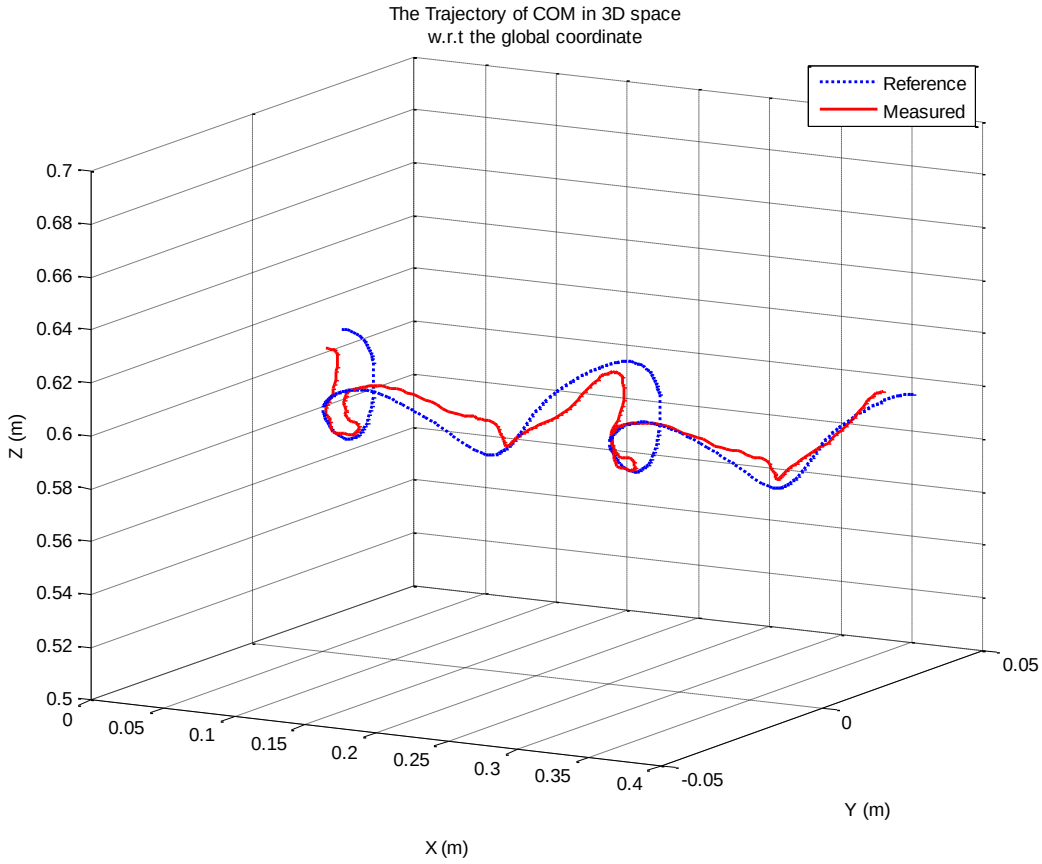

Figure 7.13 The trajectories of reference COM and measured COM in 3D space

Based on measured data, real ZMP trajectories can be estimated by Equation 4.3 as shown in Figure 7.14. It shows that ZMP was located within feet area and followed planed reference ZMP trajectory very well. The rectangular shape of Figure 7.14 shows the feet area.

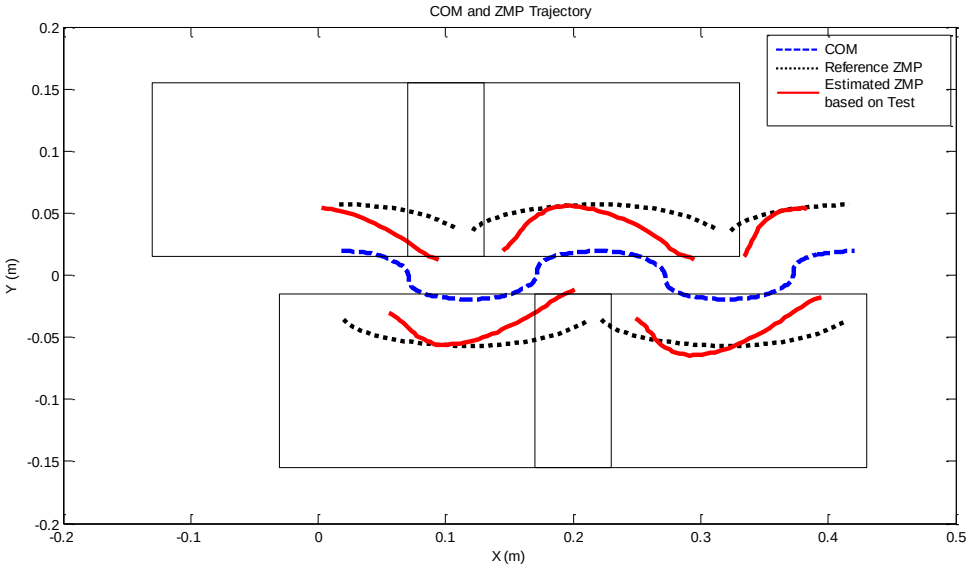

Figure 7.14 The trajectories of reference ZMP and estimated ZMP calculated by measured position data in XY plane

7.1.3 Test for Stabilization

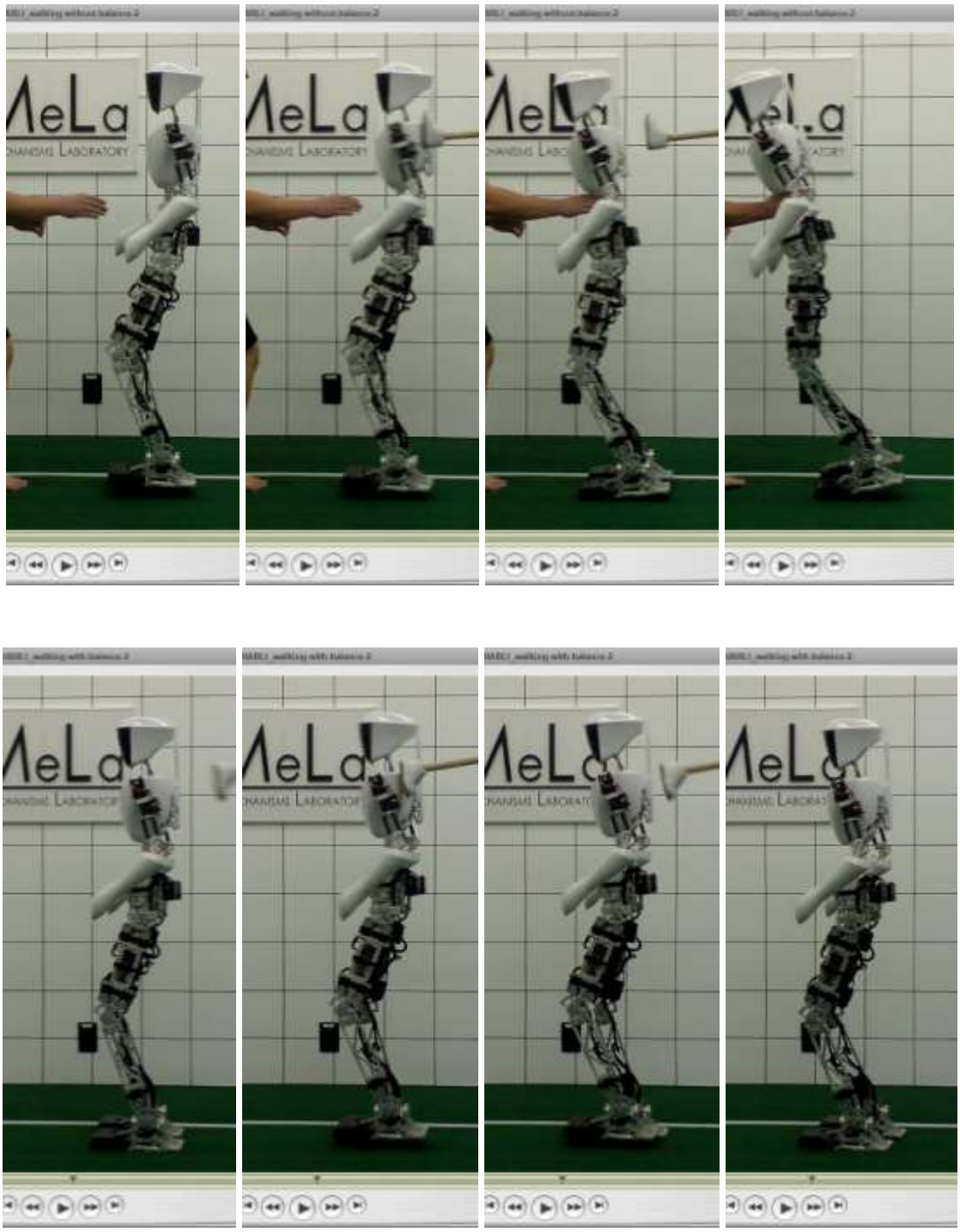

Figure 7.15 Stabilizing walking test with pushing disturbance
without feedback function for stabilization (top)
with feedback function for stabilization (Bottom)

Figure 7.15 shows the results of a balancing experiment conducted with and without the use of a feedback function for stabilization. When CHARLI-2 was pushed without stabilizing feedback while walking, it became unstable and fell. However, when using stabilizing feedback, CHARLI-2 compensated for the perturbation and did not fall.

Figure 7.16 shows the measured angular velocity and absolute angle data in the pitch and roll directions. When stabilizing feedback is used the angles converge, but when it is turned off the angles diverge. It shows how much feedback function contributes to CHARLI's stability.

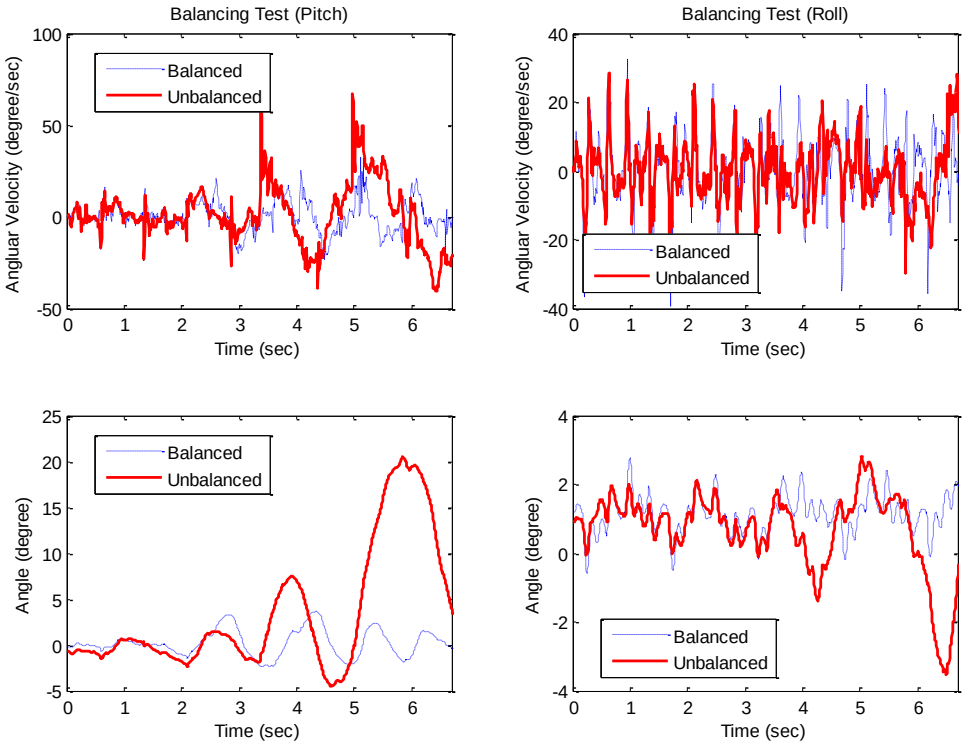

Figure 7.16 The result of stabilizing walking test with pushing disturbance
Angular velocity in pitch direction (top left)
Angular velocity in roll direction (top right)
Angle in pitch direction (Bottom left)
Angle in roll direction (Bottom right)

As shown in figure 7.17, CHARLI-2 was able to successfully walk on a real lawn using stabilizing feedback. To date, no other full-size humanoid robot has performed this kind of test. There are a number of unexpected disturbances associated with a real lawn such as uneven terrain and grass with varying elasticity, but CHARLI-2 compensated for all of these disturbances and maintained stability.

Figure 7.17 Walking test on the real lawn

7.2 Energy Consumption Test

CHARLI's actuator, Dynamixel EX-106, has the function to send actuator status back to the controller such as position, velocity, temperature, voltage or consuming current. CHARLI obtained the consuming current data from the all actuators of legs during walking. This data was used to calculate its overall energy consumption.

Figures 7.18 through 7.20 show the measured current data consumed by the actuators during walking. The voltage to drive each actuator was regulated to 5.0V. The consuming power, shown to the right hand side of each graph, can be obtained by multiplying the measured current by 5.0V. Also, energy consumption can be obtained by the definite integral of consuming power.

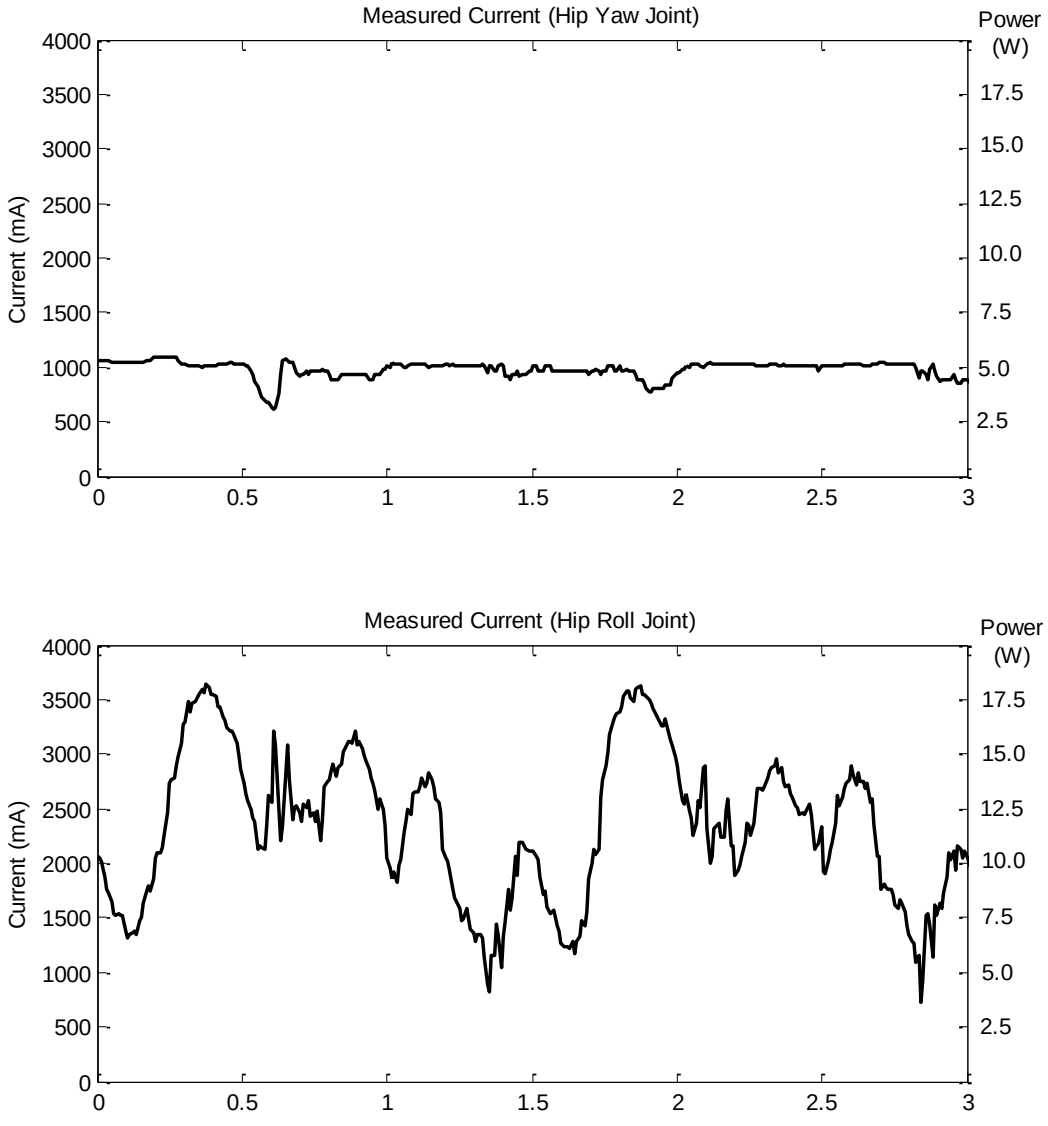

Figure 7.18 Measured Consuming Current Data
(Hip Yaw joint (top), Hip Roll joint (Bottom))

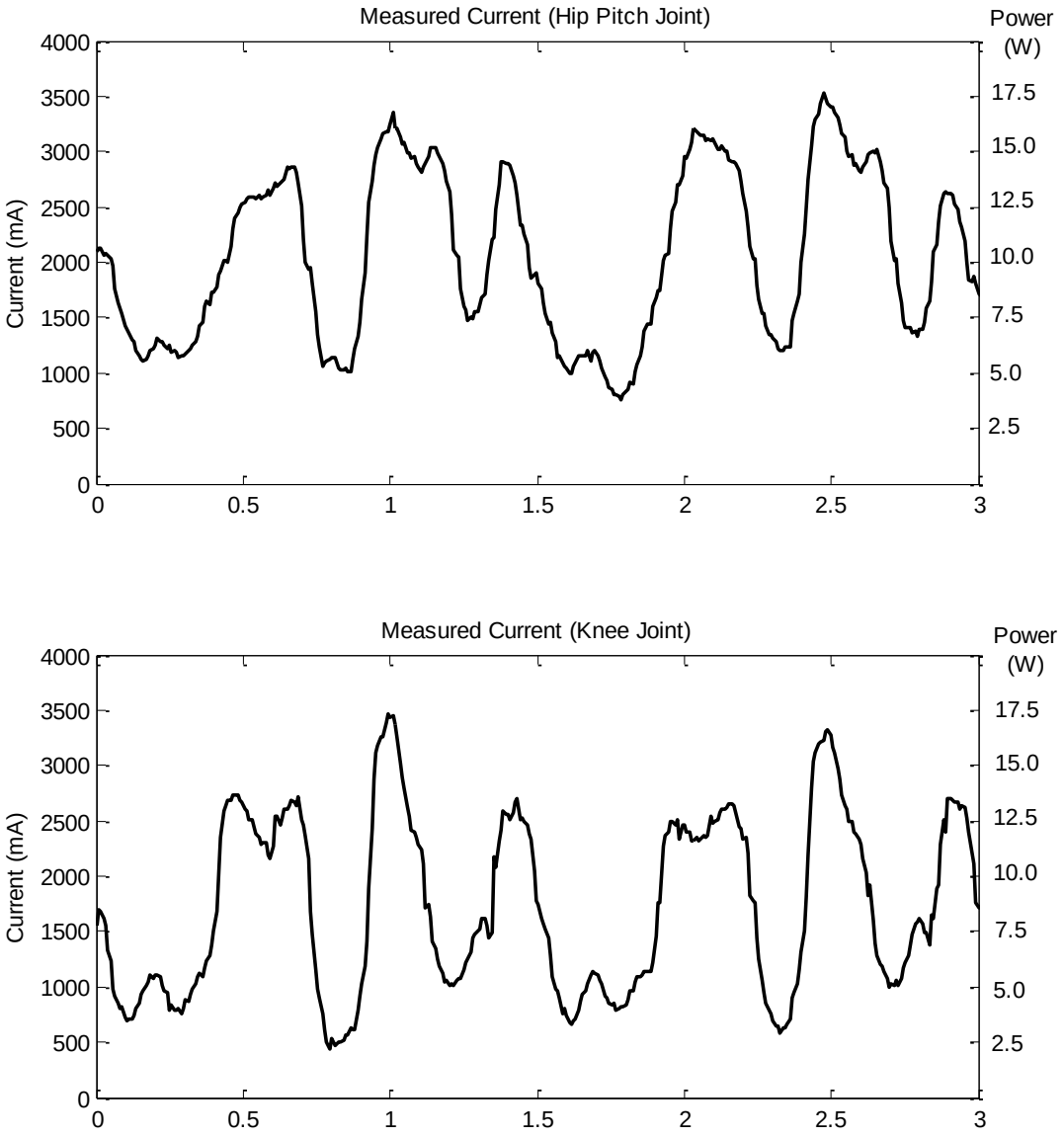

Figure 7.19 Measured Consuming Current Data
(Hip Pitch joint (top), Knee joint (Bottom))

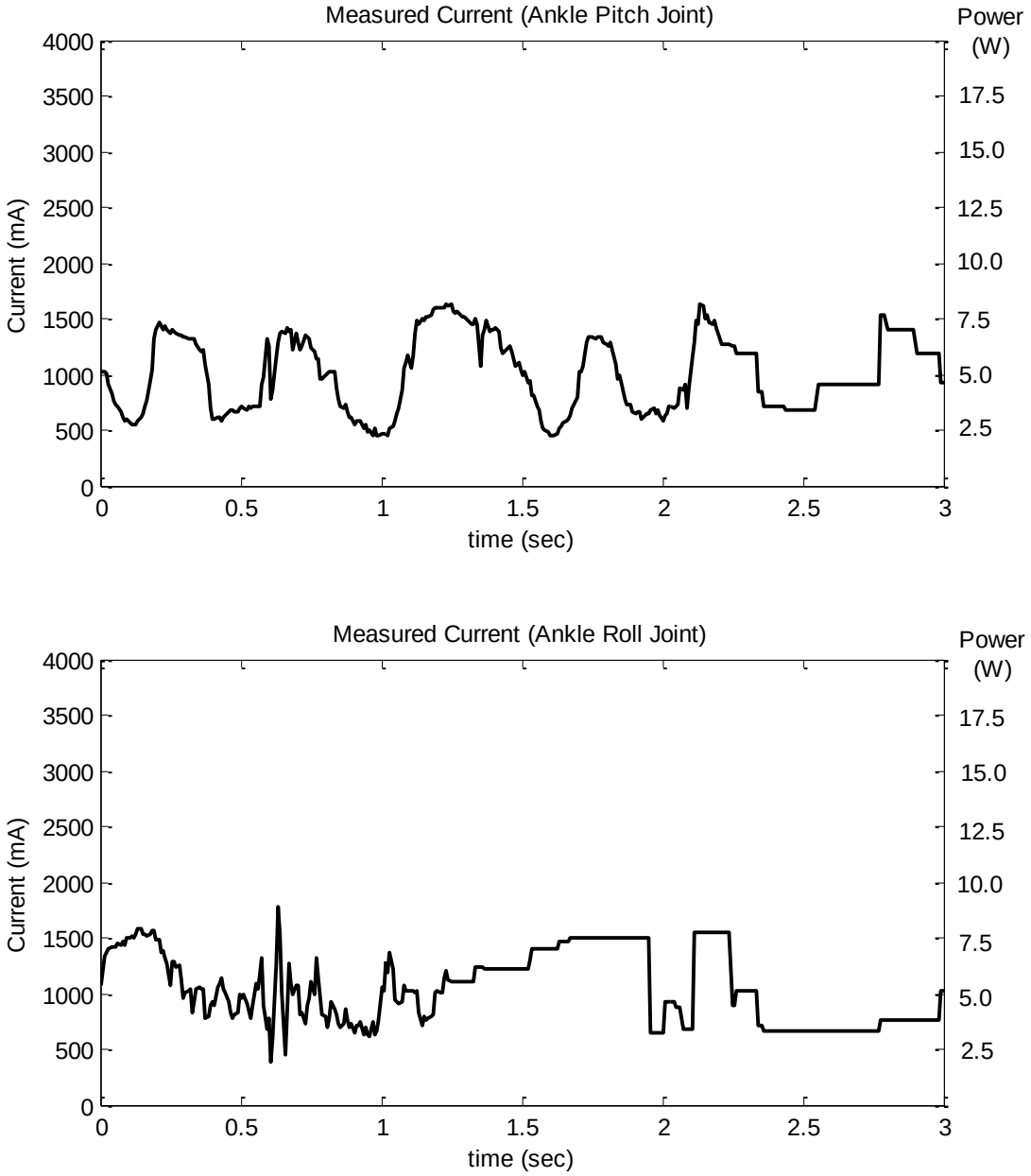

Figure 7.20 Measured Consuming Current Data
(Ankle Pitch joint (top), Ankle Roll joint (Bottom))

7.3 Discussion

The bipedal walking tests proved not only that CHARLI performed the pre-planned walking stratagem very well, but also that the intuitive walking method utilizing sinusoidal movement of each foot, which is proposed in this paper, worked very well for a full-sized humanoid robot. This method allows a full-sized humanoid robot to walk without measuring the contact force of the foot plate or the force applied to the ankle joint to use ZMP control.

In terms of current value, the consuming current of an actuator is known to have a proportional relationship with its torque value. Thus, the estimated torque graph, which is simulated in Chapter 5, was overlapped on the measured current graph, as shown in Figure 7.21. Although an arbitrary proportional rate was applied, we can see their similarities. Therefore, the dynamic simulation performed in Chapter 5 can be considered, as it has some credibility to convince its result.

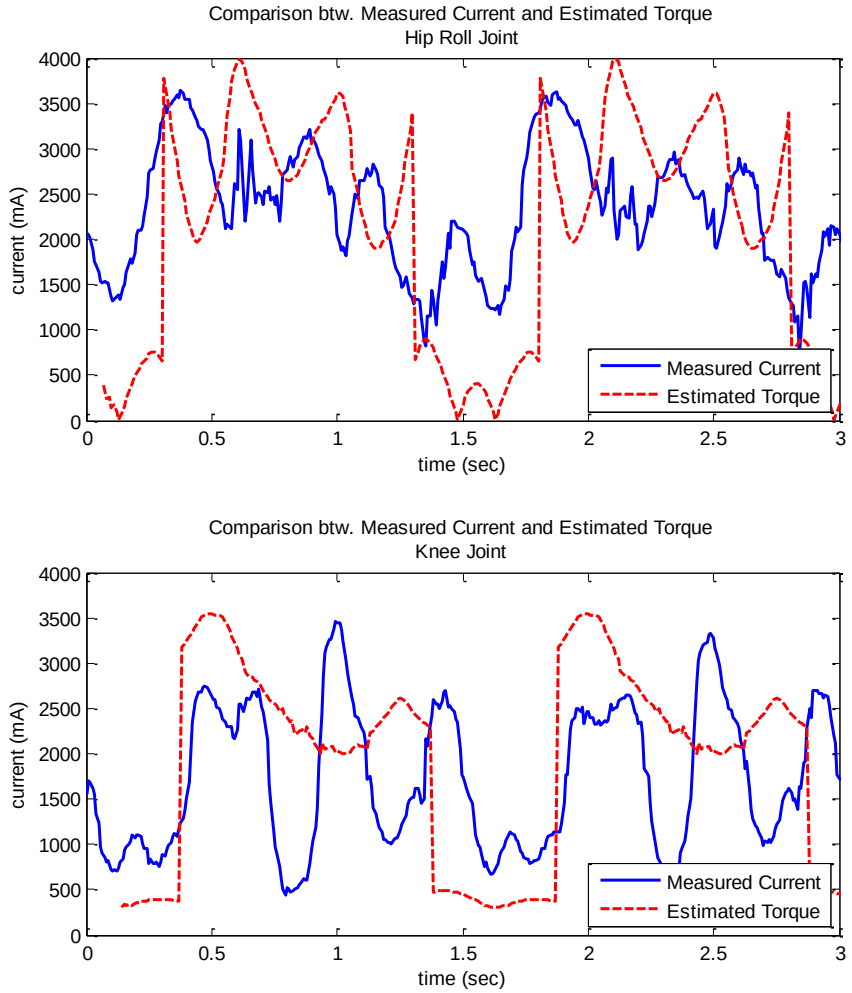

Figure 7.21 Overlapping graph Measured Current Data and Estimated Torque (Hip Roll joint (top), Knee joint (Bottom))

As mentioned in Chapter 7.2, consuming power can be obtained by multiplication of measured current and 5.0V and energy consumption can be obtained by the definite integral of consuming power. Table 7.1 and 7.2 show the average current, power and energy consumption of each joint in one leg, when walking at a speed of 1.5m/s and 2.0m/s, respectively. The energy was integrated for 9 sec.

These results show that CHARLI consumed around 100W of power to walk at a speed of 1.5m/s, and consumed around 130W of power to walk at a speed of 2.0m/s.

Table 7.1 Average current, power and energy consumption of each joint in one leg (Forward walking, speed: 1.5m/s, period of time: 9sec)

Joint	Current (A)	Power (W)	Energy (J)
Hip Yaw	1.017	5.083	45.745
Hip Roll	2.068	10.340	93.062
Hip Pitch	2.045	10.224	92.016
Knee	2.045	10.227	92.041
Ankle Pitch	1.035	5.174	46.568
Ankle Roll	0.998	4.992	44.930
Total	9.208	46.040	414.362

Table 7.2 Average current, power and energy consumption of each joint in one leg (Forward walking, speed: 2.0m/s, period of time: 9sec)

Joint	Current (A)	Power (W)	Energy (J)
Hip Yaw	1.529	7.646	68.813
Hip Roll	3.063	15.317	137.855
Hip Pitch	3.033	15.167	136.505
Knee	3.026	15.131	136.181
Ankle Pitch	1.547	7.733	69.599
Ankle Roll	1.535	7.676	69.080
Total	13.734	68.670	618.033

Section 8 Conclusions

8.1 Conclusions

The main goal of this work was to develop a bipedal walking method which allows a full-sized humanoid robot to walk. Although there have been many approaches for bipedal walking methods including ZMP method, most of them require the knowledge of contact forces at the feet or forces transmitted through the ankles. Either approach requires developers not only to install sensitive sensors on the robot but also to process and interpret the signals appropriately. Because of these difficulties, the development of a full-sized humanoid robot has been considered one of the most challenging tasks in the field of robotics.

Therefore, there is much interest in the development of a simple and reliable bipedal walking method. In this research, an intuitive bipedal walking method with sinusoidal foot movement was introduced to meet this demand. The kinematics and the dynamics were introduced to provide sound theoretical foundations in Chapter 2 and 3 respectively. Then, the way to generate the proposed bipedal walking method was described in Chapter 4 with the explanation of its principles. Next, in Chapter 5, simulations were performed to figure out how stable and reliable the proposed walking method is. The simulation was used not only to examine a walking method but also to guide the design of a humanoid robot. For example, the estimation of angular velocity and required torque were used for choosing an appropriate actuator. Also, the weight of each link calculated by simulations guided the limitation of the mechanical design. Based all this work, two full-sized humanoid robots, CHARLI-L and CHARLI-2, were fabricated.

The main goal of the mechanical design of CHARLI was to reduce the robot's weight effectively without utilizing conservative actuation or reduction systems such as harmonic drives. A light-weight design allows the use of smaller actuators – resulting in further weight reduction and decreased costs. Unlike conventional full-size humanoid robots, CHARLI-L does not use complicated gear reduction mechanisms. Instead, multiple distributed actuators are used. Synchronization of the actuators allows for smaller and lower torque actuators to be utilized with off-the-shelf components. Also, a parallel four-bar linkage system was used in the legs to reduce one more degree of freedom. CHARLI-2, on the other hand, does use a gear reduction mechanism to increase the torque of its actuator which results in a more reliable mechanism than CHARLI-L. CHARLI-2 was also carefully designed to minimize the moment of inertia of its leg.

After fabricating CAHRLI-2, experiments of bipedal walking were performed. First, the walking ability was tested and it showed to be stable and reliable. Second, a motion capture test was performed in cooperation with Locomotion Research Laboratory at Virginia Tech. Through this test, CHARLI-2 proved that it performed the pre-planned walking strategy very well. Also, it was proven that the proposed walking method utilizing sinusoidal foot movement worked very well for a full-sized humanoid robot.

Another main goal of this research was to investigate how much power and energy is consumed during walking. To determine this, the actuator currents were measured and used to calculate total power by multiplying the measured current and the regulated voltage of the motor driver. The total energy consumed was calculated by taking the integral of power.

In conclusion, this research started to build a more simple but reliable full-sized humanoid robot. Two key features were the focus of this work. One was to make a robot as light weight as possible and the other was to use as few sensors as possible. This approach was examined and proven to be effective through the use of extensive simulations and experiments based on bipedal walking theory.

8.2 Contributions

Through this research, the following technical objectives were achieved:

- The relationship between foot position and joint angles was determined using forward and inverse kinematics.
- Linear velocities of each link were expressed as a function of joint angular velocities using Jacobian matrixes.
- The torque of each joint was expressed as a function of joint angles, angular velocities, and angular accelerations by solving Euler-Lagrange equations.

- An intuitive bipedal walking method with sinusoidal foot movement was proposed to achieve a simple and reliable bipedal walking method.
- Meanings and effects of each sinusoidal function was explained in x, y and z directions.
- A stabilization algorithm was proposed to eliminate disturbances occurring during walking.

- A simulation model was built to estimate bipedal walking performance.
- Trajectories of each link, COM, and ZMP were estimated by bipedal walking simulation.
- Angles, angular velocities, and angular accelerations of each joint were estimated by dynamic simulation.
- Torque requirements of each joint were estimated by dynamic simulation.

- Two full-sized humanoid robots, CHARLI-L and CHARLI-2, were developed.
- A four bar linkage mechanism was introduced to increase torque of actuators and to decrease a degree of freedom.
- A gear reduction system synchronizing two servo motors was introduced to increase the torque of actuators.

- Tests to determine CHARLI's walking ability were performed.
- Motion capture tests were performed to determine COM and ZMP trajectories.
- The current values of each joint were measured and used to calculate the power and energy consumed during walking.

8.3 Future Work

This research was performed based on the ZMP walking method which was introduced in 1968. Its walking performance is known to be different and less effective than the natural walking strategy used by humans. Thus, many researchers have tried to develop bipedal walking methods similar to human walking. This is motivated by the belief that human walking has been optimized through evolution.

More specifically, robots using ZMP tend to walk with a constant waist height and with their knees bent while humans do not bend the knee during walking and waist height continuously moves up and down. To mimic human walking, researchers have focused on the heel-contact and toe-off aspects of walking. Doi et al. studied heel-contact motion to absorb the shock that occurs when the feet contact the ground [38]. Ralph E. Goddard et al. made a dynamic model for heel-contact and toe-off walking and then demonstrated its results in simulation [39]. Taro Takahashi and Atsuo Kawamura showed the heel joint can be controlled during walking [40]. Konno et al. proposed passive toe joints with a torsion spring in order to achieve human like gaits [41]. Based on biomechanical studies, Scarfogliero et al. equipped the passive toe joints with spring-damper buffers for smoother foot rotation [42]. Koganezawa et al. proposed a hybrid active/passive toe joint design for less energy consumption during walking [43]. Sellaouti et al. showed the effectiveness of the compliance in the toe joint in increasing walking speed through a dynamic simulation of HRP-2. [44]

Nishiwaki et al. achieved faster walking on the humanoid H6 using an active toe joint. They used rotation of the toe joint during the double support phase in order to decrease the knee joint angular velocity. The active toe joints provided a 1.8x faster walking gait [45].

Waseda University has developed another full-sized humanoid robot series, WABIAN, to realize human-like walking. They successfully carried out a stretched-knee walking method experiment in [46] [47]. Moreover, they developed passive toe joints and then tested heel-contact and toe-off walking. As a result, the WABIAN-2 is recorded as the first humanoid robot which can walk with stretched knees and heel-contact/toe-off motions in [48], [49], [50].

Although this idea was originally suggested and its benefits proven by Waseda University, they only demonstrated an improvement of walking speed and decrease of angular velocity of the knee joints. Therefore, the energy consumption effectiveness needs to be examined to illuminate the benefit of the human-like walking method in an energy consumption aspect.

A method for measuring energy consumption during walking has already been presented in this paper. If CHARLI was capable of human-like walking, the two walking methods, ZMP method and human-like walking method, could be compared with each other. For this reason, a human-like walking method is expected to be developed for CHARLI in the future.

References

[1] I. Kato, S. Ohtuu, H. Kobayashi, K Shirai, and A. Uchiyama, “Information-power machine with senses and 1imts:” in Proc. CISM-IFToMM Symposium on Theory and Practice of Robots and Manipulators, pp. 12-24.1973

[2] H. Jishikawa T. Kato, A. Takanish and I. Kato. “The realization of the quasi-dynamic walking by the biped walking machine.” Proc. 4th Symposium on Theory and Practice of Robots and Manipulators, pp. 341–351, 1981.

[3] A. Takanish, M. Ishida, Y. Yamazaki, and I. Kato. “The realization of dynamic walking by the biped walking robot WL-10RD.” Proc. Intl. Conference on Advanced Robotics, pp. 459–466, 1985.

[4] H. Karaki A. Takanish, T. Takeya and I. Kato. “A control method for dynamic biped walking under unknown external force.” Proc. IEEE Int. Workshop on Intelligent Robots and Systems, pp. 795–801, 1990.

[5] M. Tsuda A. Takanish, H. Lim and I.Kato, “Realization of dynamic biped walking stabilized by trunk motion on a sagittally uneven surface.” Proc. IEEE Int. Workshop on Interrigent Robots and Systems, pages 323–330, 1990.

[6] A. Takanishi L. Qinghau and I. Kato, “A biped walking robot having a zmp measurement system using universal force-moment sensors.” Proc. IEEE/RSJ Int. Workshop in Intelligent Robots and Systems, pp. 1568–1573, 1991.

[7] Y. Sakagami, R. Watanabe, C. Aoyama, S. Matsunaga, N. Higaki, and K. Fujimura, "The intelligent ASIMO: System overview and integration," Proc. IEEE/RSJ Int. Conference on Intelligent Robots and Systems, pp.2478-2483, 2002.

[8] Hirai, K. “The development of Honda humanoid robot,” Proc. IEEE International Conference on Robotics and Automation, pp1321 - 1326 vol.2, 1998

[9] K. Kaneko, F. Kanehiro, S. Kajita, K. Yokoyama, K. Akachi, T. Isozumi, “Design of Prototype Humanoid Robotics Platform for HRP,” Proc. IEEE/RSJ Int. Conference on Intelligent Robots and Systems, pp.2431-2436, 2002

[10] K. Nishiwaki, S. Kagami, Y. Kuniyoshi, M. Inaba, and H. Inoue, "Online Generation of Humanoid Walking Motion based on a Fast Generation Method of Motion Pattern that Follows Desired ZMP," Proc. IEEE/RSJ Int. Conference on Intelligent Robots and Systems, pp. 2684-2689, 2002.

[11] K. Loffler, M. Gienger, and F. Pfeiffer, "Sensor and Control Design of a Dynamically Stable Biped Robot," Proc. IEEE Int. Conference on Robotics and Automation, pp. 484-490, 2003.

[12] J. Kim, I. Park, J. Lee, M. Kim, B. Cho, and J. Oh, "System Design and Dynamic Walking of Humanoid Robot KHR-2," Proc. IEEE Int. Conference on Robotics and Automation, pp. 1443-1448, 2005.

[13] Vukobratovic, M., "On the stability of biped locomotion," IEEE Trans Biomed Eng, pp. 25-36, 1970

[14] Sardain, P., "Forces acting on a biped robot. Center of pressure-zero moment point," IEEE Transactions on Systems and Humans, pp. 630 – 637, 2004

[15] Qinghua Li , "A biped walking robot having a ZMP measurement system using universal force-moment sensors," Proceedings IROS '91. IEEE/RSJ International Workshop on Intelligence for Mechanical Systems, pp. 1568 - 1573 vol.3, 1991

[16] Sorao, K., "A unified approach to ZMP and gravity center control in biped dynamic stable walking," IEEE/ASME International Conference on Advanced Intelligent Mechatronics, pp. 16-20, 1997

[17] Nishiwaki Koichi, "High frequency walking pattern generation based on preview control of ZMP," Proc.IEEE International Conference on Robotics and Automation, ICRA, pp. 2667 – 2672, 2006

[18] Sugihara, T., "Real-time humanoid motion generation through ZMP manipulation based on inverted pendulum control," Proc. IEEE International Conference on Robotics and Automation, pp. 1404 - 1409 vol.2, 2002

[19] Kagami, S., "Fast Generation Method of Dynamically Stable Trajectory of Humnoid Motion based on the Characteristics of ZMP," Nippon Robotto Gakkai Gakujutsu Koenkai Yokoshu , pp.721-722, 2000

[20] Okumura, Y. "Realtime ZMP compensation for biped walking robot using adaptive inertia force control," Proc. IEEE/RSJ International Conference on Intelligent Robots and Systems, pp. 335 - 339 vol.1, 2003

[21] Kajita, S., "Biped Walking Pattern Generator allowing Auxiliary ZMP Control," IEEE/RSJ International Conference on Intelligent Robots and Systems, pp. 2993 – 2999, 2006

[22] Johannes Strom, "Omnidirectional Walking Using ZMP and Preview Control for the NAO Humanoid Robot," Robot Soccer World Cup XIII, pp. 378-389, 2009

[23] Jinsu Liu, "Online ZMP sampling search for biped walking planning," IEEE/RSJ International Conference on Intelligent Robots and Systems, pp. 185 – 190, 2008

[24] Kajita, S., "Biped walking pattern generation by using preview control of zero-moment point," IEEE International Conference on Robotics and Automation, pp. 1620 - 1626 vol.2, 2003

[25] Sato, T. "ZMP disturbance observer for walking stabilization of biped robot," IEEE International Workshop on Advanced Motion Control, pp. 290 – 295, 2008

[26] Kyu-Cheon Choi, "Fuzzy Posture Control for Biped Walking Robot Based on Force Sensor for ZMP," International Joint Conference SICE-ICASE, pp. 1185 – 1189, 2006

[27] Jong Hyeon Park, "ZMP compensation by online trajectory generation for biped robots," IEEE International Conference on Systems, Man, and Cybernetics, pp. 960 - 965 vol.4, 1999.

[28] Erbatur, K, “Humanoid Walking Robot Control with Natural ZMP References,” 32nd Annual Conference on IEEE Industrial Electronics, pp. 4100 - 4106, 2006

[29] Sugihara, T. “Standing stabilizability and stepping maneuver in planar bipedalism based on the best COM-ZMP regulator,” IEEE International Conference on Robotics and Automation, pp. 1966 – 1971, 2009

[30] Youngjin Choi, “On the stability of indirect ZMP controller for biped robot systems,” IEEE/RSJ International Conference on Intelligent Robots and Systems, pp. 1966 - 1971 vol.2, 2004

[31] Bum-Joo Lee, “Modifiable Walking Pattern of a Humanoid Robot by Using Allowable ZMP Variation,” IEEE Transactions on Robotics, Vol. 24, Issue 4, pp. 917 – 925, 2008

[32] Changjiu Zhou, “Robo-Erectus: a low-cost autonomous humanoid, soccer robot,” Advanced Robotics and Robotics Society of Japan, Vol. 18, No. 7, pp. 717–720, 2004

[33] JR. H. Hemami, C. L. Golliday, “The inverted pendulum and biped stability,” Math. Biosci, pp. 95–110, 1976.

[34] Arnaud Hamon, Yannick Aoustin, "Cross Four-Bar Linkage for the Knees of a Planar Bipedal Robot", Humanoids2010 Conference, 2-24. 2010

[35] J. McKendry, B. Brown, E.R. Westervelt, and J.P. Schmiedeler, "Kinematic Design and Dynamic Analysis of a Planar Biped Robot Mechanically Coordinated by a Single Degree of Freedom,” 2007 IEEE International Conference on Robotics and Automation , pp.1875-1880, 2007

[36] Hyeung-Sik Choi, Yong-Heon Park,"Development of a biped walking robot actuated by a closed-chain mechanism", Robotica(2006), Vol.24: Issue 1, p.31-37

[37] Thomas Buschmann, Sebastian Lohmeier, Heinz Ulbrich, "Humanoid robot Lola: Design and walking control", Journal of Physiology - Paris 103 (2009) 141–148

[38] Masahiro Doi , Takayuki Matsuno , Yasuhisa Hasegawa and Toshio Fukuda, “Proposal of Smooth Biped Walking Control by means of Heel-off Motion,” Proc. IEEE International Conference on Robotics and Automation, pp.1591-1596, 2006

[39] Ralph E. Goddard, Yuan. F. Zheng, Hooshang Hemami, “Control of the Heel-Off to Toe-Off Motion of a Dynamic Biped Gait,” IEEE Transactions on systems, man, and cybernetics, Vol. 22, No. 1, pp. 92-102, 1992

[40] Taro Takahashi and Atsuo Kawamura, “Posture Control using Foot Toe and Sole for Biped Walking Robot, Ken” Advanced Motion Control, 2002. 7th International Workshop on, pp. 437 – 442, 2002

[41] A. Konno, R. Sellaouti, F. B. Amar and F. B. Ouezdou, "Design and Development of the Biped Prototype ROBIAN," IEEE – International Conference on Robotics & Automation, pp. 1384-1389, 2002.

[42] U. Scarfogliero, M. Folgheraiter and G. Gini, "Advanced Steps in Biped Robotics: innovative Design and Intuitive Control through Spring-Damper Actuator," IEEE/RSA International Conference on Humanoid Robots, pp. 196-214, 2004

[43] K. Koganezawa and 0. Matsumoto, "Active/Passive Hybrid Walking by The Biped Robot TOKAI ROBO-HABILIS 1," IEEE/RSJ International Conference on Intelligent Robots and Systems, pp. 2461-2466, 2002.

[44] Ramzi Sellaouti, Olivier Stasse, Shuuji Kajita, Kazuhito Yokoi and Abderrahmane Kheddar "Faster and Smoother Walking of Humanoid HRP-2 with Passive Toe Joints," Proceedings of the 2006 IEEE/RSJ International Conference on Intelligent Robots and Systems, pp. 4909-4914, 2006

[45] K. Nishiwaki, S. Kagami, Y. Kuniyoshi, M. Inaba and H. Inoue, "Toe joints that Enhance Bipedal and Fullbody Motion of Humanoid Robots," IEEE International Conference on Robotics and Automation, pp. 3105-3110, 2002.

[46] H. Lim, A. Ishii, and A. Takanishi, "Motion Pattern Generation for Emotion Expression," in Proc. Int. Symp. Humanoid Robots, pp. 36-41,1999

[47] H. Lim, Y. Kaneshima, and A. Takanishi, "Online Walking Pattern Generation for Biped Humanoid with Trunk," Proc. IEEE Int. Conference on Robotics and Automation, pp.3111-3116, 2002

[48] Y. Ogura, H. Lim, A. Takanishi, "Stretch Walking Pattern Generation for a Biped Humanoid Robot," Proc. IEEE/RSJ Int. Conference on Intelligent Robots and Systems, pp. 352-357, 2003.

[49] Y. Ogura, H. Ailrawa, H. Lim, A. Takanishi, "Development of a Human-like Walking Robot Having Two 7.DOF Legs and a 2-DOF Waist," Proc. IEEE Int. Conference on Robotics and Automation, pp. 134-139, 2004

[50] Yu Ogura, Hun-ok Lim, Atsuo Takanishi "Human-like Walking with Knee Stretched, Heel-contact and Toe-off Motion by a Humanoid Robot," Proc. IEEE/RSJ Int. Conference on Intelligent Robots and Systems, pp 3976-3981, 2006